



**US Army Corps
of Engineers®**
Engineer Research and
Development Center



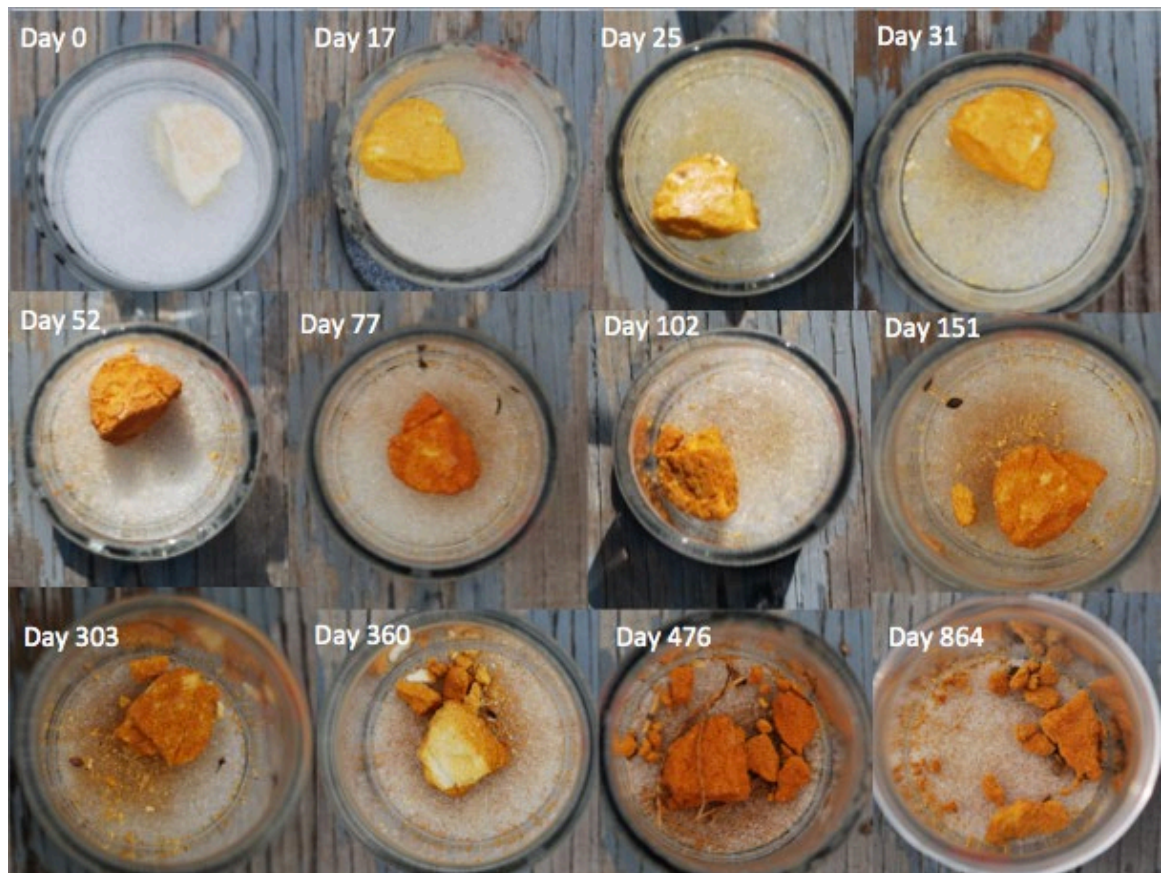
Strategic Environmental Research and Development Program (SERDP)

Dissolution of NTO, DNAN, and Insensitive Munitions Formulations and Their Fates in Soils

SERDP ER-2220

Katerina M. Dontsova, Susan Taylor, Jennifer D. Arthur, Julie
B. Becher, Mark L. Brusseau, Edward Hunt, Noah W. Mark,
Dave B. Ringelberg, Jiří Šimůnek, and Marianne E. Walsh

November 2022



The US Army Engineer Research and Development Center (ERDC) solves the nation's toughest engineering and environmental challenges. ERDC develops innovative solutions in civil and military engineering, geospatial sciences, water resources, and environmental sciences for the Army, the Department of Defense, civilian agencies, and our nation's public good. Find out more at www.erdclibrary.on.worldcat.org/discovery.

To search for other technical reports published by ERDC, visit the ERDC online library at <http://www.erdclibrary.on.worldcat.org/discovery>.

Dissolution of NTO, DNAN, and Insensitive Munitions Formulations and Their Fates in Soils

SERDP ER-2220

Katerina M. Dontsova, Jennifer D. Arthur, Edward Hunt, Mark L. Brusseau,
and Noah W. Mark

*University of Arizona
Biosphere 2 and Soil, Water, and Environmental Science Department
845 N. Park Avenue
Tucson, AZ 85721-0158*

Susan Taylor, Dave B. Ringelberg, and Marianne E. Walsh

*US Army Engineer Research and Development Center (ERDC)
Cold Regions Research and Engineering Laboratory (CRREL)
72 Lyme Road
Hanover, NH 03755-1290*

Julie B. Becher

*Dartmouth College
Hanover, NH 03755*

Jiří Šimůnek

*University of California, Riverside
Department of Environmental Sciences
2258 Geology Building
Riverside, CA 92521-0424*

Final Report

Approved for public release; distribution is unlimited.

Prepared for Strategic Environmental Research and Development Program
Environmental Restoration Program Area
4800 Mark Center Drive, Suite 16F16
Alexandria, VA 22350

Under Project Number ER-2220, “Dissolution of NTO, DNAN, and Insensitive
Munitions Formulations and Their Fates in Soils”

Abstract

The US military is interested in replacing TNT (2,4,6-trinitrotoluene) and RDX (1,3,5-hexahydro-1,3,5-trinitro-1,3,5-triazine) with DNAN (2,4-dinitroanisole) and NTO (3-nitro-1,2,4-triazol-5-one), which have similar explosive characteristics but are less likely to detonate unintentionally. Although these replacements are good explosives, basic information about their fate and transport was needed to evaluate their environmental impact and life-cycle management. This project measured their dissolution, photodegradation, and how aqueous solutions interact with soils, data critical to determining exposure potential and, consequently, risk.

DISCLAIMER: The contents of this report are not to be used for advertising, publication, or promotional purposes. Citation of trade names does not constitute an official endorsement or approval of the use of such commercial products. All product names and trademarks cited are the property of their respective owners. The findings of this report are not to be construed as an official Department of the Army position unless so designated by other authorized documents.

DESTROY THIS REPORT WHEN NO LONGER NEEDED. DO NOT RETURN IT TO THE ORIGINATOR.

Contents

Abstract	ii
Figures and Tables	v
Preface	x
1 Introduction	1
1.1 Background.....	1
1.2 Objective.....	5
1.3 Approach.....	5
2 Outdoor Dissolution and Photodegradation Tests of IM Formulations	7
2.1 Introduction.....	7
2.2 Methods.....	8
2.2.1 High-performance chromatography.....	8
2.2.2 Gas chromatography–mass spectrometry (GC-MS).....	9
2.2.3 Other analytical methods.....	10
2.3 Results.....	11
2.3.1 Appearance of explosive pieces.....	11
2.3.2 Dissolution of explosive pieces.....	13
2.3.3 Mass balance for the outdoor tests.....	17
2.3.4 UV–vis.....	19
2.3.5 Photodegradation of explosive pieces.....	23
2.3.6 HPLC and GC-MS analyses.....	25
2.3.7 Compounds detected in the effluent and on the frits of the outdoor IM formulations.....	26
2.3.8 Unknowns HPLC.....	32
2.3.9 Unknowns GC-MS.....	33
2.4 Conclusion.....	36
3 Outdoor Dissolution Studies in Arizona	38
3.1 Introduction.....	38
3.2 Methods.....	38
3.3 Results.....	41
3.3.1 Weather conditions during the experiment.....	41
3.3.2 Particle appearance.....	42
3.3.3 Dissolution of IM constituents.....	43
3.3.4 Mass balance.....	51
3.4 Conclusions.....	55
4 Dissolution and Transport of Insensitive Munitions Formulations IMX-101 and IMX-104 in Saturated Soil Columns	58
4.1 Introduction.....	58
4.2 Method.....	58
4.2.1 Soils.....	58

4.2.2 Column experiments	59
4.2.3 Analytical method	61
4.2.4 Numerical analysis	62
4.3 Results.....	64
4.3.1 Breakthrough curves.....	64
4.3.2 pH of the insensitive munitions solutions	82
4.3.3 Mass balance.....	83
4.4 Conclusion.....	85
5 Predicting Dissolution and Transport of IMX-101 and IMX-104 Constituents Using HYDRUS-1D	88
5.1 Introduction.....	88
5.2 Methods	88
5.3 Results.....	91
5.3.1 IMX-101 dissolution and transport to a 20 cm depth in Camp Guernsey and Plymouth soils	91
5.3.2 IMX-101 dissolution and transport to groundwater in Camp Guernsey soil	92
5.3.3 IMX-101 dissolution and transport to groundwater in Camp Swift Soil	93
5.3.4 IMX-101 dissolution and transport to groundwater in Plymouth soil	95
5.3.5 IMX-104 dissolution and transport to groundwater in Camp Guernsey soil	96
5.4 Conclusions.....	98
6 Summary	99
References.....	101
Appendix A: Solubility of DNAN, NQ, and NTO as a Function of Temperature.....	109
Appendix B: Studies Investigating the Transformation Products of DNAN.....	110
Appendix C: Properties of DNAN and Its Transformation Products	112
Appendix D: GC-MS Retention Times and Mass Spectra for Compounds Discussed in This Report	115
Appendix E: Additional Figures for Dissolution and Transport of Insensitive Munitions Formulations IMX-101 and IMX-104 in Saturated Soil Columns	125
Abbreviations.....	133
Report Documentation Page (SF 298).....	137

Figures and Tables

Figures

1.	Composition of IM formulations IMX-101, IMX-104, and PAX-21 (modified from Taylor et al. 2013).....	1
2.	Appearance of a piece of IMX-101, IMX-104, and PAX-21 set outdoors to weather and dissolve. The top row shows particles at 17 days, and the bottom row shows the same particles at 363 days.....	7
3.	IMX-101#1 set outside to weather and dissolve. The images show how the surface of the piece changed over the 864 days of the experiment.	12
4.	We found that IM formulations are very friable compared to traditional explosives.....	12
5.	The μ CT cross sections of (a) a detonated piece of IMX-101#1; (b) a detonated piece of IMX-101#2 at 0, 437, and 864 days of outdoor dissolution; (c) a piece of IMX-104#4; and (d) a piece of PAX-21#2. All of these pieces split during the test, so the images taken at day 437 and 864 are the largest fragments of the original piece.	13
6.	Dissolved mass vs. precipitation volume for five IMX-101 (a), five IMX-104 (b), and two PAX-21 (c) chunks placed outside: NTO (blue), NQ (orange), DNAN (green), RDX (red), AP (purple).	14
7.	Dissolved DNAN plotted against water volume for outdoor samples of IMX-101, IMX-104, and PAX-21.	15
8.	Dissolved NTO (a) and NQ (b) plotted against water volume for outdoor samples of IMX-101, IMX-104, and PAX-21.	17
9.	The UV-vis spectra of IM formulation constituents.	20
10.	UV-vis spectra of known transformation products of DNAN.	21
11.	Plots showing the UV-vis spectra for the first (black), tenth (green), and eighteenth (orange) water sample collected from IM pieces placed outside to weather.....	22
12.	Plot of NTO concentration in effluent collected from IMX-104 outdoor chunks vs. the UV-vis peak position (nm) for NTO.	23
13.	Chromatograms from a NovaPak C8 column plotting absorption units at 230 nm vs. minutes for a water sample collected from an IMX-104 indoor dissolution test (top, no sunlight exposure, Taylor et al. 2015a) and an outdoor test (bottom). DNAN, RDX, and HMX peaks are well defined; but there are many unknown peaks and a large presolvent peak (arrow) in the outdoor sample.....	24
14.	Microbial biofilm found in the first PAX-21#1 aqueous sample collected (at T = 1, day 17) and GC-MS analysis of this sample. Note the high concentrations of 2-methoxy-5-nitroaniline (arrow) and the absence of the other methoxy nitroaniline and nitrophenol compounds. Present are MNA (N-methyl-p-nitroaniline); 4-nitroaniline; and 2,4-dinitroaniline.	29
15.	Hypercarb analyses of effluent from frit samples, showing elution times of the methoxy aniline and phenol compounds (red arrows) and the elution time of three unknown compounds (dashed lines).	30
16.	Three unknowns were paired using two HPLC methods. The third and	

	fourth panels show the UV-vis spectrum of the peak at 5.5 min on the NovaPak C8 (panel 1) and at 37 min on the Hypercarb column (panel 2) of effluent collected from IMX-104 (at T = 18). The next four panels show the elution time of the unknown peaks and their UV-vis spectra from the IMX-101#1 frit extracts.	33
17.	(a) Mass spectrum of an unknown compound having a slightly shorter retention time than that of 2,4-DNAN and a similar pattern of mass fragments, tentatively identified as 2,6-DNAN; (b) mass spectrum of 2,4-DNAN; and (c) DNAN solution before and after exposure to sunlight. Note that the peak we think corresponds to 2,6-DNAN disappears after sunlight exposure while 4-methoxy-3-nitrophenol, the methoxy nitoaniline isomers, and UK- A are formed.....	35
18.	Experimental setup to examine dissolution and phototransformation of insensitive munitions: (a) an unweathered particle of IMX-104 in a bottle with a funnel attached for collecting solution, (b) a particle of IMX-104 (from a low-order detonation) on a glass frit and PTFE mesh in the funnel after one month of exposure to sunlight (no rain), and (c) a light-protected container with bottles and funnels with the particles exposed to sun and rainfall. The container is equipped with temperature sensors and the LPO2 pyranometer to measure solar radiation.	40
19.	Global radiation expressed as average irradiance per 15 min, $W\ m^{-2}$, measured next to the experimental setup over the course of the experiment (top) and a close up to show daily variation (bottom).....	41
20.	Mean rainfall amount and distribution during the experiment across all samples.	42
21.	Images of particles of IMX-101, IMX-104, and PAX-21 over time as they were exposed to sunlight and rainfall in Oracle, AZ.	43
22.	Dissolution of (a) NTO, NQ, and DNAN from IMX-101; (b) NTO, RDX, and DNAN from IMX-104; and (c and d) perchlorate, RDX, and DNAN from PAX-21 as a function of time.....	44
23.	Dissolution of NTO, NQ, and DNAN from six IMX-101 particles as a function of rainfall amount. NTO is indicated in green, NQ in burgundy, and DNAN in blue.....	45
24.	Dissolution of NTO, RDX, and DNAN from six IMX-104 particles as a function of rainfall amount. NTO is indicated in green, NQ in burgundy, and DNAN in blue.....	46
25.	Dissolution of ClO_4^- , RDX, and DNAN from six PAX-21 particles as a function of rainfall amount. NTO is indicated in green, NQ in burgundy, and DNAN in blue.....	46
26.	Correlation between concentrations of HMX and RDX in solutions resulting from dissolution of IMX-101 and PAX-21 particles.....	48
27.	The relationship between ammonium and nitrate concentrations in solutions of IMX-101 and IMX-104 and blank samples without explosives.	50
28.	The relationship between pH and NTO concentrations for solutions resulting from dissolution of IMX-101 and IMX-104 particles. Data was combined for all studied particles.	51
29.	The relationship between particle size and mass loss of the particles for outdoor dissolution of traditional and insensitive munitions in New Hampshire and Arizona. Data for traditional munitions is from Taylor et al.	

	(2010) and for IMs from Taylor et al. (2015a).	54
30.	The relationship between mass loss during particle dissolution and phototransformation and recovery of products of dissolution and phototransformation in solution analyzed by HPLC, using IMX-101 FB, IMX-104 MB, and PAX-21 MA particles as examples.	55
31.	Image of IMX-101 on top of the soil profile during dissolution experiments.	60
32.	Breakthrough curves for individual explosives for detonated IMX-101 in Camp Swift soil: NTO, 3-nitro-1, 2, 4-triazol-5-one; NQ, nitroguanidine; DNAN, 2, 4-dinitroanisole; 2-ANAN, 2-amino-4-nitroanisole; and 4-ANAN, 4-amino-2-nitroanisole. The vertical gray solid line indicates a switch to background solution.	66
33.	Breakthrough curves for individual explosives for detonated IMX-101 flow interruption in Camp Swift soil: NTO, 3-nitro-1, 2, 4-triazol-5-one; NQ, nitroguanidine; DNAN, 2, 4-dinitroanisole; 2-ANAN, 2-amino-4-nitroanisole; 4-ANAN, 4-amino-2-nitroanisole. The vertical dashed line indicates the start of 24 hr flow interruption. The vertical gray solid line indicates a switch to background solution.	69
34.	Correlation between simulated Ymax of individual components in IMX-101 formulation from continuous flow experiments: NTO, 3-nitro-1, 2, 4-triazol-5-one, and DNAN, 2,4-dinitroanisole. The Thompson Tau method was used to reject one outlier in the data set.	73
35.	Breakthrough curves for individual explosives for the detonated IMX-104 particle in Camp Swift soil: NTO, 3-nitro-1, 2, 4-triazol-5-one; RDX, hexahydro-1,3,5-trinitro-1,3,5-triazine; HMX, octahydro-1,3,5,7-tetranitro-1,3,5,7-tetrazocine; DNAN, 2, 4-dinitroanisole; 2-ANAN, 2-amino-4-nitroanisole; and 4-ANAN, 4-amino-2-nitroanisole. The vertical gray solid line indicates a switch to the background solution.	75
36.	Flow interruption breakthrough curves for individual explosives for detonated IMX-104 particle in Camp Swift soil: NTO, 3-nitro-1, 2, 4-triazol-5-one; RDX, hexahydro-1,3,5-trinitro-1,3,5-triazine; HMX, octahydro-1,3,5,7-tetranitro-1,3,5,7-tetrazocine; DNAN, 2, 4-dinitroanisole; 2-ANAN, 2-amino-4-nitroanisole; and 4-ANAN, 4-amino-2-nitroanisole. The vertical dashed gray line indicates the start of 24 hr flow interruption. The vertical solid gray line indicates a switch to the background solution.	76
37.	Correlations between simulated Ymax and Ymin of individual propellants in IMX-104 formulation from continuous flow experiments: NTO, 3-nitro-1, 2, 4-triazol-5-one; RDX, hexahydro-1,3,5-trinitro-1,3,5-triazine; HMX, octahydro-1,3,5,7-tetranitro-1,3,5,7-tetrazocine; and DNAN, 2, 4-dinitroanisole.	81
38.	The pH of samples collected during analysis for IMX-104 flow interruption experiments. The vertical dashed gray line indicates the start of 24 hr flow interruption. The vertical solid gray line indicates a switch to saturated solution.	83
39.	Breakthrough curves of NTO, DNAN, and 2-ANAN in Camp Guernsey soil at a 20 cm depth with 1 year of rainfall (a and b). Plot of flow rate vs. time (c). Zero flow rate indicates periods of no flow.	91
40.	Forward simulations of NTO, NQ, DNAN, and 2-ANAN in Camp Guernsey soil with rainfall over 1 year, 10 years, and 25 years. Note that the depth profiles for NTO, DNAN, and 2-ANAN for the three time periods overlap.	93
41.	Forward simulations of NTO, NQ, DNAN, and 2-ANAN in Camp Swift soil	

	with rainfall over 1 year, 10 years, and 25 years. Note that the depth profiles for NTO, DNAN, and 2-ANAN for the three time periods overlap.....	94
42.	Forward simulations of NTO, NQ, DNAN, and 2-ANAN in Plymouth soil with rainfall over 1 year, 10 years, and 25 years. Note that the depth profiles for NTO, DNAN, and 2-ANAN for the three time periods overlap.	95
43.	Forward simulations of NTO, RDX, HMX, DNAN, and 2-ANAN in Camp Guernsey soil with rainfall over 1 year, 10 years, and 25 years. The depth profiles for NTO, DNAN, and 2-ANAN for the three time periods overlap.....	97

Tables

1.	Environmentally relevant chemical and physical properties of DNAN, NTO, NQ, and RDX, including solubility at 25 °C, octanol-water partition coefficient (Kow), and soil organic carbon adsorption coefficient (KOC).....	4
2.	Parameters measured or calculated (life spans) for the 12 pieces of IM explosives set outdoors to weather and dissolve.....	16
3.	List showing the initial mass (Mi) of the outdoor samples and the percentage not recovered. The recovered mass is the final mass (Mf) of the particle added to the mass analyzed from the effluent via HPLC. Data are given for both IM and high explosives formulations.	18
4.	Retention times and peak absorbance wavelengths for standard, identified, and unknown (blue) compounds. We found that the HPLC retention times shifted depending on what other compounds were present in the sample. Here we listed the times for the pure standards, when available.	26
5.	Results from the GC-MS (X), NovaPak C8 (NP; ✓), and Hypercarb (HC; ◇) HPLC columns for samples analyzed. (MW = molecular weight.).....	27
6.	Temperature and rainfall conditions in Hanover, NH, where the original dissolution experiments were conducted, and Oracle, AZ, location of the current study.	38
7.	Removal of munitions constituents in solution as percent of original mass in the particle.	47
8.	Removal of IM constituents in solution, percent of original present in the particle, after 390 days of exposure to sunlight and rainfall outdoors.	52
9.	Measured physical and chemical properties of soils used in dissolution and transport studies with IMX-101 and IMX-104 (Mark et al. 2016).	59
10.	The Ymax, χ , and Ymin estimates obtained from Taylor et al. 2015b for IMX-101 and IMX-104.	66
11.	Dissolution and transport parameters obtained by HYDRUS-1D for saturated column experiments involving Br ⁻ tracer and IMX-101 (19.7% NTO, 36.8% NQ, and 43.5% DNAN) in Camp Swift and Camp Guernsey soils. λ was estimated from Br ⁻ breakthrough, whereas Kd; χ ; Ymax; Ymin; and mass-loss rate coefficient, k, were estimated from explosives breakthrough curves. FI = flow interruption for 24 hr, D = detonated, UD = undetonated, and NA= not applicable and Kd fixed to zero.	70
12.	Solute transport and dissolution parameters obtained by HYDRUS-1D for column-saturated experiments involving Br ⁻ and IMX-104 (53.0% NTO, 15.3% RDX, and 31.7% DNAN) in Camp Swift and Camp Guernsey soils. λ was estimated from Br ⁻ BTCs, whereas Kd; Ymax; Ymin; and mass-loss	

	rate coefficient, k, were estimated from explosives. D = detonated, UD = undetonated, and NA = not applicable and Kd fixed to zero.	77
13.	Mass recoveries of IMX-101 and IMX-104 constituents in effluent and soil and extractions of remaining IM particles during dissolution column transport studies. FI = flow interruption for 24 hr, D = detonated, UD = undetonated, and na = data not available.....	86
14.	Dissolution and transport parameters used for forward simulation of energetic compounds in IMX-101: 3-nitro-1,2,4-triazol-5-one (NTO); nitroguanidine (NQ); 2,4-dinitroanisole (DNAN); and DNAN product, 2-amino-4-nitroanisole (2-ANAN).....	90
15.	Dissolution and transport parameters used for forward simulation of IMX-104 compounds: 3-nitro-1,2,4-triazol-5-one (NTO); 2,4-dinitroanisole (DNAN); hexahydro-1,3,5-trinitro-1,3,5-triazine (RDX); octahydro-1,3,5,7-tetranitro-1,3,5,7-tetrazocine (HMX); and DNAN product, 2-amino-4-nitroanisole (2-ANAN).....	90

Preface

This study was conducted for the Strategic Environmental Research and Development Program (SERDP) under ER-2220, “Dissolution of NTO, DNAN, and Insensitive Munitions Formulations and Their Fates in Soils.” The program manager was Dr. Andrea Leeson, SERDP.

The work was performed by the Biogeochemical Sciences Branch of the Research and Engineering Division, US Army Engineer Research and Development Center, Cold Regions Research and Engineering Laboratory (ERDC-CRREL). At the time of publication, Mr. Nathan Lamie was branch chief, and Dr. Caitlin A. Callaghan was division chief. The acting deputy director of ERDC-CRREL was Mr. Bryan E. Baker, and the director was Dr. Joseph L. Corriveau.

SERDP funded this work under its environmental restoration program, and we thank our program manager, Dr. Andrea Leeson, for her support. The ERDC 6.1 Basic Research program funded a portion of the DNAN (2,4-dinitroanisole) photo transformation work. We thank Mr. Anthony Di Stasio and Ms. Erika Rivera, US Army Armament Research, Development, and Engineering Center (ARDEC), Picatinny Arsenal, for providing IMX-101 and IMX-104. Finally, we thank Dr. Bonnie M. Packer, Ms. Rosa Gwinn, Ms. Lisa DeGrazia, Ms. Bethany Keller, Ms. Jessica Milose, Ms. Amibeth Sheridan, Ms. Laurie Stenberg, and Ms. Sarah Gettier (all from the Army National Guard–Environmental Directorate) and URS Corporation, Germantown, Maryland, for collecting the soils from Army National Guard installations used in these experiments.

COL Christian Patterson was commander of ERDC, and Dr. David W. Pittman was the director.

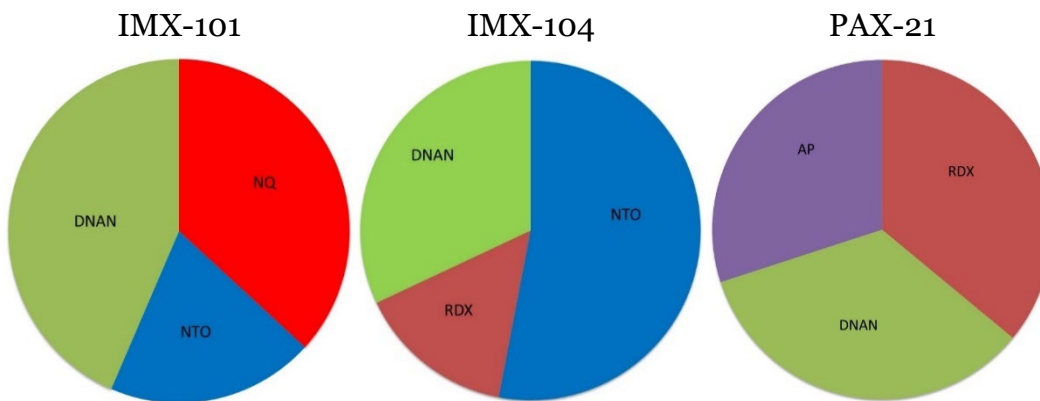
1 Introduction

By Jenifer D. Arthur¹

1.1 Background

The US military is using new explosive compounds, insensitive munitions (IM), that are less sensitive to shock and high temperatures as replacements for TNT (2,4,6-trinitrotoluene) and RDX (1,3,5-hexahydro-1,3,5-trinitro-1,3,5-triazine). Two of these explosives, DNAN (2,4-dinitroanisole) and NTO (3-nitro-1,2,4-triazol-5-one), were shown to have good detonation characteristics and are less likely to detonate unintentionally. Several new explosive formulations use them as the main ingredients: IMX-101, composed of 19.7% NTO, 36.8% nitroguanidine (NQ), and 43.5% DNAN; IMX-104 (53.0% NTO, 15.3% RDX, and 31.7% DNAN); and PAX-21 (30% ammonium perchlorate [AP], 34% DNAN, and 36% RDX) (Figure 1).² NTO, NQ, RDX, and AP are used as explosive fill whereas DNAN is used as a binder in these melt-cast explosive formulations.

Figure 1. Composition of IM formulations IMX-101, IMX-104, and PAX-21 (modified from Taylor et al. 2013).



When munitions do not completely detonate, a low-order detonation, a significant mass of the explosive compounds originally present in a round can become deposited on the ground. Training ranges are a particular concern due to the great number of rounds fired in the same location,

¹ This material is a part of the dissertation defended by Jenifer Arthur as one of the requirements for her PhD degree.

² IMX stands for Insensitive Munitions Explosive, and PAX stands for Picatinny Arsenal Explosive.

resulting, in some cases, in contamination of the groundwater with munition constituents (Jenkins et al. 2001). The likelihood of IM rounds having incomplete detonation is higher than that for traditional explosives (Walsh et al. 2013), resulting in more munition constituents on the ground. When explosives are exposed to rainfall, they gradually dissolve; and laboratory and outdoor studies have demonstrated that NTO and DNAN readily dissolve from IM formulations (Taylor et al. 2013, 2015a, 2015b). Transport of residues off military ranges by wind or water can limit training or result in closure of the ranges.

Exposure to explosive compounds has adverse health effects. The toxicity of the chemical compounds in IMX-101 and IMX-104 is used to quantify the threat to the environment and human health. Health and environmental effects associated with exposure to explosive compounds vary by the explosive. Toxicological reports of NTO showed that it is not toxic to rats and mice when given orally ($LD_{50}^3 > 5 \text{ g kg}^{-1}$);⁴ however, skin application studies with rabbits showed it to be mildly irritating (London and Smith 1985). Microbial degradation studies of NTO in soils show nitroreduction followed by the cleavage of the primary amine, 5-amino-1,2,4-triazol-3-one (ATO) (Le Campion et al. 1999b). Metabolic intermediates produced during the process of nitroreduction of nitro-compounds displayed cytotoxicity and neurotoxicity (Koch et al. 1979; Walton and Workman 1987; Le Campion et al. 1999b).

The oral LD_{50} for NQ is 3.9 g kg^{-1} in mice and 10.2 g kg^{-1} in rats. Direct contact with NQ may cause irritation to the eyes and burning of the skin. Exposure to sublethal doses of NQ in rodents has caused gastrointestinal, respiratory, and central nervous system effects. Chronic exposure may result in slight hematological and liver function changes (Deeter 2000). NQ also has low acute and chronic toxicity to a range of aquatic organisms; however, products of NQ photolysis are 100-fold more toxic (Burton et al. 1993; Sunahara 2009).

Information on the health effects of HMX (high explosive 1,3,5,7-octahydro-1,3,5,7-tetranitrotetrazocine, an impurity in RDX) is limited. It does have low toxicity to aquatic organisms. No deaths of humans and animals

³ Lethal dose (LD_{50}) is the amount of an ingested substance that kills 50 percent of a test sample.

⁴ For a full list of the spelled-out forms of the units of measure used in this document, please refer to *US Government Publishing Office Style Manual*, 31st ed. (Washington, DC: US Government Publishing Office, 2016), 248–252, <https://www.govinfo.gov/content/pkg/GPO-STYLEMANUAL-2016/pdf/GPO-STYLEMANUAL-2016.pdf>.

have resulted from inhalation exposure (Sunahara 2009; Pichtel 2012). RDX's reported LD₅₀ in literature ranges from 44 to 300 mg kg⁻¹ in rats. The major toxic effects of RDX include anemia with secondary splenic lesions, hepatotoxicity, possible central nervous system involvement, and urogenital lesions. In humans and animals, RDX is slowly absorbed from inhalation and from the stomach after ingestion. Chronic exposure via inhalation of fine particles causes epileptiform seizures and unconsciousness. RDX is poorly adsorbed through the skin (Etnier 1986; Deeter 2000).

Toxicological reports for DNAN indicate that it is toxic to bacteria *Vibrio fischeri* and freshwater green algae *Pseudokirchneriella subcapitata* in the milligrams per liter range and to earthworm *Eisenia andrei* and perennial ryegrass *Lolium perenne* in the milligrams per kilogram range (Dodard et al. 2013). It can be metabolized in the body to 2,4-dinitrophenol, which is a chemical with a high acute and chronic toxicity. DNAN is a skin and eye irritant (Davies and Provatas 2006); but the behavior of its amino derivatives, 2-ANAN and 4-ANAN, has not been established: studies have shown 2-ANAN and 4-ANAN to have both lower (Liang et al. 2013) and higher (Olivares et al. 2016) microbial toxicity than DNAN.

The two major processes that influence potential transport of explosive compounds off-site once they dissolved from IM particles are adsorption and transformation in soils. Knowing the physical and chemical properties of the explosive compounds can aid in analyzing the environmental fate and transport (Table 1). High aqueous solubility of NTO and NQ indicates that both compounds will readily dissolve in water, while lower solubilities of DNAN and RDX indicate that their dissolution would be slower.

Taylor et al. (2013, 2015a, 2015b) conducted a series of experiments evaluating dissolution of IM compositions. Laboratory drip tests under controlled conditions mimicking those found on military training ranges indicated that IMX formulations dissolution is controlled by the aqueous solubility of the explosive compounds, with NTO dissolving first followed by NQ and DNAN in IMX-101 and by RDX and DNAN in IMX-104 (Taylor et al. 2013, 2015b). Dissolution of most soluble components removed them from the outer layers of the particle and created a porous structure (Taylor et al. 2013). Taylor et al. (2015a) also observed these patterns in outdoor dissolution studies and additionally observed phototransformation of IM compounds. While dissolution of NTO and NQ was high initially and then

decreased over time as these compounds were removed from the outer shell of IM particles, DNAN dissolution tended to be more constant over time.

Table 1. Environmentally relevant chemical and physical properties of DNAN, NTO, NQ, and RDX, including solubility at 25 °C, octanol-water partition coefficient (K_{ow}), and soil organic carbon adsorption coefficient (K_{oc}).

Property	DNAN	NTO	NQ	RDX	HMX
Solubility, mg L ⁻¹	276.2 ^{a1}	16642.0 ^{c2}	2600 to 5000 ^{b3}	59.9 ^{a4}	5 ⁵
Log K_{ow}	1.7 to 1.92 ^b , 1.62 ^{a6} , 1.58 ⁷	0.37 to 1.03 ^{b6}	-0.83 ^{b8}	0.81 to 0.87 ^{b3}	0.19 ^{a9}
Log K_{oc}	3.11 ^{a10} , 2.2 ^{b11}	3.03 ^{a10} , 2.1 ^{b11}	0.356 ^{b12} , 1.41 ^{b13}	0.88 to 2.4 ^{b4}	0.54 to 2.8 ^{a14}

^a Measured

7 Hawari et al. (2015)

^b Estimated

8 Dave et al. (2000)

^c Interpolated from measured values

9 Yoon et al. (2002)

1 Boddu et al. (2008)

10 Rose Pesce-Rodriguez, Army Research Laboratory (unpublished)

2 Spear et al. (1989)

11 Chen (1977)

3 Mirecki et al. (2006)

12 Burrows et al. (1989)

4 Brannon and Pennington (2002)

13 Ruge et al. (1998)

5 Glover and Hoffsommer (1973)

14 Boyer et al. (2007)

6 Sokkalingam et al. (2008)

Sorption coefficients, such as the soil adsorption coefficient (K_d), the soil organic carbon adsorption coefficient (K_{oc}), and the octanol-water partition coefficient (K_{ow}), are available for NQ, RDX, and HMX; but less information is published for NTO and DNAN.

NQ and NTO are both very mobile and have low K_d , K_{oc} , and K_{ow} values (Mirecki et al. 2006; Mark et al. 2016) (Mirecki et al. 2006; Mark et al. 2016). Mark et al. (2016) examined NTO interactions with a number of soils and concluded that adsorption was low and not related to the amount of organic carbon in the soil. It was, however, strongly influenced by the soil's pH due to the ionic character of the NTO molecule. NQ is not adsorbed or transformed in soils (Dontsova et al. 2007, 2008; Taylor et al. 2012), which is consistent with its low K_{ow} values (Burrows et al. 1989; Dave et al. 2000).

Hawari et al. (2015) reported log K_{ow} values for DNAN and its transformation products. DNAN has a higher K_{ow} value, indicating that it would be less mobile than NQ, NTO, and RDX in soil. Arthur et al. (2017) conducted batch and column soil adsorption experiments to determine the fate and transport parameters for DNAN in soil. They observed that DNAN

strongly adsorbed to soils with linear adsorption coefficients ranging between 0.6 and 6.3 L kg⁻¹ and Freundlich coefficients between 1.3 and 34 mg¹⁻ⁿ Lⁿ kg⁻¹. Both linear and Freundlich adsorption coefficients positively correlated with cation exchange capacity and the amount of organic carbon in the soil. The column studies confirmed the impact of sorption on retardation of DNAN during transport. DNAN also readily transformed to its amino transformation products, 2-ANAN and 4-ANAN.

For comparison, RDX has higher K_{ow} and K_{OC} values than NTO and NQ but lower values than DNAN. RDX's low K_d , K_{OC} , and K_{ow} values indicate that it will be mobile (Haderlein et al. 1996; Singh et al. 1998).

Richard and Weidhaas (2014) conducted dissolution and sorption experiments with IMX-101 and then examined leaching of IM compounds in effluent produced as a result of simulated rainfall. They found that IMX-101 particles dissolved slowly under simulated rainfall conditions with NQ and NTO dissolving first, leaving DNAN crystals. The results of the sorption experiments showed that DNAN and NTO sorption to soils fit the Freundlich isotherm best and that desorption was limited.

1.2 Objective

The objective of this project was to measure the dissolution, photodegradation, and soil adsorption properties of DNAN, NTO, and insensitive munitions (IM) formulations that contain them: IMX-101, IMX-104, and PAX-21 (Figure 1). This information, coupled with the mass of IM formulations scattered on a range, will allow us and others to estimate and model the dissolved IM mass loads, their subsequent transport and fate, and their likelihood of reaching groundwater.

1.3 Approach

We measured the dissolution of IM particles under simulated rainfall in the lab and natural rainfall and sunshine outside at two locations, one in New Hampshire and one in Arizona. Solution concentrations of NTO, NQ, DNAN, RDX, HMX, and AP were also measured to calculate the amount of IM constituents dissolved into solution. The photodegradation of DNAN and NTO in solid (outdoors) and aqueous (in the lab) form was measured to determine if these compounds degrade in sunlight either before or after dissolution.

Transport of products of dissolution of IM particles was studied in several soils collected on training facilities to determine how DNAN and NTO interact with the soils. Lastly, the measured dissolution and transport parameters were used in HYDRUS-1D, a software package for simulating water, heat, and solute movement in one-dimensional variably saturated media, to predict the environmental fate of IM explosives for several locations.

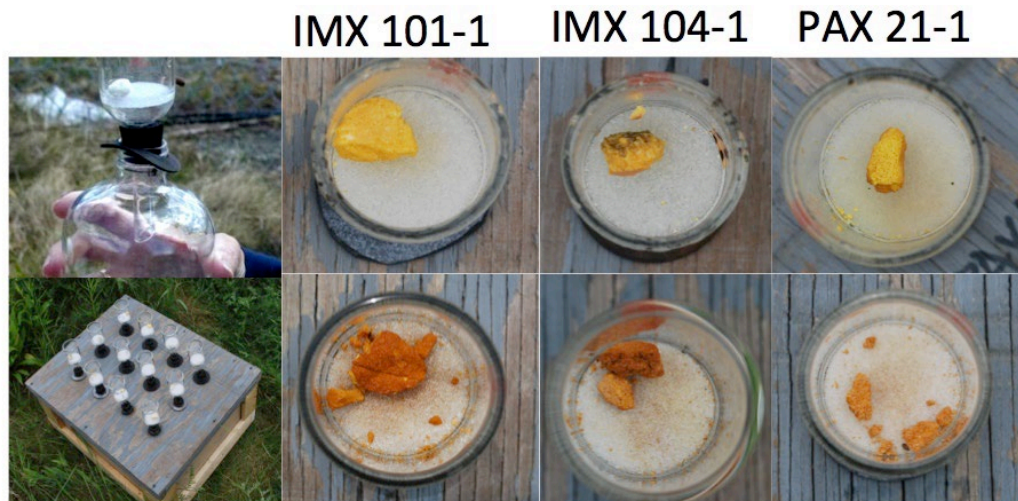
2 Outdoor Dissolution and Photodegradation Tests of IM Formulations

By Susan Taylor, Julie B. Becher, Marianne E. Walsh, and Dave B. Ringelberg

2.1 Introduction

To measure the outdoor dissolution of IM formulations, we placed 5 chunks of IMX-101, 5 chunks of IMX-104, and 2 chunks of PAX-21 on glass frits in dedicated 4 cm diameter Buchner funnels (Figure 2). The funnels were attached to 1 L bottles, which fit snugly into an insulated wooden box to both insulate and keep the bottles upright. Rainwater or snowmelt that interacted with the chunks collected in the bottles. About every month, except during the winter when the experiment was snow covered, we exchanged the bottles for clean ones and measured the volume and explosive concentrations in the water samples. Each time we collected samples, we also photographed the pieces of IM in situ to document changes in their appearance and size (Figure 2.). Our experiment was set up in an area enclosed with a locked chain link fence and next to a dedicated rain gauge and are similar to experiments conducted for high explosives (Taylor et al. 2009, 2010).

Figure 2. Appearance of a piece of IMX-101, IMX-104, and PAX-21 set outdoors to weather and dissolve. The top row shows particles at 17 days, and the bottom row shows the same particles at 363 days.



Our tests allowed us to collect and analyze the dissolved constituents and monitor changes in the appearance of the chunks while at the same time exposing the IM formulations to conditions similar to those experienced on a range—where rain, snow, sun, and freeze–thaw cycles weather the IM. These experiments were conducted in Hanover, New Hampshire, where the yearly temperature varies between -12°C and 28°C . These tests ran between June 2013 and October 2015 during which time we collected 19 sets of water samples for each IM chunk. The average volume of precipitation interacting with these chunks was 3.7 ± 0.27 L.

2.2 Methods

We analyzed by high-precision liquid chromatography (HPLC) all solutions from the outdoor tests and, using an ion selective probe, analyzed solutions from PAX-21 particles for perchlorate. Two different columns, NovaPak C8 and Hypercarb, and stationary phases were used for chromatographic separation of the IM components and transformation products.

2.2.1 High-performance chromatography

Using the NovaPak C8 column, determinations of DNAN were made on a modular system from Thermo Scientific composed of a Spectra-System Model P4000 pump, a Spectra-System UV2000 dual wavelength UV–vis (ultraviolet to visible) absorbance detector (cell path 1 cm), set at 295 nm for DNAN, and a SpectraSYSTEM AS3000 autosampler. Samples were introduced with a 100 μL sample loop. Additional determinations were made for select samples on an Agilent 1200 Series HPLC equipped with a Diode Array Detector (Model G1315B). The spectrum range was 200 to 800 nm. Separations were achieved on a 15 cm \times 3.9 mm (4 μm) NovaPak C8 column (Waters Chromatography Division, Milford, Massachusetts) at 28°C and eluted with 1.4 mL min^{-1} of 15/85 (v/v)⁵ isopropanol/water. All samples were introduced to the HPLC in a matrix of 1/3 v/v acetonitrile/water. This matrix provides excellent chromatographic peak shapes. Calibration standards, which were acetonitrile solutions, were prepared by mixing 1.00 mL of each standard with 3.00 mL Type I reagent grade water (MilliQ). To maintain the same proportions volumetrically as the calibration standards, aqueous solutions were prepared by mixing 1.00 mL of each sample with 2.00 mL of MilliQ water and 1.00 mL acetonitrile. Each

⁵ Volume/volume

sample was filtered prior to injection using a Polytetrafluoroethylene (PTFE) (0.45 μm) 25 mm filter unit (Millipore Millex-FH).

Using the Hypercarb column (100% porous graphitic carbon), NTO, NQ, and DNAN were determined following the Standard Operating Procedure DLS810 obtained from M. Hable⁶, which was based on the methods of Le Campion et al. (1997). Samples were injected using a matrix of 3/1 acetonitrile/water. Determinations were made using the same modular systems as above except that the column was a 15 cm \times 4.6 mm (5 μm) Hypercarb (Thermo Scientific) eluted with 1.5 mL min^{-1} of 3/1 acetonitrile/water with 0.1% trifluoroacetic acid (Fisher HB9813-4) at 28°C. The ultraviolet (UV) detector was set at 315 nm for NTO, 263 nm for NQ, and 295 for DNAN. Additional determinations of select samples were made on an Agilent 1200 Series HPLC equipped with a Diode Array Detector (Model G4212B). The spectrum range was 200 to 600 nm. For the chromatographic separation on the Hypercarb we used 3/1 acetonitrile/water stationary phase. To maintain the same volumetric proportions, 1.00 mL of each calibration standard was mixed with 2.00 mL of acetonitrile and 1.00 mL MilliQ water. Solutions were filtered as for the NovaPak C8 separation.

2.2.2 Gas chromatography–mass spectrometry (GC-MS)

Mass spectra were obtained using an Agilent 5973 Mass Selective Detector. The ionization voltage was 70 eV. The Mass Selective Detector was operated in scan mode ($m/z^7 = 29$ to 400) and in selective ion monitoring (SIM) for masses 169, 182, and 30. The gas chromatography column was a Restek-RTx-5MS (Crossbond 5% diphenyl/95% dimethyl polysiloxane) (15 m \times 0.25 mm, 1.00 μm film thickness). The carrier gas was helium at constant flow (1.4 mL min^{-1}) with a linear velocity of 62 cm/s. The oven temperature was 75°C for 2 min, then ramped at 20°C per minute to 220°C and held for 10 min. The injection port temperature was 200°C; splitless 1 μL injections with a deactivated liner were used.

Standards of known compounds and matrix samples were introduced to the gas chromatography as solutions in acetonitrile that were filtered through PTFE (0.45 μm) filter units (Millipore Millex-FH) into 2 mL amber autosampler vials just prior to injection. Analytes from the aqueous

⁶ M. Hable, US Army Public Health Command, unpublished analysis of the components of IMX-101 by liquid chromatography and gas chromatography, 2013.

⁷ mass / atomic number

samples from the outdoor dissolution experiments were transferred to acetonitrile using two procedures. The first procedure was solid phase extraction where each PoraPak RDX Sep-Pak Vac (Waters) cartridge was preconditioned with acetonitrile and reagent-grade water according to the manufacturer's instructions. Then 5.00 mL of each aqueous sample was passed through using gravity flow. Each cartridge was placed under a vacuum for 1 hr to remove residual water, then eluted with 5.00 mL acetonitrile, of which approximately 4.5 mL were recovered. The second procedure involved evaporating aqueous samples, followed by dissolution of the dried residue in acetonitrile and filtration through a PTFE (0.45 μm) 25 mm filter unit (Millipore Millex-FH).

2.2.3 Other analytical methods

An ion-selective electrode (Cole Parmer) was used to quantify the AP. To generate a standard line from which we could determine the AP concentration of the samples, we prepared and analyzed a series of concentrations from a perchlorate standard. Using a Mettler Toledo SevenEasy meter and a pH probe, we measured the pH of the water samples; and we completed a three-point calibration by using pH 4, 7, and 10 solutions.

Micro computed tomography (μCT) images were taken using a SkyScan 1172 X-ray micro tomograph, run at a 40 kV with a 250 μA source current. Radiographs (X-ray images) were taken of one chunk of each formulation before being set outside and again near the end of the tests. The images were taken with a 1.3 Megapixel X-ray camera and the cross sections reconstructed using a modified Feldkamp cone-beam algorithm. For more information on how IM particles were imaged, see Taylor et al. (2015b).

UV-vis spectra were acquired of the outdoor samples using a Jasco V-630 spectrophotometer and quartz cuvettes that are UV transparent to 200 nm (YeHui Instruments). UV-vis spectra for the samples were obtained in the wavelength range of 200–800 nm. The data interval was set to 1 nm, the UV-vis bandwidth was set to 1.5 nm, the response was set to fast, and the scan speed was set to 200 nm min^{-1} . The D2/WI (deuterium/tungsten) light source changed at 340 nm with a continuous filter exchange. A Spectra Measurement program on the instrument was used to collect each sample's UV-vis spectrum. Before analyzing samples, we ran the quartz cuvette filled with deionized water as a background, which was used to remove the water signal from the aqueous samples. Between each sample,

the cuvette was rinsed with deionized water three times and then dried with a lint-free cloth.

2.3 Results

2.3.1 Appearance of explosive pieces

The three formulations were initially white (IMX-101), cream colored (IMX-104), and yellow (PAX-21); but their surfaces turned light orange after two weeks (Figure 2) and orange to brick red after a year of exposure to sunlight (Figure 3). Microscopic examination of the surfaces of particles exposed to light in a windowsill showed that, of the IM constituents, only DNAN changed color. Phototransformation of the other constituents may also be occurring but to colorless products.

During the 16-month dissolution test, all of the IM chunks split and all shed millimeter-sized particles (Figure 3), a faster splitting rate than observed for TNT, Comp B (60-40 RXD-TNT mix), and Tritonal (TNT + aluminum) (Figure 4) as each had only three of 29 chunks split during a three-year test (Taylor et al. 2010). The friability of the IM formulations may be due to the large (~300 μm) crystals they contain, to the voids left when the crystals dissolve, or to fractures produced during detonation (Figure 5a) (Taylor et al. 2013). Note that the fractures predominantly follow the crystal boundaries and, in some cases, surround the crystal. We think these fractures debond crystals from the matrix (Taylor et al. 2013) and explain why AP, NTO, and NQ are found after “high order” detonations when all of the DNAN is consumed (Walsh et al. 2013, 2014); the debonded crystals are scattered instead of being detonated. The μCT images of one particle each of IMX-101#2, IMX-104#4, and PAX-21#2 taken before, part way through, and at the end of the outdoor tests (Figure 5b, c, d) show that IMX-101 has lost crystals in its interior and periphery but less so than IMX-104 where all the NTO crystals have dissolved. The ammonium perchlorate in PAX-21 dissolved in the first rainfall, leaving voids throughout.

Figure 3. IMX-101#1 set outside to weather and dissolve. The images show how the surface of the piece changed over the 864 days of the experiment.

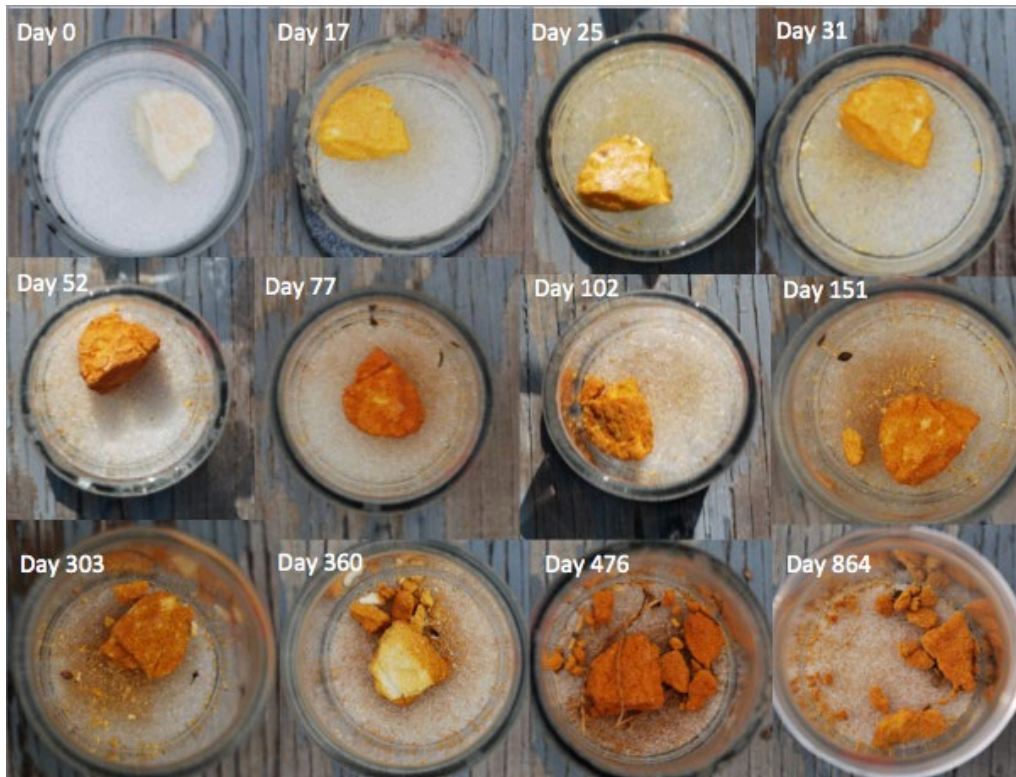


Figure 4. We found that IM formulations are very friable compared to traditional explosives.

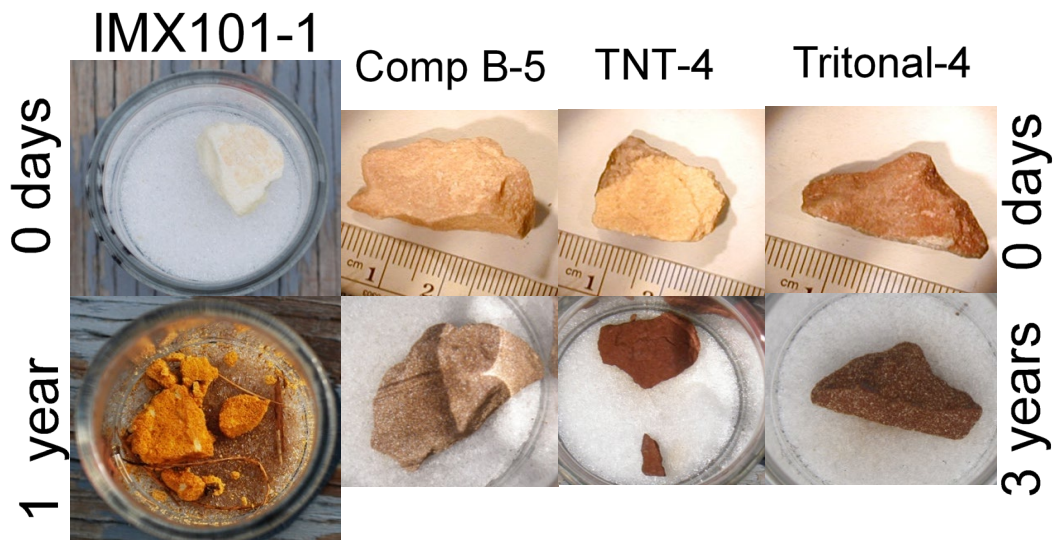
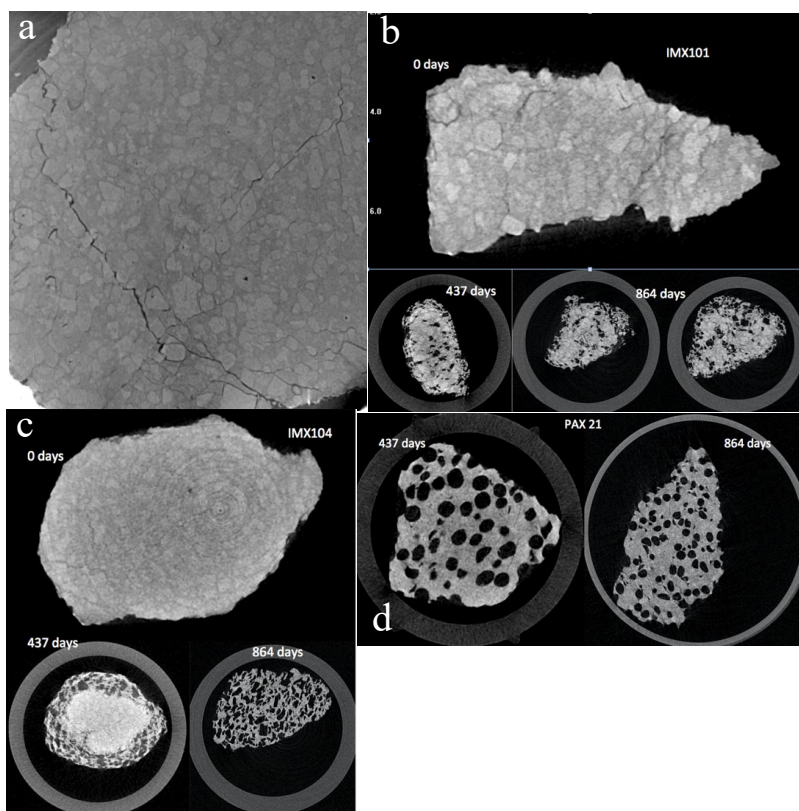


Figure 5. The μ CT cross sections of (a) a detonated piece of IMX-101#1; (b) a detonated piece of IMX-101#2 at 0, 437, and 864 days of outdoor dissolution; (c) a piece of IMX-104#4; and (d) a piece of PAX-21#2. All of these pieces split during the test, so the images taken at day 437 and 864 are the largest fragments of the original piece.



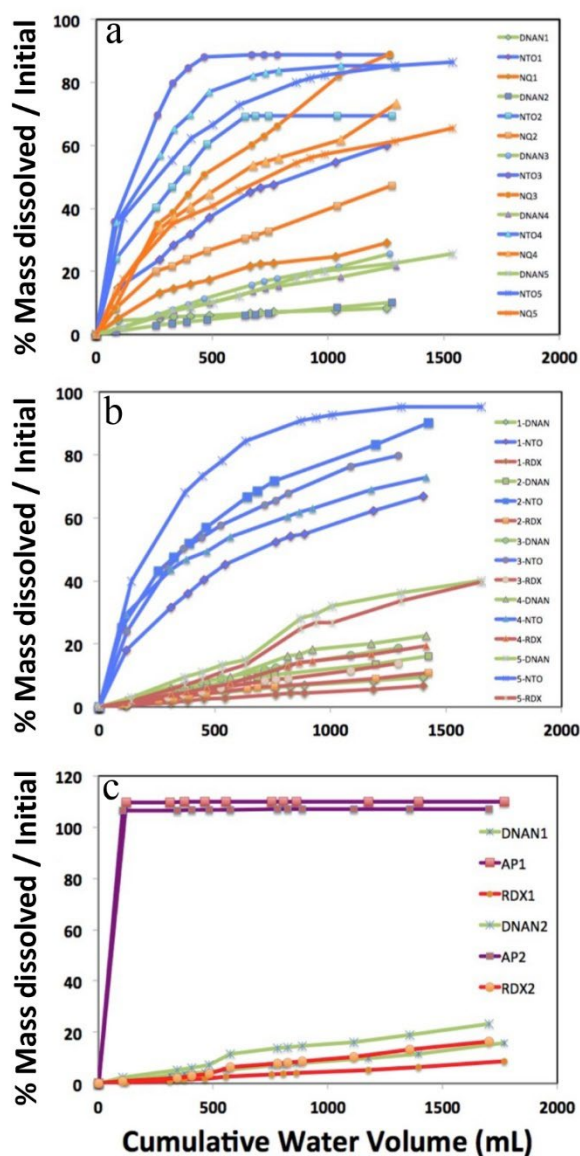
2.3.2 Dissolution of explosive pieces

Figure 6 shows the percent cumulative mass dissolved for each constituent in the IM formulation plotted against the cumulative volume of water collected. We calculated the percent cumulative mass by dividing the mass of each constituent measured in the water samples by the putative starting mass of each constituent. The latter value was obtained by multiplying the initial mass of the chunk by the fraction of each constituent in the formulation. The plots help to highlight compositional variations among the pieces.

Figure 6a plots the mass loss data for the five IMX-101 pieces. We see that NTO dissolves first, followed by NQ and finally DNAN. The dissolution rates of NTO and NQ are higher at the start of the test and decrease during the test. The shape of the NTO mass loss with water volume is more clearly seen for IMX-104, which contains no NQ (Figure 6b). In Figure 6c, we see

that the AP in PAX-21 dissolved in the first water sample, leaving DNAN and RDX as the only constituents. As found in laboratory experiments (Taylor et al. 2013; Richard and Weidhaas 2014), the constituents of the formulations dissolve in the order of their solubility. None of these pieces had completely dissolved after 16 months.

Figure 6. Dissolved mass vs. precipitation volume for five IMX-101 (a), five IMX-104 (b), and two PAX-21 (c) chunks placed outside: NTO (blue), NQ (orange), DNAN (green), RDX (red), AP (purple).



Any increases or decreases in the temperature of rain or surface water, due to changes in the ambient temperature, will affect the dissolution rate of the individual compounds and of the formulations. For example, the

solubility of DNAN and NQ doubles between 20°C and 40°C and almost doubles for NTO (Appendix A).

Unlike high explosives, IM formulations dissolve throughout their volumes due to their soluble crystal constituents. We cannot, therefore, use dissolution models that assume dissolution from the surface (Lever et al. 2005) to calculate particle life times. For all three formulations, however, the mass loss of DNAN (and RDX) is fairly linear when plotted against water volume (Figure 7). The best linear fits to the DNAN data have slopes ranging from 0.0114 to 0.0572 and coefficient of determination (R^2) between 0.94 and 0.99 (Table 2). As DNAN is a main constituent in the matrix, its quasi-linear dissolution allows us to estimate chunk life times. Using the rate of DNAN mass loss vs. water volume, the area of the funnel opening and the average yearly precipitation for Hanover, New Hampshire (~ 100 cm yr⁻¹, US Climate Data 2018), we estimate that 3 to 21 years are needed to completely dissolve these chunks. Using the average water volume measured (1.7 L yr⁻¹), the time to dissolution would be 3 to 16 years (Table 2).

Figure 7. Dissolved DNAN plotted against water volume for outdoor samples of IMX-101, IMX-104, and PAX-21.

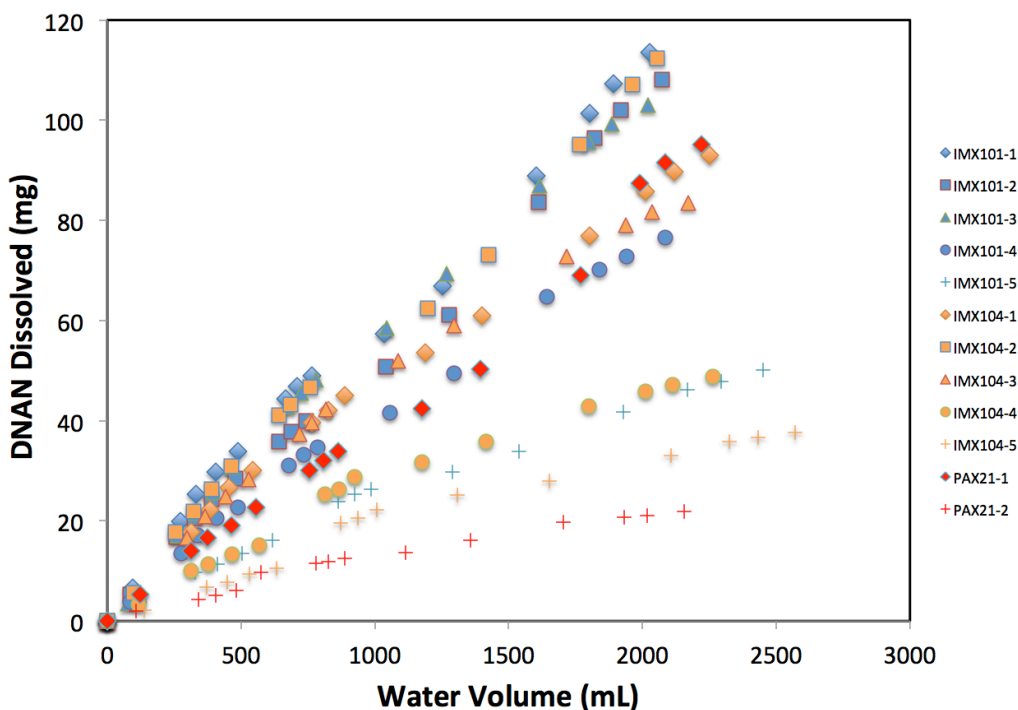
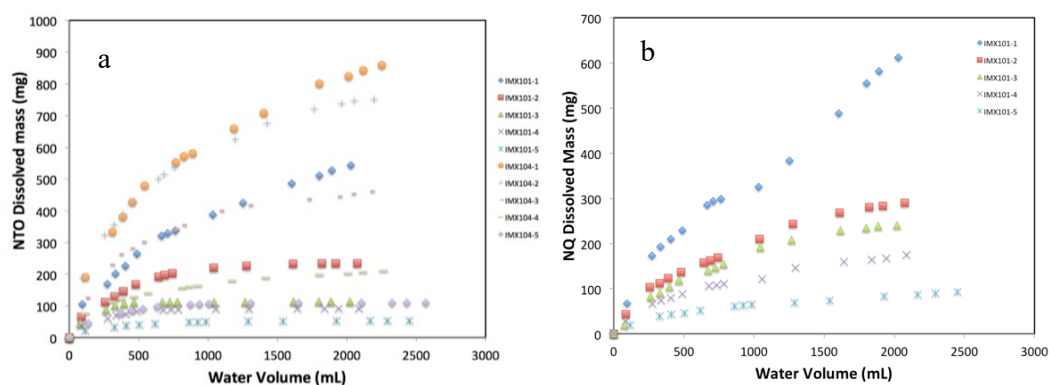


Table 2. Parameters measured or calculated (life spans) for the 12 pieces of IM explosives set outdoors to weather and dissolve.

Sample	Sample Number	Initial Mass (mg)	Cumulative Dissolved Explosive (mg)	% Mass Loss	Cumulative Water Vol. (mL)	Max. # Pieces	Explosive Initial DNAN (mg)	Slope Line DNAN	R ²	Liters to Dissolve Chunk	Life Span of Chunk at 1.3 L yr ⁻¹	Life Span of Chunk at 1.7 L yr ⁻¹
IMX-101	#1	3551.53	1270.37	35.8	2027	11	1527	0.0572	0.98	27	21	16
	#2	1390.93	633.84	45.6	2075	11	598	0.0523	0.99	11	9	7
	#3	631.51	458.84	72.7	2021	9	272	0.0541	0.99	5	4	3
	#4	532.36	344.29	64.7	2086	12	229	0.0388	0.98	6	5	3
	#5	306.00	198.43	64.8	2452	1	132	0.022	0.97	6	5	4
IMX-104	#1	1996.85	986.56	49.4	2252	8	639	0.0437	0.98	15	11	9
	#2	1418.93	908.07	64.0	2196	10	454	0.055	0.99	8	6	5
	#3	988.69	579.09	58.6	2170	8	316	0.0425	0.96	7	6	4
	#4	491.44	281.35	57.3	2264	1	157	0.024	0.95	7	5	4
	#5	217.19	165.30	76.1	2569	3	70	0.0162	0.94	4	3	3
PAX-21	#1	1279.67	576.47	45.0	2219	10	435	0.0414	0.99	11	8	6
	#2	248.70	118.57	47.7	2156	3	85	0.0114	0.94	7	6	4

Quasi-linear dissolution does not occur for the NTO or NQ (Figure 8), for most millimeter-sized particles of these formulations (Taylor et al. 2015a), or for Comp B and TNT (Lever et al. 2005; Taylor et al. 2009). In all these cases, the explosive pieces lose more mass initially when soluble constituents are at or near the surface of the chunk, and then mass loss decreases as constituents are depleted or as water has a harder time contacting the constituents. For DNAN, its low solubility coupled with increases in its surface area explain the linear mass loss. When the IM chunks split, the numerous fragments that result increase the DNAN surface area and dissolution. This idea is supported by the fact that more fragments result in a better linear fit to the mass loss vs. water volume data (Table 2). Although fragmentation also affects the dissolution of NTO, NQ, and AP, none of these compounds show quasi-linear dissolution because the time scales over which they dissolve are shorter than the fragmentation rate.

Figure 8. Dissolved NTO (a) and NQ (b) plotted against water volume for outdoor samples of IMX-101, IMX-104, and PAX-21.



2.3.3 Mass balance for the outdoor tests

We stopped the outdoor experiment after 864 days both to calculate a mass balance for the individual particles (Table 3) and to scrape off or dissolve their surfaces to analyze for phototransformation products. Table 3 lists the initial and final masses for the IM pieces. Also shown are initial and final masses of high explosives particles for comparison. For IM, the difference between the initial and ending masses averaged 0.8 ± 0.6 g, and about 80% of this value was recovered in the water samples. This suggests that about 20% was lost via photodegradation.

Table 3. List showing the initial mass (M_i) of the outdoor samples and the percentage not recovered. The recovered mass is the final mass (M_f) of the particle added to the mass analyzed from the effluent via HPLC. Data are given for both IM and high explosives formulations.

IM Formulations							High Explosives Formulations						
Sample	M_i (g)	M_f (g)	Diff (g)	M_{diss} (g)	M_{miss} (g)	M_{diss} /Diff	Sample	M_i (g)	M_f (g)	Diff (g)	M_{diss} (g)	M_{miss} (g)	M_{diss} /Diff
IMX-101#1	3.55	1.43	2.12	1.65	0.48	0.78	TNT#1	1.97	1.75	0.22	0.071	0.15	0.32
IMX-101#2	1.39	0.28	1.11	0.75	0.36	0.68	TNT#2	0.4	0.31	0.10	0.033	0.06	0.34
IMX-101#3	0.63	0.02	0.61	0.49	0.12	0.80	TNT#3	0.52	0.28	0.24	0.074	0.16	0.32
IMX-101#4	0.53	0.04	0.49	0.38	0.11	0.77	CompB#1	0.78	0.65	0.13	0.065	0.06	0.50
IMX-101#5	0.31	0.05	0.26	0.23	0.03	0.89	CompB#2	0.43	0.31	0.11	0.056	0.06	0.50
IMX-104#1	2.00	0.70	1.30	1.15	0.15	0.88	CompB#3	5.07	4.85	0.22	0.066	0.15	0.30
IMX-104#2	1.42	0.13	1.29	0.99	0.30	0.77	Trit#1	2.97	2.77	0.20	0.047	0.16	0.23
IMX-104#3	0.99	0.23	0.76	0.65	0.11	0.86	Trit#2	5.32	4.99	0.33	0.054	0.28	0.16
IMX-104#4	0.49	0.13	0.36	0.33	0.03	0.91	Tri#3	2.47	2.22	0.24	0.054	0.19	0.22
IMX-104#5	0.22	0.01	0.21	0.18	0.03	0.85	C4#1	4.93	4.62	0.31	0.037	0.27	0.12
PAX-21#1	1.28	0.41	0.87	0.67	0.20	0.77	C4#2	3.97	3.64	0.33	0.059	0.27	0.18
PAX-21#2	0.25	0.08	0.17	0.14	0.03	0.80	C4#3	2.30	2.10	0.20	0.030	0.17	0.15

Diff = $M_i - M_f$

M_{diss} = Mass dissolved determined from effluent samples via HPLC

M_{miss} = Mass missing = $M_i - (M_f + M_{diss})$

The high explosives (TNT, Comp B, Tritonal, and Composition 4 [C4]) were found to lose less mass than the IM formulations because their constituents are less soluble and their particle is less friable (Taylor et al. 2011). The difference between the initial and ending mass averaged 0.2 ± 0.08 g, but only about 20% of this value was recovered in the water samples. This suggests that approximately 80% was phototransformed into compounds not analyzed for in the effluent samples (Taylor et al. 2010). Unlike the high explosives, the percent mass loss of the IM formulations is not inversely related to the mass of the chunks.

2.3.4 UV-vis

The UV-vis spectra of the IM constituents are quite distinct and have absorption features in the UV portion of the spectrum (Figure 9). DNAN has a very distinctive spectrum with absorbance features at 214, 260, and 299 nm. NQ has a peak at 264 nm and NTO at 345 nm. RDX's spectrum decreases between 200 and 300 nm and is featureless except for a small shoulder at 235 nm. Ammonium perchlorate, another constituent of PAX-21, has a flat UV-vis spectrum.

We also made UV-vis measurements of some of the known degradation products of DNAN: 2,4-diaminoanisole; 4-methoxy-3-nitrophenol (4-MeO-3-NP); 2,4-dinitrophenol; 2-methoxy-5-nitrophenol (2-MeO-5-NP); 2-methoxy-5-nitroaniline (MENA, or 2-MeO-5-NA, also called 2-amino-4-nitroanisole, or 2-ANAN); and 4-methoxy-3-nitroaniline (4-MeO-3-NA, also called 4-amino-2-nitroanisole, or 4-ANAN) (Figure 10). The 2,4-diaminoanisole has a spectrum with peaks at 307 nm and 204 nm with a slight shoulder at 240 nm. The UV-vis spectrum for 4-methoxy-3-nitrophenol exhibits strong absorption peaks at 374 nm and 218 nm and two shoulders at 275 nm and 245 nm. The 2-methoxy-5-nitrophenol spectrum is weak with a broad peak centered around 350 nm.

The 2,4-dinitrophenol spectrum has a large absorption peak at 366 nm and smaller ones at 235 and 268 nm. The 2-methoxy-5-nitroaniline had strong absorption peaks at 368, 318, 258, and 224 nm. Its overall shape resembled that of the 2,4-dinitrophenol spectrum but shifted to shorter wavelengths. The 4-methoxy-3-nitroaniline also had strong absorption peaks with a large peak at 386 nm and a sharp peak at 231 nm. Its overall shape was quite similar to that of 2,4-diaminoanisole, just shifted towards longer wavelengths.

We made UV–vis measurements of the 218 effluent samples and plotted the spectra of the first, tenth, and eighteenth water samples collected from the outdoor tests (Figure 11). The results show temporal changes in the UV–vis spectra of each IM formulation, but these are due to changes in the composition of the effluent and not to degradation products. For example, IMX-101 initially has absorption features consistent with the presence of NTO and NQ. The tenth sample shows an absorption peak dominated by NQ while the eighteenth sample is starting to show a DNAN signature. Similarly, IMX-104 initially has a spectrum that matches that of NTO, but the spectrum becomes more like that of DNAN and RDX in latter samples. PAX-21 has a spectrum that matches that of DNAN, there being no NTO or NQ in this formulation.

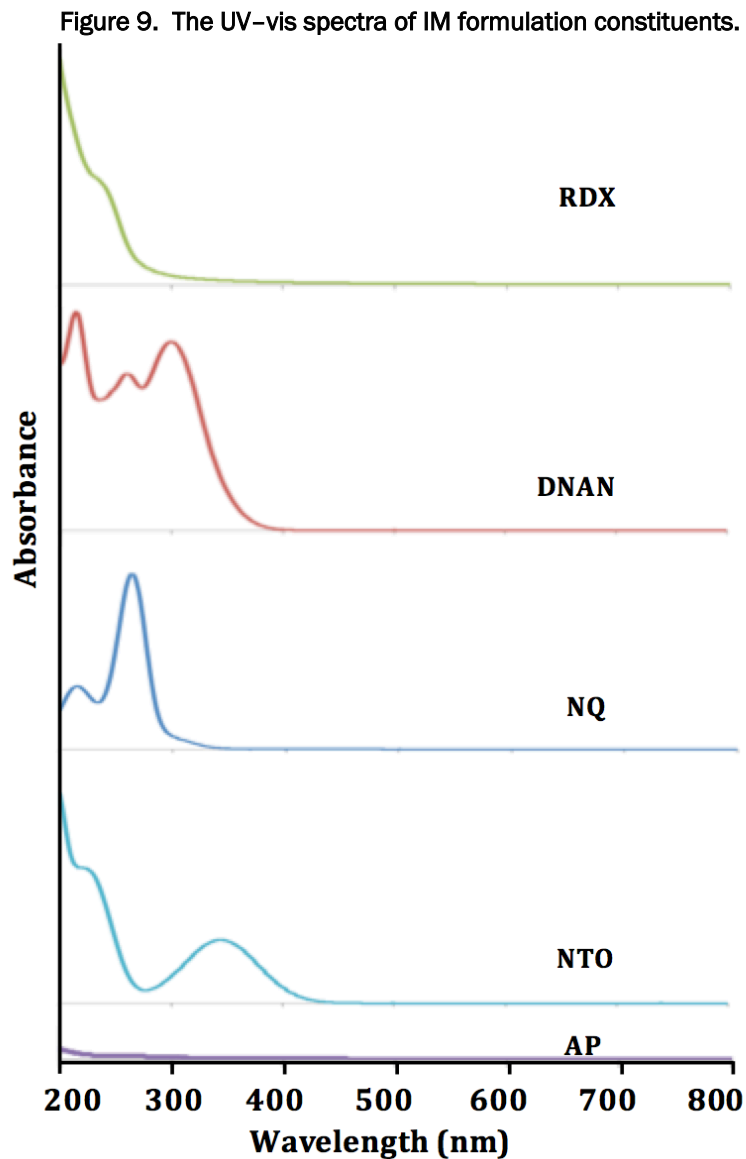


Figure 10. UV-vis spectra of known transformation products of DNAN.

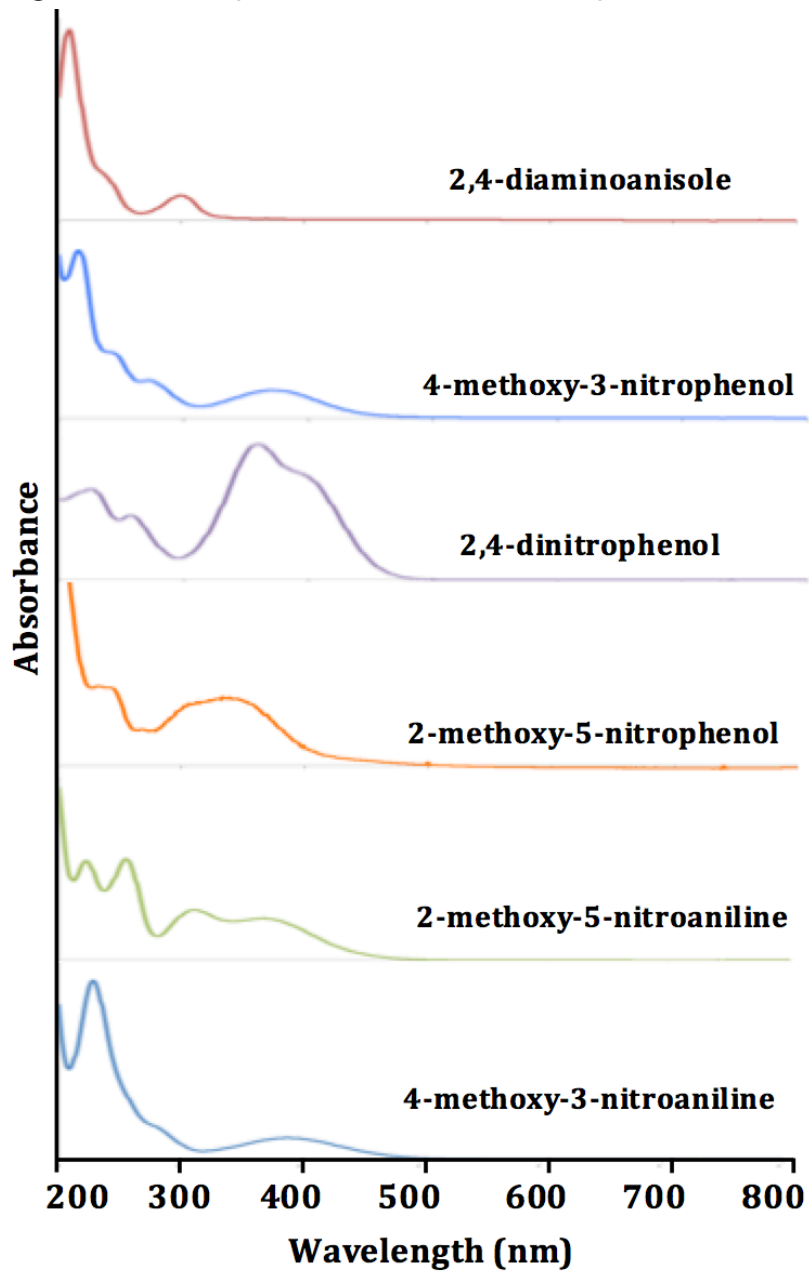
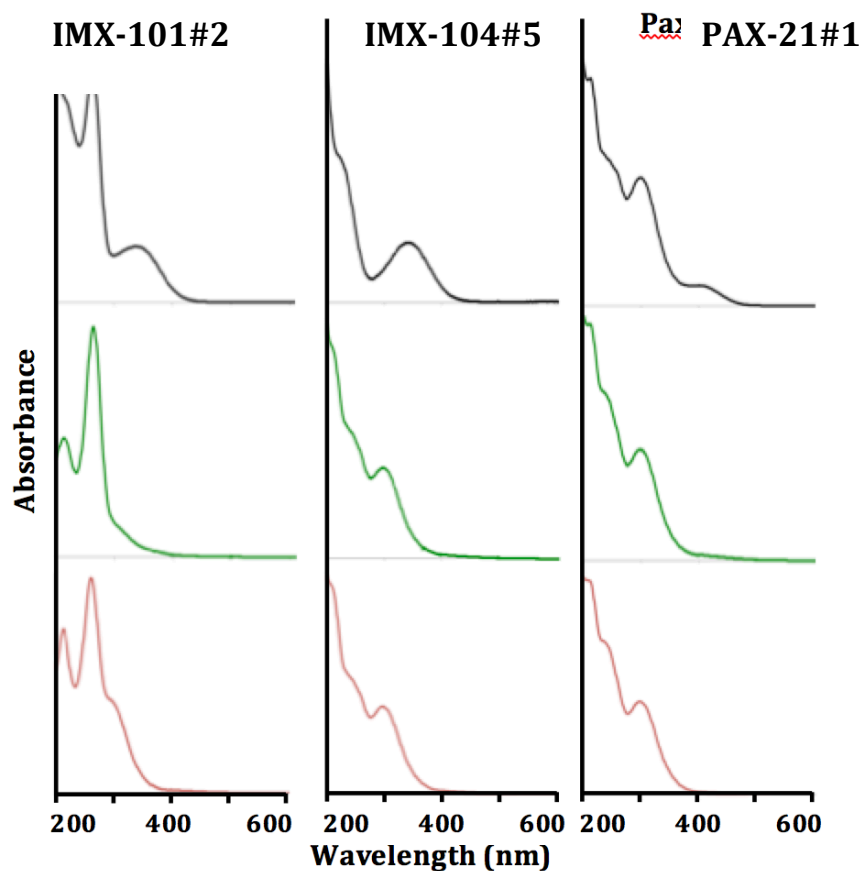
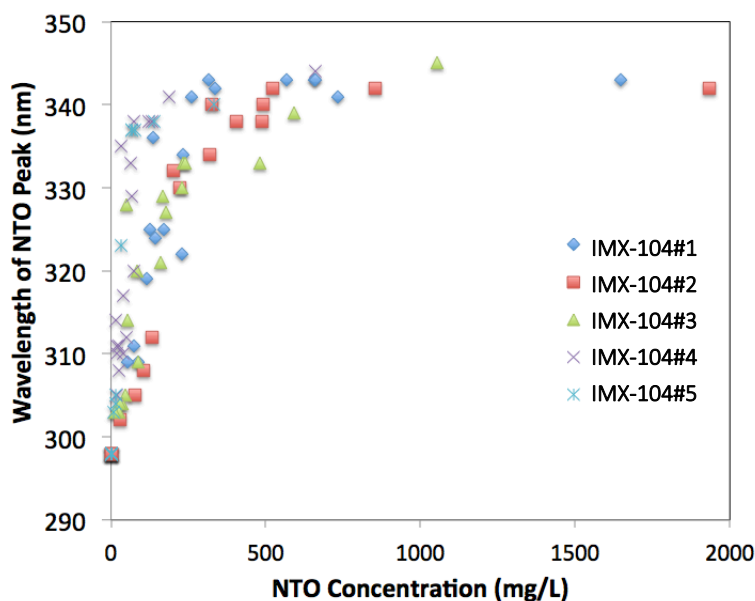


Figure 11. Plots showing the UV-vis spectra for the first (*black*), tenth (*green*), and eighteenth (*orange*) water sample collected from IM pieces placed outside to weather.



The absence of DNAN peaks in IMX-101 and IMX-104 is due to the presence of the much more soluble constituents, NTO and NQ. As the NTO is dissolved and depleted from IMX-101 particles, NQ dominates the UV-vis spectrum. Once NQ is depleted, the spectrum of the much less soluble DNAN appears. For IMX-104, as the NTO is depleted, the spectrum of DNAN starts to emerge. This transition can be tracked by a shift to shorter wavelengths of NTO's main absorption peak (Figure 12). The NTO peak position holds steady at 340 nm until the NTO concentration in the sample drops below 500 mg/L, at which point the peak position decreases to 300 nm. For PAX-21, as AP completely dissolves in the first sample, only the spectra of DNAN and RDX are present. We can see the absorption features corresponding to DNAN, but they are superimposed on a steep slope characteristic of RDX. The spectra of the IM formulations are consistent with the compositional change occurring in the individual particles as constituents of the particles dissolve.

Figure 12. Plot of NTO concentration in effluent collected from IMX-104 outdoor chunks vs. the UV-vis peak position (nm) for NTO.

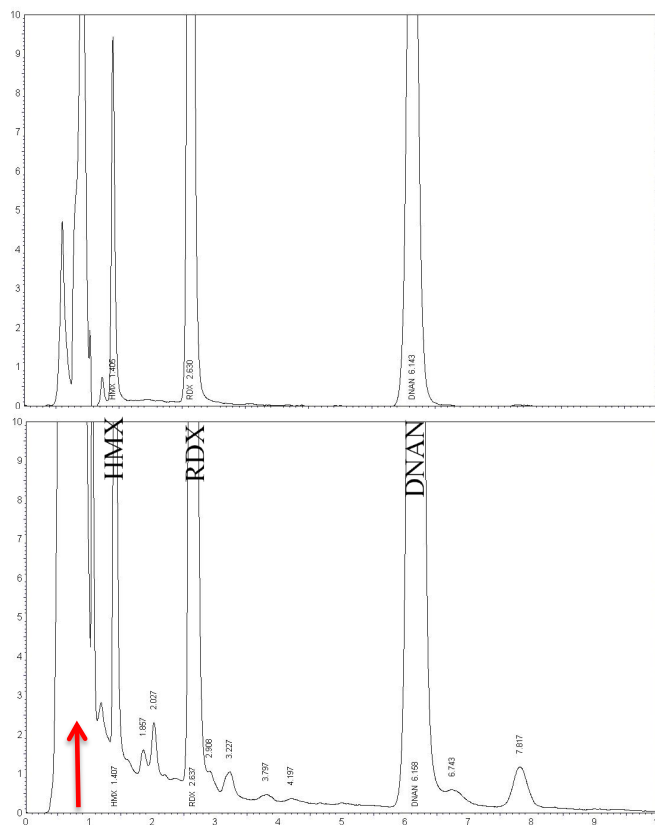


None of the UV-vis spectra had absorbance features near 600 nm, features we would expect from degradation products responsible for the color change on the explosive samples and in the effluent from those samples (Figure 11). The samples, however, were all diluted to between 3 and 6 mg/L to obtain absorption values between 0 and 2 absorbance units. To check if small amounts of other compounds were being diluted to near 0 absorbance units, we also analyzed some undiluted samples. Here, most of the absorption features were out of the linear range (>2); but we still saw no features in the visible portion of the spectrum, suggesting the colored compounds occur at very low concentrations.

2.3.5 Photodegradation of explosive pieces

We think that, similar to light-induced changes on the surfaces of high explosives (Taylor et al. 2010), phototransformation of the IM particle surfaces is also occurring. Evidence of phototransformation includes color changes of the outdoor IM pieces (Figures 3 and 4), the presence of unknown peaks in their HPLC chromatographs (Figure 13), large presolvent peaks in the HPLC chromatographs where polar substances elute, and the absence of unknown peaks and good mass balances ($100\% \pm 5\%$) in samples from laboratory tests not exposed to sunlight (Taylor et al. 2015b). Some of these photoproducts are soluble and cause the water samples to become reddish.

Figure 13. Chromatograms from a NovaPak C8 column plotting absorption units at 230 nm vs. minutes for a water sample collected from an IMX-104 indoor dissolution test (*top*, no sunlight exposure, Taylor et al. 2015a) and an outdoor test (*bottom*). DNAN, RDX, and HMX peaks are well defined; but there are many unknown peaks and a large presolvent peak (*arrow*) in the outdoor sample.



We focused on the degradation of DNAN because microscopic observation of IM formulations showed that only DNAN changed color. DNAN transformation pathways and products have been published for several matrices, including cell cultures, soil microcosms, sludge bioassays, treated wastewater (alkaline hydrolysis, zero-valent iron, fluidized-bed bioreactors), toxicity test organisms, irradiated aqueous solutions, and oxic aqueous solutions (Appendix B). No studies have reported on the phototransformation products that form on the surface of solid pieces of DNAN or DNAN in IM formulations.

Most of the studies listed in Appendix B focused on biological transformation products (see Olivares et al. 2016 for a review). The physical, chemical, and toxicological properties of some of DNAN's transformation products are known because the products are used in dyes or as reagents for chemical synthesis (o). The most commonly reported transformation product is 2-

methoxy-5-nitroaniline, which is abbreviated as MENA. MENA forms by reducing the *ortho* nitro group of DNAN, reported to be favored over reduction of the *para* nitro group. Under anaerobic conditions, reduction of both nitro groups forms 2,4-diaminoanisole (Olivares et al. 2016).

There are fewer studies of phototransformation products of DNAN in aqueous solutions. Both Hawari et al. (2015) and Rao et al. (2013) found 2-methoxy-5-nitroaniline and 2,4-dinitrophenol intermediates, not end products. Hawari et al. (2015) also reported formamide derivatives, from amino-nitro-anisole and amino-nitro-phenol, as intermediates. The final products of a DNAN aqueous solution photolyzed over 21 days were, 0.7 mole nitrate anion, 1 mole ammonium, and 0.9 mole formaldehyde/formic acid per mole of DNAN degraded (Hawari et al. 2015). Using Fourier Transfer Infrared (FTIR) analyses, Rao et al. (2013) found -COOH or -C=O in aqueous DNAN samples after 5 days of irradiation.

To help identify the photodegradation compounds in our samples, we purchased standards of six compounds known to form from DNAN (2,4-diaminoanisole; 4-methoxy-3-nitrophenol; 2,4-dinitrophenol; 2-methoxy-5-nitrophenol; 2-methoxy-5-nitroaniline; and 4-methoxy-3-nitroaniline) and analyzed them at the same time as the aqueous samples from our outdoor tests. We used a suite of instruments, including UV-vis, HPLC (two columns and a diode array detector), and GC-MS. Determining any phototransformation products of IM constituents is important because these could be toxic, soluble, and a threat to groundwater (O).

2.3.6 HPLC and GC-MS analyses

Table 4 shows the HPLC and GC-MS retention times for some of DNAN's transformation products. Unknowns could sometimes be identified by matching their GC-MS chromatograms with those in the National Institute of Standards and Technology (NIST) library (Appendix D).

After analyzing the standards, we analyzed (1) water samples for IMX-101, IMX-104, and PAX-21 collected from the beginning (at T = 1, 17 days), middle (T = 10, 360 days), and end (at T = 18, 800 days) of the outdoor dissolution experiment; (2) the acetonitrile used to extract frits for IMX-101#1, IMX-104#1, and PAX-21#1; (3) DNAN thin films that were exposed to sunlight and some also to UV radiation; and (4) a saturated DNAN solution. We were interested in determining if the photodegradation products formed on these various samples were different.

Table 4. Retention times and peak absorbance wavelengths for standard, identified, and unknown (*blue*) compounds. We found that the HPLC retention times shifted depending on what other compounds were present in the sample. Here we listed the times for the pure standards, when available.

Analyte	Retention time (min)			Mol Mass (g/mole)	λ_{max} (nm)
	GC-MS	NovaPak C8	Hypercarb		
1,2,4-benzenetriol ^a	7.8, 8.2	0.7	2.7, 6.0, 13.3	126	254, 374
2,4-dinitrophenol ^a	8.02	4.9 ^c	33.8	184	212, 257, 294
Unknown A	8.45			182	
Unknown 1		5.5	37.1		215, 270, 400
4-nitroaniline	8.65	2.56	35.58	138	240, hump 380
2-methoxy-5-nitrophenol ^a	8.67	4.5	19.7	169	212, 242, 304, 344
Unknown C	9.03			214	
Unknown 3		12	14.5		222, 314
4-methoxy-3-nitrophenol ^a	9.05	3.5	7.8	169	216, 241, 273, 372
NTO ^a	9.1 ^d	0.67 ^b	1.7	128	214, 312
4-methoxy-3-nitroaniline ^a	9.18	2.2	2.8	168	228, 386
<i>N</i> -methyl- <i>p</i> -nitroaniline (MNA)	9.28	7.58	13.56	152	<i>Broad peak 228 and 372</i>
Unknown B	9.37			198	
Unknown 2		10.2	12.2		220, 275, 330
2-methoxy-5-nitroaniline ^a	9.40	4.0	24	168	221, 255, 309, 370
DNAN ^a	9.6	7.3	26	198	214, 260, 299
NQ ^a	9.65 ^d	0.76 ^b	1.5	104	216, 266
Unknown D	9.81			184	
1-Ethoxy-2,4-dinitrobenzene	9.85			212	
HMX	9.9	1.5	3.1	228	228
RDX ^a	10.3	2.9	2.2	222	231- shoulder
2,4-Dinitroaniline	11.2	3.88	24.46	183	226, 260, 306, 378
Unknown			2.4		featureless

^a Pure standard

^b Elutes close to the solvent peak

^c To retain 2,4- dinitrophenol (DNP) on the C8 column, we lowered the pH of the mobile phase (acetic acid added to 85/15 water/isopropanol) below the pK_a (acid dissociation constant) of 2,4-DNP (4.09) to ensure that the compound was in the nondissociated form. Above the pK_a , the very polar phenolate ion forms and elutes with the solvent peak.

^d Not compatible with high temperature of the gas chromatography and elutes as a broad, asymmetrical peak

Note: Italicized values highlight uncertain matches between compounds identified by HPLC and GC-MS.

2.3.7 Compounds detected in the effluent and on the frits of the outdoor IM formulations

We analyzed both the solid products dried onto the frits holding the IM samples and the effluent derived from the IM surfaces (Table 5).

Table 5. Results from the GC-MS (X), NovaPak C8 (NP; ✓), and Hypercarb (HC; ◇) HPLC columns for samples analyzed. (MW = molecular weight.)

Compound	2,4-DNP			UK-A			2-MeO-5-NP			UK-C			4-MeO-3-NP			4-MeO-3-NA			UK-B			2-MeO-5-NA			UK-D	
MW	184			182			169			214			169			168			198			168			184	
Analysis Method	GC-MS	HPLC		GC-MS	HPLC UK-1		GC-MS	HPLC		GC-MS	HPLC UK-3		GC-MS	HPLC		GC-MS	HPLC		GC-MS	HPLC UK-2		GC-MS	HPLC		GC-MS	
		NP	HC		NP	HC		NP	HC		NP	HC		NP	HC		NP	HC		NP	HC		NP	HC		NP
Retention Time (min)	8.02	4.9*	33.8	8.45	5.5	37.8	8.67	4.5	20	9.03	12	14.6	9.05	3.5	8	9.19	2.67	2.8	9.37	10	12.2	9.41	4.0	24.5	9.81	
IM Outdoor																										
IMX-101, T = 1	X	-	-	-	✓	◇	X	-	◇	-	-	-				X	-	◇	X	✓	-	X	✓	-	-	
IMX-101, T = 10	X	-	-	-	✓	◇	X	-	◇	-	-	-							-	-	-					-
IMX-101, T = 18	-	-	-				X	-	◇	-	-	-							-	-	-					-
IMX-104, T = 1	X	-	-	-	✓	◇				-	-	-				X	-	-	-	-	-	X	✓	-	X	
IMX-104, T = 10	-	-	-	-	✓	◇	X	-	◇	-	-	-				X	-	◇	-	-	-					X
IMX-104, T = 18	-	-	-							-	-	-				-	-	◇	-	-	-					-
PAX-21, T = 1	-	-	-	-	-	-	-	-	◇	-	-	-							-	-	-					-
PAX-21, T = 10	X	-	-				X	-	◇	-	-	-				-	-	◇	-	-	-					-
PAX-21, T = 18	X	-	-	X	✓	-	X	✓		-	-	-				-	-	◇	-	-	-					-
IMX-101 Frit	-	-	◇				X	-	◇				-	-	◇	-	-	◇				X	-	◇	-	
IMX-104 Frit	-	-	-				-	✓	-	-	✓	◇										-	✓	◇	-	
PAX-21 Frit	-	-	-	-	✓	◇	-	-	-	-	-	◇	-	✓	◇	-	-	◇	-	✓	◇	-	✓	◇	-	
DNAN Indoor																										
SS film	-	-	-				-	-	◇	-	-	-				X	✓	-								X
Crystal 4 film	-	-	-				-	-	-	-	-	-										X	✓	-	X	
Crystal 7 film	-	na	-	X	na	◇	-	na	-	-	na	-	X	na	◇	X	na	◇	-	na	◇	X	na	-	X	
Aqueous Evap	-	-	-				-	-	-	-	-	-							-	✓	◇	X	✓	-	X	

Note: For GC-MS, all effluent samples were solid-phase extracts analyzed by single ion monitoring at mass 169. We exposed crystal 7 to both sunlight and to 18 hr of UV irradiation.

IMX-101 Frit: Acetonitrile rinse of IMX101 particle supporting glass frit from the outdoor dissolution studies.

IMX-101 Surface: Acetonitrile solution formed by a brief, partial, immersion of an IMX-101 particle outdoor dissolution studies.

SS Film: DNAN film on a glass surface that was formed from a volume of a stock solution of DNAN in acetonitrile.

Crystals: DNAN crystal thin films exposed to ambient light and UV light (312 nm) from a FOTO/Phoresis Transilluminator (FOTODYNE Incorporated, Hartland, Wisconsin).

Aqueous Evap: Saturated aqueous solution of DNAN set in the windowsill.

- Not detected.

na Not analyzed.

■ All three techniques found the compound.

Though we tabulate only the degradation compounds (Table 5), NQ and NTO were also present in all IMX-101 samples; NTO, RDX, and HMX were in all IMX-104 samples; AP, RDX, and HMX were in the PAX-21 (T = 1) sample; and RDX and HMX were in the other PAX-21 samples. We also detected unknowns (UK). The most prominent were labeled using numbers for HPLC unknowns, and we used letters for those detected by GC-

MS. Note that for most of these samples, the quantities of degradation products were small relative to DNAN; and as the DNAN concentration decreased, the concentrations of the products were undetectable.

2.3.7.1 Effluent samples

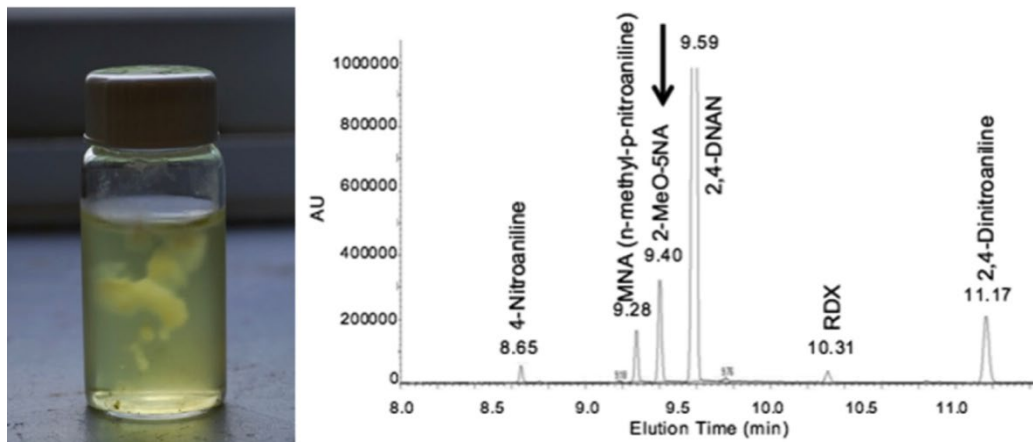
All the effluent samples had 4-MeO-3-NP and most had 2-MeO-5-NA. The concentrations of 4-MeO-3-NA, 2-MeO-5-NP, and UK-1 were lower and consequently not always detected by all three analytical methods. Trace quantities of DNP were observed by GC-MS only, and 2-MeO-5-NP could be detected using only selective ion monitoring at $m/z = 169$ whereas the higher concentrations of 4-MeO-3-NP were also detected in full scan mode.

PAX-21 at T = 1 was unusual in having a high concentration of 2-MeO-5-NA (10% of the DNAN) and a microbial biofilm (Figure 14). This is the only sample we analyzed that contained ammonium perchlorate, and we think that the latter promoted the microbial growth that transformed DNAN into 2-MeO-5-NA. PAX-21 also contained small amounts of 4-MeO-3-NP and 4-MeO-3-NA and three compounds that we identified by matching their mass spectra to ones in the NIST database. They are *N*-methyl-*p*-nitroaniline (MNA); 2,4-dinitroaniline; and 4-nitroaniline (Figure 14). MNA is added to DNAN during the production of PAX-21 to reduce DNAN's melting temperature (Doll et al. 2006). We think that the 2,4-dinitroaniline was an impurity in the DNAN and the structure of 4-nitroaniline suggests it formed from MNA.

PAX-21 was one of the first insensitive explosive manufactured and initially contained DNAN purchased from China that was of lower purity than the DNAN produced at Holston Army Ammunition Plant (Fung et al. 2010). DNAN at Holston is produced by direct nitration of *para*-nitroanisole (Fung et al. 2010) or by the reaction of 4-chloro-1,3-dinitrobenzene (Fedoroff et al. 1960). We tested with PAX-21 manufactured using DNAN from Holston, and our GC-MS analysis showed trace amounts of chloronitrobenzenes and 1-Ethoxy-2,4-dinitrobenzene, and we occasionally detected these compounds in our DNAN crystal samples (Appendix D).

The T = 10 and T = 18 effluent samples still contained small amounts of 4-nitroaniline, but MNA and 2,4-dinitroaniline were not detected. The GC-MS chromatograms for these samples showed a sharp DNAN peak superimposed on two broad peaks; the one at 10.3 is RDX, and the one at 9.9 is thought to be HMX. Both RDX and HMX degrade in the GC-MS column (Appendix D). Except for PAX-21 at T = 1, the effluent samples were similar to one another.

Figure 14. Microbial biofilm found in the first PAX-21#1 aqueous sample collected (at T = 1, day 17) and GC-MS analysis of this sample. Note the high concentrations of 2-methoxy-5-nitroaniline (*arrow*) and the absence of the other methoxy nitroaniline and nitrophenol compounds. Present are MNA (*N*-methyl-*p*-nitroaniline); 4-nitroaniline; and 2,4-dinitroaniline.



2.3.7.2 Compositional changes of effluent samples with time

Two effluent samples, IMX-101#18 and IMX-104#18, were analyzed immediately after collection and then reanalyzed after being refrigerated for 6 months.

The HPLC Hypercarb analyses for the initial IMX-101 sample shows that it contained an unknown peak at 1.1 min; the NQ, NTO, 4-MeO-3-NA, and 4-MeO-3-NP peaks; two unknown peaks at 21.3 and 24 min; and DNAN. After 6 months, the sample contained NQ; NTO; an unknown peak at 2.4 min; 4-MeO-3-NA; 4-MeO-3-NP; unknown peaks at 15.5, 19.6, and 22.2 min; 2-MeO-5-NA; DNAN; and UK-1. These comparisons suggest that 2-MeO-5-NA, an unknown peak at 2.4 min, and UK-1 all developed in the solution.

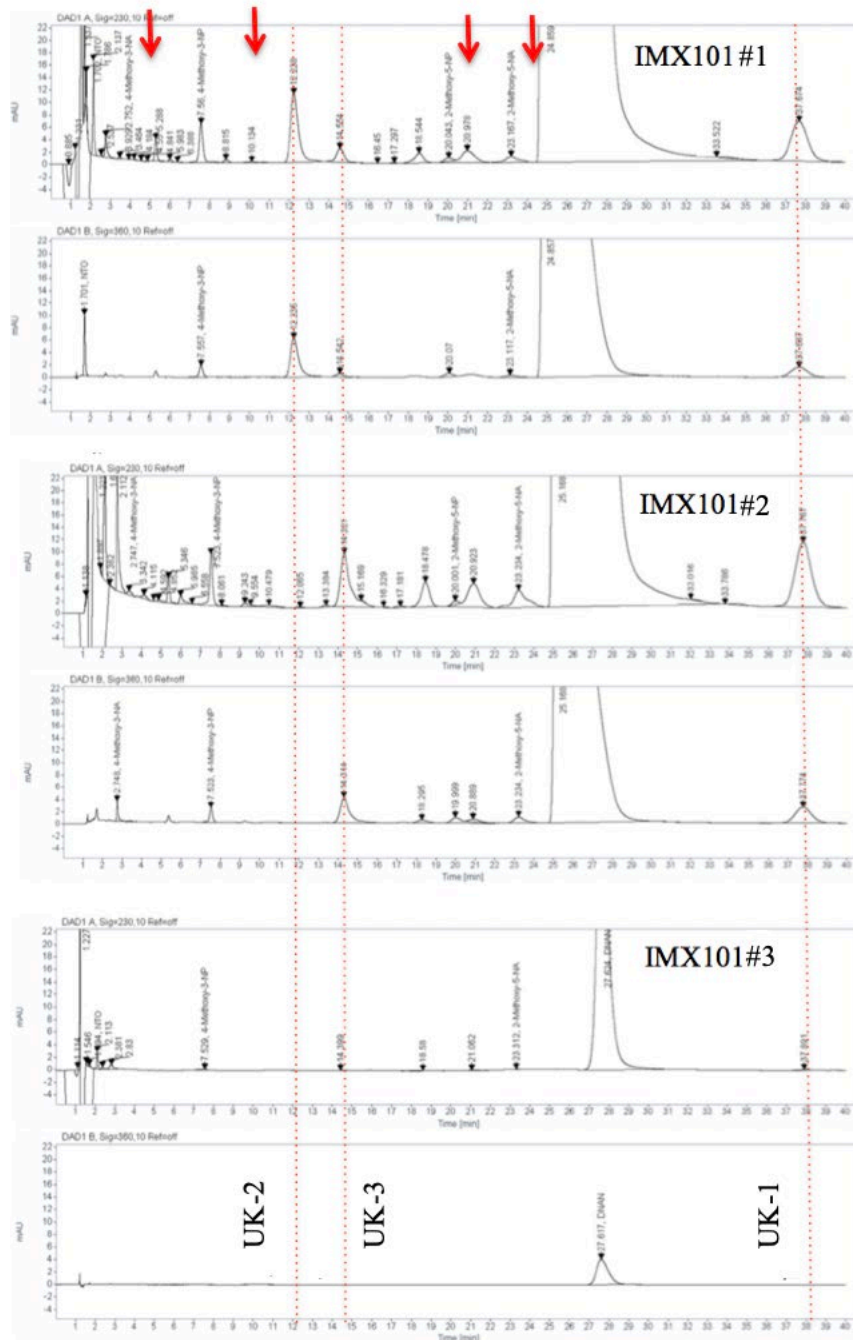
Hypercarb analyses done on IMX-104 show that initially the effluent sample contained some small peaks in the presolvent peak area: NTO, RDX, HMX, 4-MeO-3-NA, 4-MeO-3-NP, two small unknown peaks at 21.3 and 23.4 min, and DNAN. After 6 months, the sample contained NTO, RDX, an unknown peak at 2.4, HMX, 4-MeO-3-NP, DNAN, and UK-1. Again, the peak at 2.4 min and UK-1 developed in the solution.

2.3.7.3 Frit samples

The frit samples appear to have more compounds than the effluent samples, including an unknown (UK-3). HPLC Hypercarb analyses of the IMX-101 frit samples show DNP; the methoxy phenols and anilines; UK-1, UK-2, and UK-3 (Figure 15); and an unknown at 18.5 min. GC-MS for this

sample found both methoxy phenol and aniline isomers and UK-A, UK-B, and UK-C.

Figure 15. Hypercarb analyses of effluent from frit samples, showing elution times of the methoxy aniline and phenol compounds (red arrows) and the elution time of three unknown compounds (dashed lines).



The IMX-104 frit samples contained 4-MeO-3-NP; 2-MeO-5-NP; 2-MeO-5-NA; 4-MeO-3-NA; and UK-1, UK-2, and UK-3. Similar to the frit analyses for the other formulations, the PAX-21 frit sample also contained small amounts of 4-MeO-3-NP; 2-MeO-5-NA; 4-MeO-3-NA; and UK-1, UK-2, and UK-3 (Table 5). The greater number of compounds detected is likely attributable to sample concentration, which was greater for the solid material extracted off the frit than for the effluent samples.

2.3.7.4 DNAN crystals and aqueous DNAN solutions

Products formed on solid DNAN may be different from those formed in IM formulations or in aqueous DNAN solutions. To find out, we dissolved DNAN crystals and evaporated the solution into thin films, thus maximizing the surface area exposed to sunlight.

HPLC analyses of the DNAN thin films contained 4-MeO-3-NA, 4-MeO-3-NP, 2-MeO-5-NA, UK-1, and UK-2. Interestingly, we found what appear to be two isomers of DNAN, one that eluted at about 12 min and the other at about 20 min. Using the GC-MS, we identified small amounts of 4-MeO-3-NA, 4-MeO-3-NP, 2-MeO-5-NA, and UK-B and larger amounts of UK-A. We also found small amounts DNAN manufacturing impurities: chloronitrobenzenes eluting at 6.05 and 6.9 min; 2-propanol, 1-chloro-, phosphate (3:1) eluting at 9.73; and 1-ethoxy-2,4-dinitrobenzene eluting at 9.85 min. Compounds were identified if their GC-MS chromatograms matched chromatograms in the NIST database by more than 90%.

Initially, the DNAN-saturated solution contained only DNAN and UK-2. With time, the DNAN solution contained 4-MeO-3-NA, 4-MeO-3-NP, 2-MeO-5-NA, UK-1, and a peak at 9.8 min; and the UK-2 peak disappeared. We think UK-2 is an isomer of DNAN and that the other compounds derive from the phototransformation of DNAN.

In summary, the effluent samples tend to have fewer compounds than the frit samples or the irradiated thin films. As the effluent samples were collected about every 2–3 weeks, compounds washed off the IM formulations had time to interact with one another in solution, albeit in the dark. Such interaction might explain results from irradiation studies of DNAN aqueous solutions that appear to reach a stable end state after 3 weeks (Hawari et al. 2015).

2.3.8 Unknowns HPLC

We used the UV–vis spectra from the diode array detectors on the HPLC to pair unknown peaks seen using the two HPLC methods. Figure 16 shows examples of three unknown peaks that we were able to pair. UK-1 was found in most of the samples we analyzed, UK-2 appears to be a DNAN isomer, and UK-3 is unique to the frits.

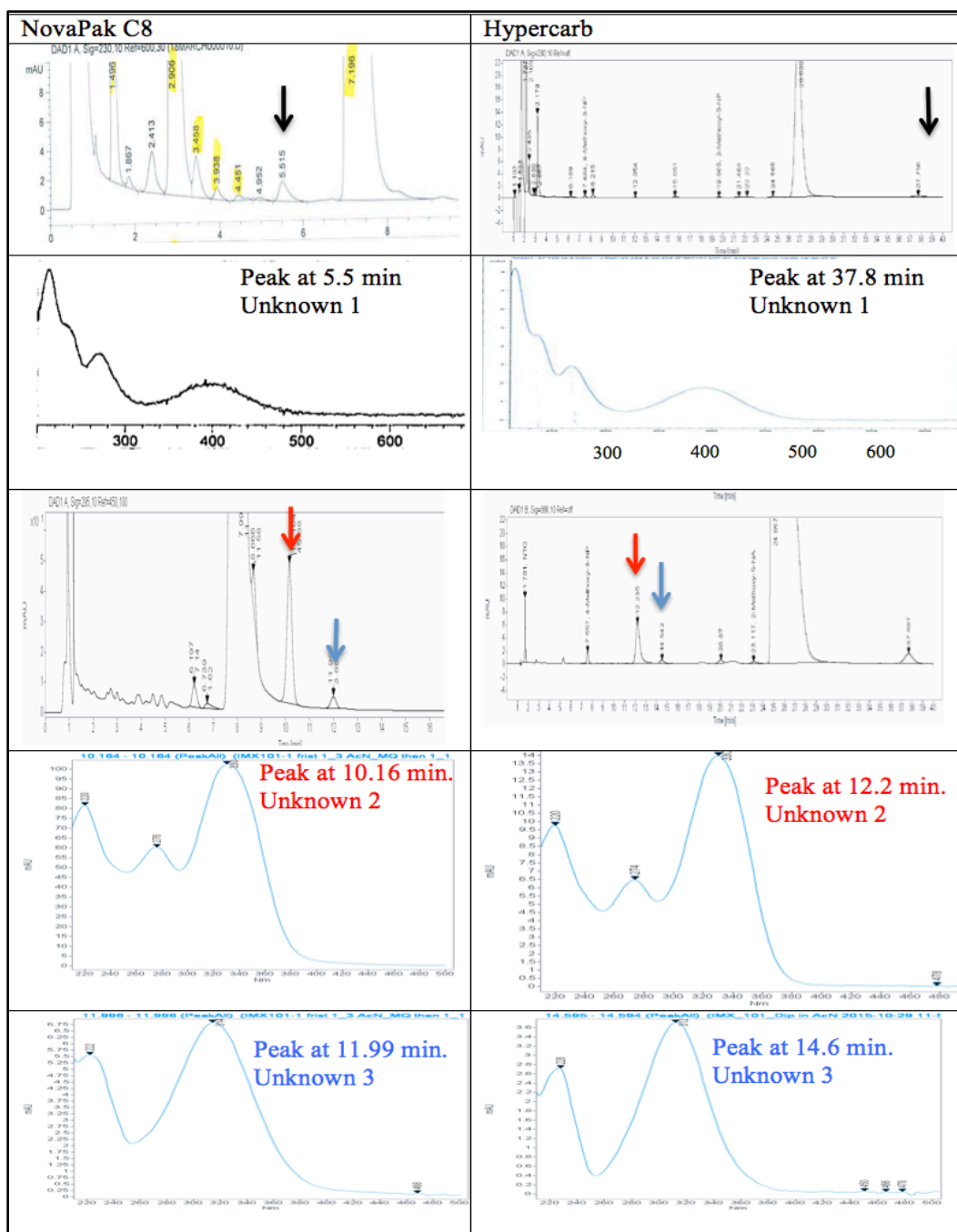
Unknown 1: The first panel shows the HPLC chromatograms for an IMX-104 effluent sample (T = 18) collected on day 800 of the test. Below the chromatograms are the UV–vis spectra of the compound producing the peaks. The compound eluting at 5.5 min on the NovaPak C8 has a very similar UV–vis spectrum to that eluting at 37 min on the Hypercarb.

Unknown 2: The second set of chromatograms is from the IMX-101#1 frit extract. One compound (red arrows) eluted at 10.2 min on the NovaPak C8 and 12.2 and occasionally at 20.5 min on the Hypercarb column (UK-2). Their UV–vis spectra resemble that of DNAN, but the wavelengths at which the major absorption peaks occur are shifted to longer wavelengths. For example, DNAN has absorption peaks at 214, 260, and 299 nm, whereas this compound has absorption peaks at 220, 276, and 330 nm. We think this compound is 2,6-DNAN.

Unknown 3: The IMX-101#1 frit extract had another unknown compound (UK-3) unique to these samples. This compound (blue arrows in Figure 16) eluted at 12 min on the NovaPak C8 and at 14.6 min on Hypercarb column.

We saw many transient peaks in the HPLC chromatograms. The UV–vis spectra of some of these resemble those of the known degradation products, suggesting similar structures.

Figure 16. Three unknowns were paired using two HPLC methods. The third and fourth panels show the UV-vis spectrum of the peak at 5.5 min on the NovaPak C8 (*panel 1*) and at 37 min on the Hypercarb column (*panel 2*) of effluent collected from IMX-104 (at T = 18). The next four panels show the elution time of the unknown peaks and their UV-vis spectra from the IMX-101#1 frit extracts.



2.3.9 Unknowns GC-MS

The GC-MS analyses provide the molecular weight and information about the structure of unknown compounds. We have labeled the unknowns

found by GC-MS using letters as we are still trying to match them to the unknown compounds found by HPLC.

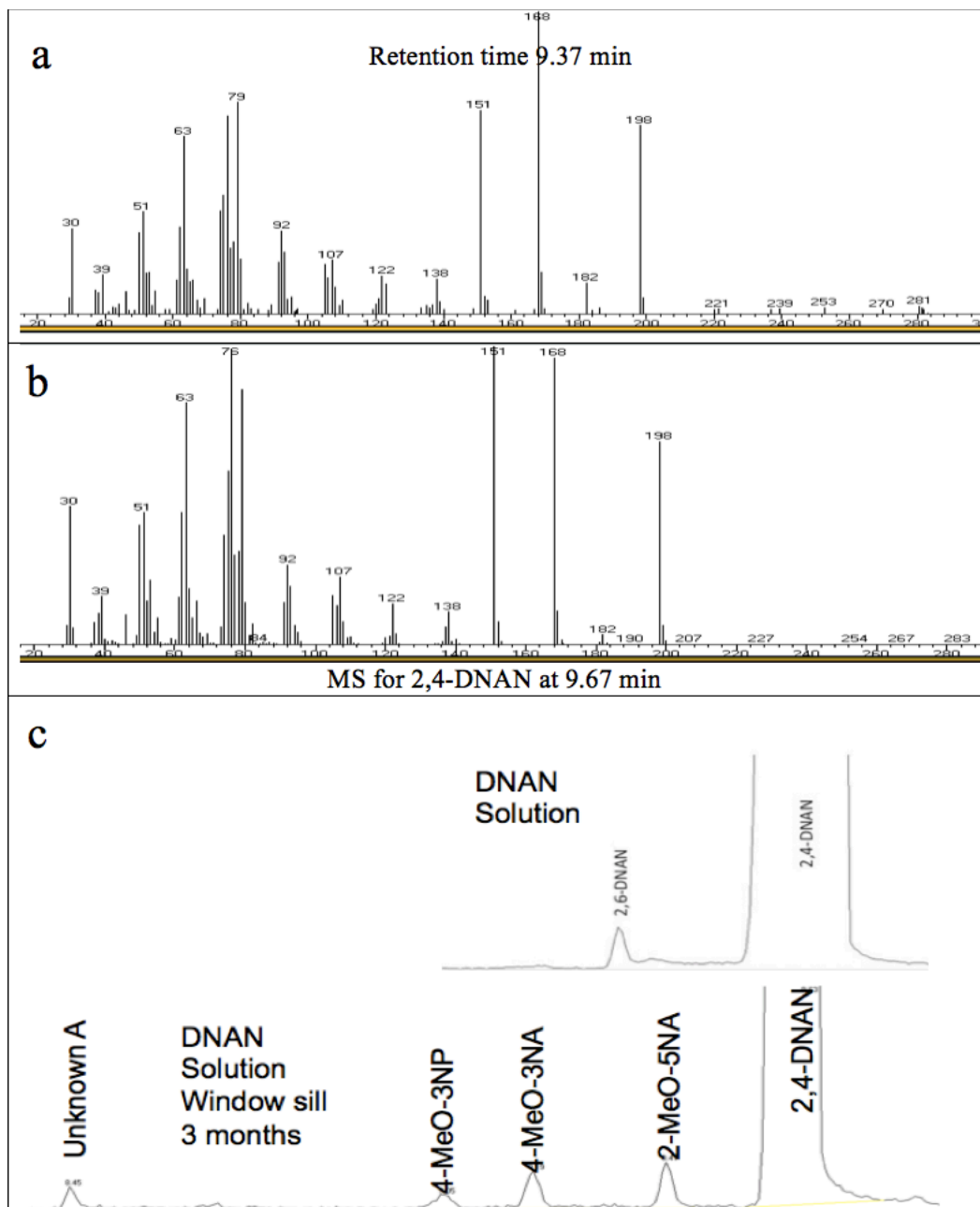
Unknown A: In the GC-MS chromatograms of the most samples, we saw a peak with a retention time of 8.45 min and a base peak of $m/z = 182$. The unknown compound has the characteristics of a nitroaromatic that includes an ion ($m/z = 136$) resulting from loss of 46 (NO_2)⁸ and the presence of $m/z = 30$ (NO). The ion $m/z = 106$ corresponds to a mass loss of 76 (CH_2ONO_2).

The mass spectrum did not produce a high-quality match in the NIST database. Hawari et al. (2012) reported a compound with a molecular weight of 182 that he suggested was 4-nitrophenol with a -NH-CHO group in the *ortho* position, $\text{C}_7\text{H}_6\text{N}_2\text{O}_4$ (Appendix D). An alternative structure is the nitroso compound, 1-methoxy-4-nitro-2-nitrosobenzene (Appendix D). The photodecomposition of nitrobenzene to nitrosobenzene has been reported by Hastings and Matsen (1948), and our data support either structure. Regardless of its structure, the compound must be fairly stable or continually produced or both as it is seen in most samples. We think this compound is the same as UK-1 found by HPLC because the latter is present in the same samples and has a UV-vis spectrum consistent with that of a nitroaromatic compound.

Unknown B (DNAN isomer): A peak with a retention time of 9.34 min and a mass spectrum consistent with DNAN (probably 2,6-DNAN) was present in the DNAN samples that were analyzed within the first few days of exposure to sunlight or UV light (312 nm) (Figure 17) and in the frit samples. The compound was detected in only one of the effluent samples (IMX-101#1, T = 1). If this compound is 2,6-DNAN, it is likely a manufacturing impurity of 2,4-DNAN, analogous to the presence of 2,6-DNT (dinitrotoulene) in military-grade 2,4-DNT. We think this compound corresponds to UK-2 seen in the HPLC chromatograms because both unknowns are found in the same samples and because the UV-vis spectrum of UK-2 is very similar to that of DNAN.

⁸ For a full list of the spelled-out forms of the chemical elements used in this document, please refer to *US Government Publishing Office Style Manual*, 31st ed. (Washington, DC: US Government Publishing Office, 2016), 265, <https://www.govinfo.gov/content/pkg/GPO-STYLEMANUAL-2016/pdf/GPO-STYLEMANUAL-2016.pdf>.

Figure 17. (a) Mass spectrum of an unknown compound having a slightly shorter retention time than that of 2,4-DNAN and a similar pattern of mass fragments, tentatively identified as 2,6-DNAN; (b) mass spectrum of 2,4-DNAN; and (c) DNAN solution before and after exposure to sunlight. Note that the peak we think corresponds to 2,6-DNAN disappears after sunlight exposure while 4-methoxy-3-nitrophenol, the methoxy nitroaniline isomers, and UK- A are formed.



Unknown C: A peak with a retention time of 9.03 min and a mass spectrum of 214 was found only in the frit samples. We think this may be the same compound as UK-3 found by HPLC because it too was found in only

these samples. Although we have a mass and possibly a UV–vis spectrum for this compound, its identity is not known.

Unknown D: A small peak at 9.8 min (just after the 2,4-DNAN peak) had a base peak at $m/z = 184$. Assuming this base peak corresponds to the molecular ion, a molecular weight of 184 is consistent with 2-hydroxylamino-4-nitroanisole that is a precursor to 2-methoxy-5-nitroaniline (2-MeO-5-NA). As described by McCormick et al. (1976) for TNT and other nitroaromatics, a nitro ($-\text{NO}_2$) group is reduced to an amino (NH_2) group via a nitroso ($-\text{NO}$), followed by hydroxylamino ($-\text{NHOH}$) intermediates. Given that we detected 2-MeO-5-NA in most of our samples and possibly a nitroso (UK-A), detection of this intermediate is plausible.

2.4 Conclusion

Insensitive formulations differ from conventional explosives in that they deposit more of their fill onto range soils during high-order and blow-in-place detonations, contain crystalline components that have widely different aqueous solubility, are orders-of-magnitude more soluble than TNT or RDX, and have a DNAN matrix that is less soluble than the crystal constituents. Our work shows that for the same mass deposited, IM formulations will dissolve more quickly than high explosives formulations. Not only are their components more soluble but also IM formulations are more friable than TNT and Comp B and crumble into many pieces, thereby increasing the surface area available to dissolve.

As was found for laboratory tests on millimeter-sized particles, the outdoor tests show that the constituents of these formulations dissolve in the order of their solubility. Unlike the laboratory tests, the outdoor results reveal that DNAN dissolves quasi-linearly as a function of precipitation. We think fragmentation of these centimeter-sized particles is responsible for this quasi-linear dissolution and use this relationship to estimate decadal particle life spans for centimeter-sized particles.

DNAN (2,4-dinitroanisole) is one of the main ingredients in IM formulations and one of the least soluble of the multiple constituents of IMX-101, IMX-104, and PAX-21 studied here. Its low solubility suggests that solid DNAN persists on range soils and can be photodegraded. To determine what products formed on pieces of IM formulations, we analyzed precipitation that had wetted chunks of three IM formulations set outdoors and

analyzed the glass frits holding these samples. We also exposed DNAN films and a DNAN solution to sunlight in the laboratory.

In most cases, the peaks of transformation products detected by HPLC and GC-MS were small, less than 1%, compared to the peak for 2,4-DNAN, suggesting that DNAN will be the main compound entering the soil. Many peaks appeared in the chromatograms, most associated with transient compounds that were found in only a couple of samples. The exception was UK-1, possibly a nitrosobenzene, which was found in the majority of the samples. It, along with the methoxy phenols and methoxy anilines, are the most common DNAN degradation products found in our samples. Microbes are likely responsible for producing the methoxy-nitroanilines in our nonsterile samples, and PAX-21#1 (T = 1) had high concentrations of 2-MeO-5-NA and a microbial biofilm. We think the ammonium perchlorate present in this sample stimulated microbial growth. DNP is occasionally present in small quantities, but it does not appear to be a persistent phototransformation product of DNAN under the conditions tested here.

Our results differ from those found for aqueous DNAN samples irradiated in solution possibly because during those tests the compounds in solution interacted and continued to be irradiated, a process that produced a few end products. We studied phototransformation products formed on the surfaces of explosive compounds that were dissolved by precipitation. Once dissolved, the compounds were no longer exposed to sunlight, similar to what would occur in the field where explosive aqueous solutions would enter the soil quickly. DNAN and small quantities of the compounds identified here are likely entering training range soils.

3 Outdoor Dissolution Studies in Arizona

By Katerina M. Dontsova, Edward Hunt, and Susan Taylor

3.1 Introduction

To determine if climatic conditions affect dissolution of IM, we conducted experiments in Oracle, Arizona, which complemented the ones previously performed in New Hampshire by Dr. Taylor for traditional and IM. Taylor et al. (2009, 2015a) conducted outdoor weathering and dissolution tests for four high explosives (2,4,6-trinitrotoluene, TNT, Comp B, Tritonal [TNT + aluminum], and C4) and three IM formulations (IMX-101, IMX-104, and PAX-21). Less dissolution should occur in Arizona than New Hampshire given the lower rainfall rate (60 cm yr⁻¹ vs. 100 cm yr⁻¹) (Table 6). The pattern of rainfall distribution is also different between New Hampshire and Arizona with two monsoon seasons in Arizona (larger in the summer and smaller in the winter), when several high intensity rainstorms can happen per week, little rainfall between monsoons, and lack of snow cover. Mean solar radiation is higher in Arizona than in New Hampshire (approximately 3.5 kWh m⁻² day⁻¹ in New Hampshire and 7.2 kWh m⁻² day⁻¹ in Arizona). However, we also expect that phototransformation on the surface could shield the underlying explosives so that the weathering rind will develop, slowing further transformation under conditions when rainfall does not remove products from the surfaces.

Table 6. Temperature and rainfall conditions in Hanover, NH, where the original dissolution experiments were conducted, and Oracle, AZ, location of the current study.

Location	Average temperature (°C)				Annual precipitation	
	January low	January high	July low	July high	in.	mm
Hanover, NH	-12	-2.2	15	28	40.11	1019
Oracle, AZ	1.7	13	19	33	24.92	633

3.2 Methods

We performed outdoor dissolution and phototransformation experiments under natural rainfall and sunlight and determined the amount of IM constituents that were dissolved or phototransformed relative to the total deposited on the soils. We used methodology developed by Dr. Taylor for the outdoor dissolution experiments in New Hampshire. As in her study, we tested three different formulations: IMX-101 (43% DNAN, 20% NTO, and

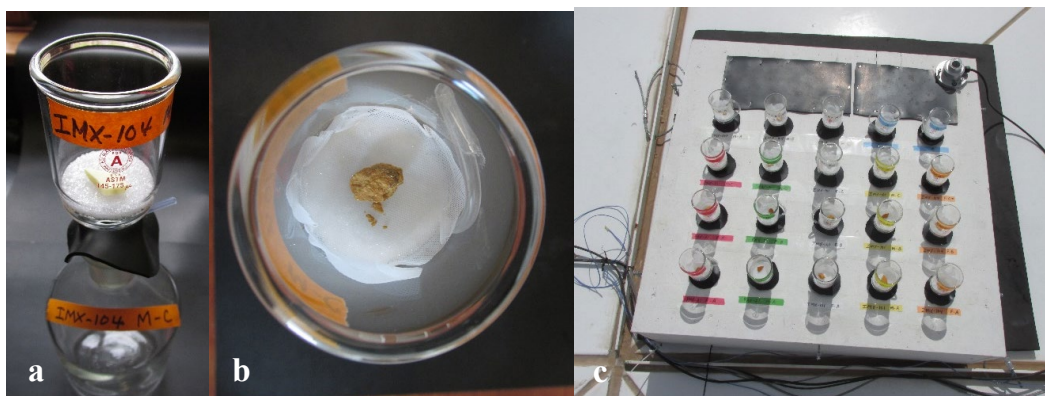
37% NQ); a TNT replacement; IMX-104 (32% DNAN, 53% NTO, and 15% RDX); a Comp B replacement; and PAX-21 (DNAN 34%, AP 30%, and RDX 36%), a formulation that has been discontinued but provides valuable insight into patterns of IM dissolution. Some of the explosive particles used for these experiments were obtained from blow-in-place studies (Walsh et al. 2013, 2014, 2015), while others were obtained from the manufacturer. Particles were previously characterized using micro-computed tomography (μ CT) (Taylor et al. 2013) to determine their internal structure.

Individual pieces of explosives were placed in Buchner funnels with glass frits (4 cm diameter with 145–175 μ m openings) attached to 0.5 L bottles (Figure 18). Particles in the funnels were exposed to sunlight and rainfall. When it rained, precipitation wetted the particles, dissolved energetic ingredients in the formulations and products of their phototransformation, and traveled through the funnels to the bottles shielded from sunlight and temperature extremes by the isolated box. In the sample box, we also placed solutions of NTO, DNAN, and NQ at 1 and 10 mg L⁻¹ concentrations and solutions of IMX-101 and IMX-104 that were sampled regularly to control for degradation in solution. The bottles were exchanged after rainfall, and the explosive pieces were photographed in situ and weighed. Since the IM particles tend to become fragile after initial exposure to rainfall due to NTO dissolution, we placed them in PTFE mesh cradles, which allowed removal of a particle for weighing without disturbing it. We measured precipitation volumes and determined concentrations of explosives (NTO, DNAN, RDX, AP, and NQ), their known transformation products (2-ANAN and its isomer 4-ANAN, products of DNAN transformation) and explosive impurities (such as HMX found in RDX) in the water samples. An adjacent LPO2 pyranometer (Hukseflux USA, Center Moriches, NY) provided solar radiation data, while collected solution volumes were used to estimate the amount of rainfall that the particles were exposed to during the study period.

Solutions were analyzed for energetic compounds and their transformation products and impurities by using a Dionex Ultimate 3000 HPLC equipped with a diode array detector (ThermoFisher, MA) and a Dionex ICS 5000 ion chromatography (IC) system with conductivity detectors (ThermoFisher, MA). The method for NTO, adapted from Le Champion et al. (1999a), used 75:25 acetonitrile to deionized water mobile phase, which was acidified with 0.1% trifluoroacetic acid (TFA) and run isocratically at 1 mL min⁻¹. NTO and its transformation product (5-amino-1,2,4-triazol-3-one, ATO) were separated using a Thermo Scientific Hypercarb column at

32°C. NTO was detected at approximately 2.8 min using a 315 nm wavelength while the 220 nm wavelength was monitored for ATO (Le Campion et al. 1999a). DNAN, RDX, NQ, HMX, and DNAN transformation products 2-ANAN and 4-ANAN were analyzed using the Thermo Scientific Acclaim reversed phase column C-18 with a 5 µm particle size, mobile phase ratio of 43:57 methanol and water, and a flow rate of 1 mL min⁻¹ (Olivares et al. 2013). The wavelengths used for detection and quantification were 300 nm for DNAN and NQ; 254 nm for 2-ANAN, 4-ANAN, RDX, and HMX; and 210 nm for DAAN. The retention time on HPLC for DNAN was approximately 21 min, 11 min for 2-ANAN, 6 min for 4-ANAN, 8 min for RDX, 5 min for HMX, and 3 min for NQ. Detection limits were 0.015 mg L⁻¹ for DNAN, 2-ANAN, 4-ANAN, NQ, RDX, and HMX and 0.020 mg L⁻¹ for NTO.

Figure 18. Experimental setup to examine dissolution and phototransformation of insensitive munitions: (a) an unweathered particle of IMX-104 in a bottle with a funnel attached for collecting solution, (b) a particle of IMX-104 (from a low-order detonation) on a glass frit and PTFE mesh in the funnel after one month of exposure to sunlight (no rain), and (c) a light-protected container with bottles and funnels with the particles exposed to sun and rainfall. The container is equipped with temperature sensors and the LPO2 pyranometer to measure solar radiation.



The perchlorate ion (ClO₄⁻) was analyzed using IC: Dionex IonPac AS20 capillary IC Column and AG20 guard column with 22 min run at 0.012 mL min⁻¹ and 35 mM KOH (potassium hydroxide) isocratic eluent. Concentrations of ammonium (NH₄⁺) and nitrate (NO₃⁻), known products of NTO transformation (Krzmarzick et al. 2015; Madeira et al. 2017) and phototransformation of DNAN (Hawari et al. 2015), were also determined using IC (Thermo Scientific Dionex ICS-5000+ Ion Chromatography System). For nitrates, we incorporated the capillary IC using an Ion Swift MAX-100 0.25 mm × 250 mm column with a flow rate of 0.012 mL min⁻¹. The ammonium method used an analytical microbore column (2 mm × 250 mm IonPac 12A) with a flow rate of 0.25 mL min⁻¹.

3.3 Results

3.3.1 Weather conditions during the experiment

The experiment started 4 February 2016 when we put six particles each of IMX-101, IMX-104, and PAX-21—three from manufacturers (named MA, MB, and MC for 3 replicate particles) and three resulting from low-order detonations (FA, FB, and FC) (Walsh et al. 2013, 2014, 2015; Taylor et al. 2015a)—outside to dissolve. Particle weight varied between 0.1718 and 2.6151 g. While the experiment still continues with the particles exposed, we present the results here through 390 days of the experiment. Figures 19 and 20 show global radiation measured close to the particles and average rainfall in millimeters (determined from the weight of the solution collected in each bottle) as a function of time from the beginning of the experiment. Both annual (Figure 19, top) and daily (Figure 19, bottom) variation can be observed in the amount of light particles were exposed to during the experiment. There was little rainfall in the first 150 days of the experiment followed by summer and winter monsoons with more frequent rains after that (Figure 20).

Figure 19. Global radiation expressed as average irradiance per 15 min, W m^{-2} , measured next to the experimental setup over the course of the experiment (*top*) and a close up to show daily variation (*bottom*).

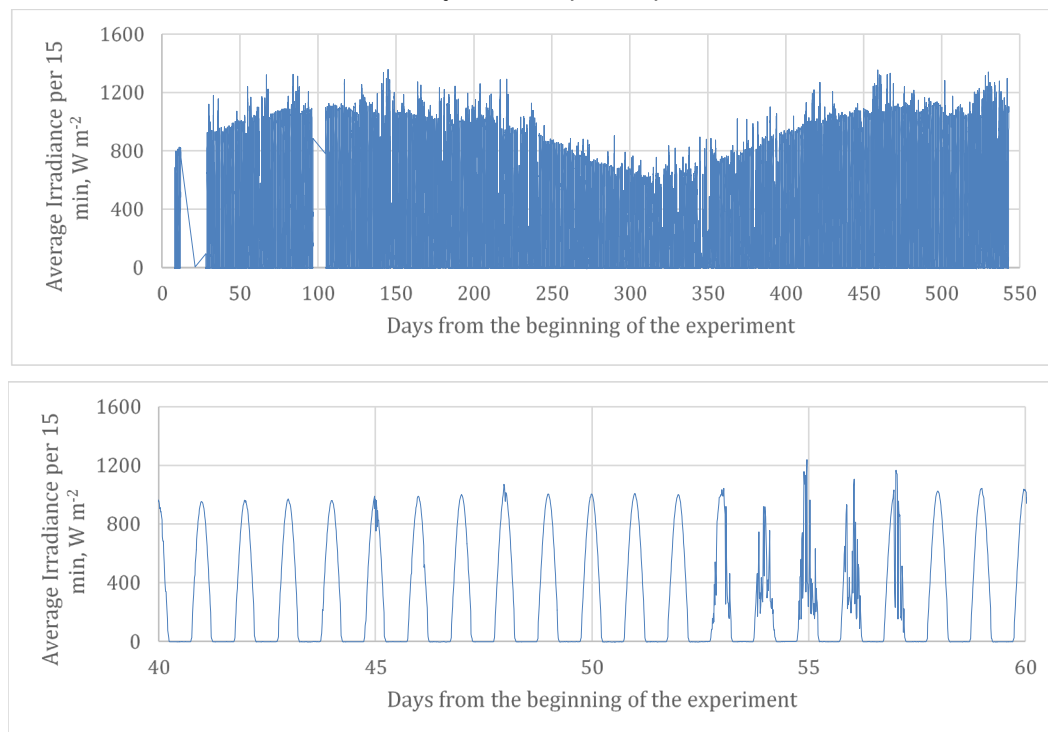
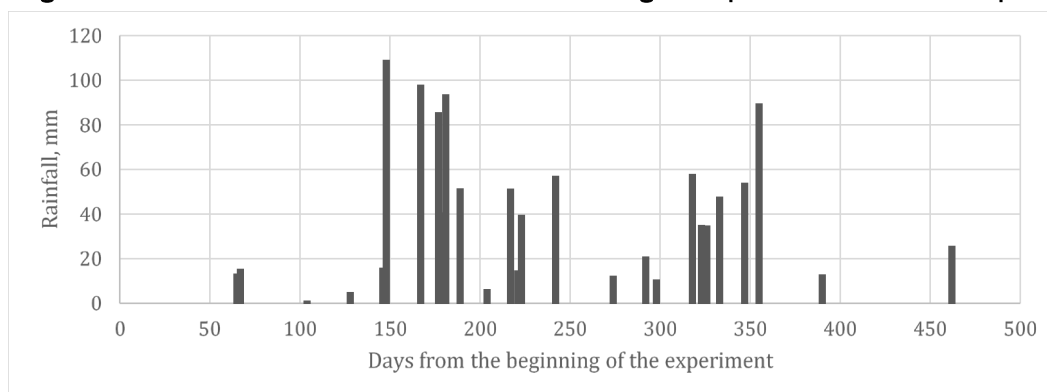


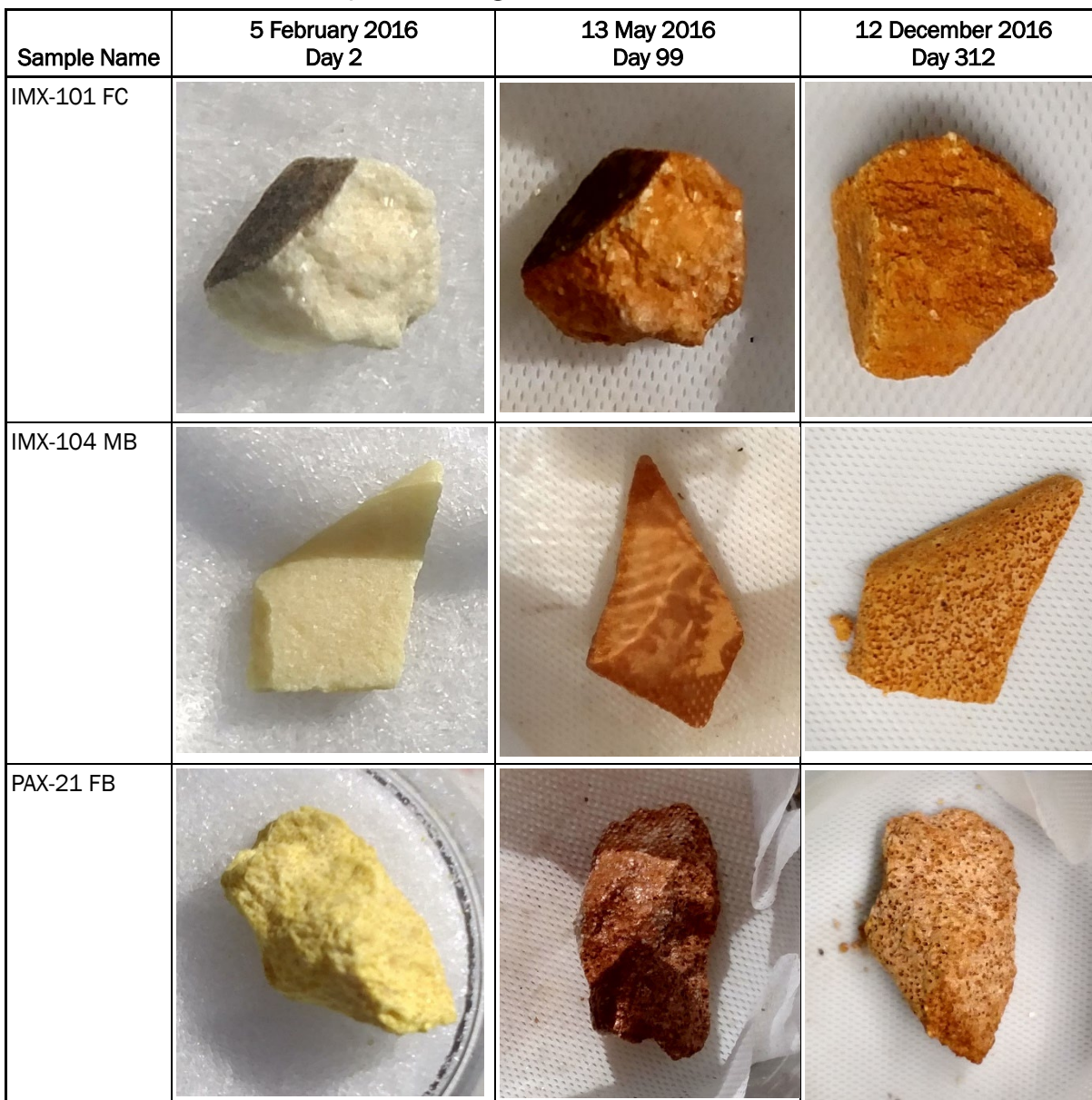
Figure 20. Mean rainfall amount and distribution during the experiment across all samples.



3.3.2 Particle appearance

The appearance of particles exposed to sun and rainfall changed over time (Figure 21). They changed color from cream colored or yellowish to brick red, indicative of the phototransformation products of DNAN. The color intensity generally increased over time, except for PAX-21, which initially became brighter but later developed a paler cover on the surface as a result of armoring of the surface with undissolved crystals of RDX. Color intensity also was higher before the rainfall periods and lower after. Particles of all studied formulations developed pits on the surface where crystals of more soluble constituents, such as NTO and NQ in IMX-101, NTO in IMX-104, and AP in PAX-21, were originally present. Several particles also broke apart.

Figure 21. Images of particles of IMX-101, IMX-104, and PAX-21 over time as they were exposed to sunlight and rainfall in Oracle, AZ.



3.3.3 Dissolution of IM constituents

As observed in previous indoor and outdoor experiments (Taylor et al. 2015a, 2015b), energetic components dissolved in order of their solubility, with NTO and NQ in IMX-101, NTO in IMX-104, and AP in PAX-21 dissolving first followed by DNAN and RDX (Figure 22). There were distinct steps in the dissolution plots corresponding to dry periods between the periods of frequent rainfall. In general, plots appeared less gradual than ones obtained for IM in New Hampshire under wetter conditions (Taylor et al. 2015a).

Perchlorate dissolved the fastest and plateaued for several particles, indicating that all perchlorate in those particles had dissolved. Calculated percent dissolved was not necessarily 100% when this happened due to deviation from ideal mixture composition in the particle. There was a difference in behavior of fired and unfired particles of PAX-21 with quick initial dissolution of perchlorate in manufactured particles (Figure 22c) and more gradual release in detonated particles (Figure 22d). This is better seen in the plots of IM dissolution as a function of cumulative rainfall (Figure 23). The pattern was attributed to the difference in shape between the two groups of particles: detonated and not detonated. While detonated particles were chunky, manufactured particles were slivers with higher specific surface area and the majority of perchlorate accessible to water from the surface.

Figure 22. Dissolution of (a) NTO, NQ, and DNAN from IMX-101; (b) NTO, RDX, and DNAN from IMX-104; and (c and d) perchlorate, RDX, and DNAN from PAX-21 as a function of time.

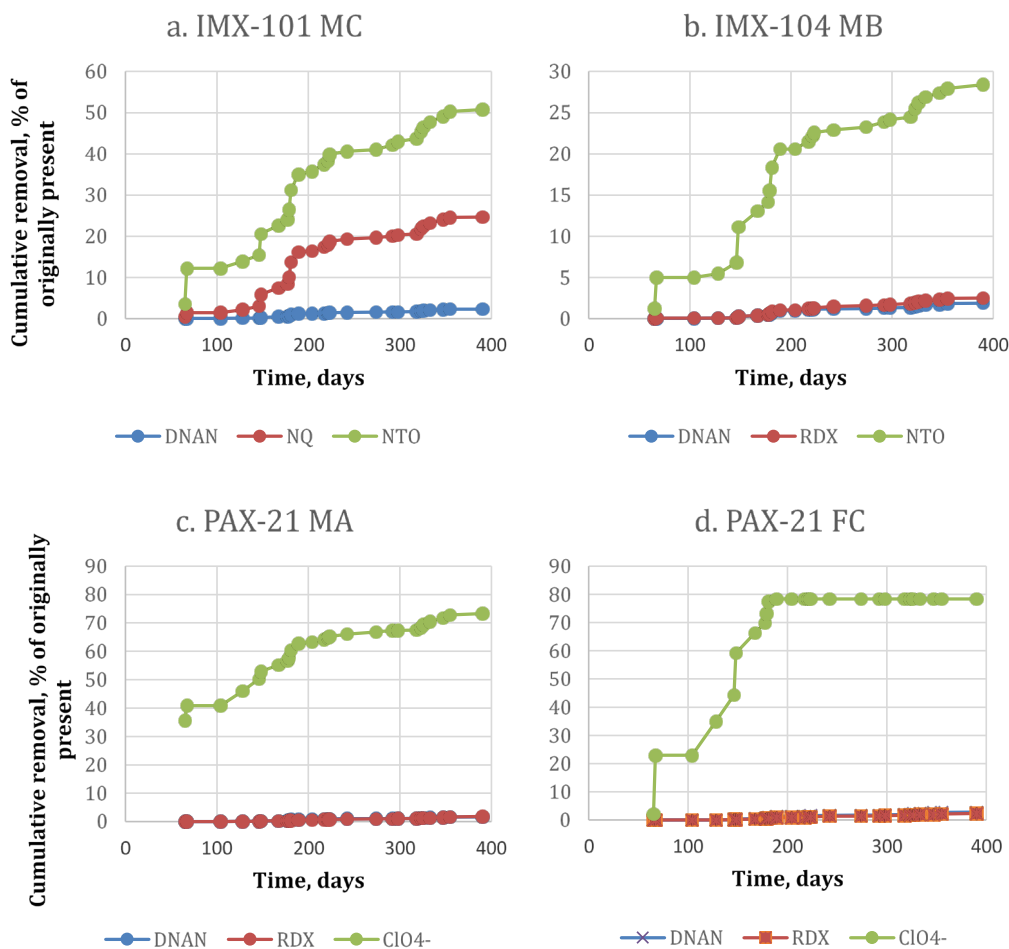
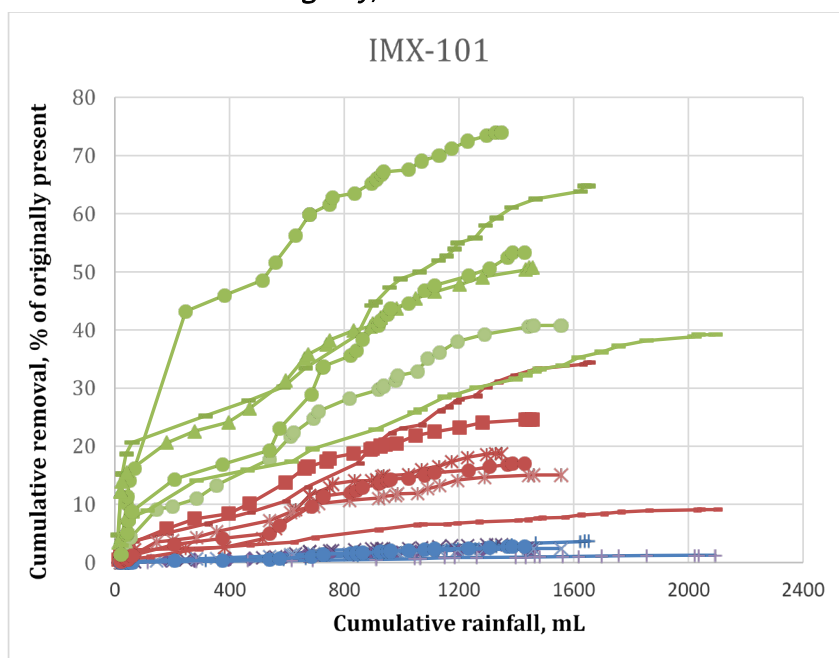


Figure 23. Dissolution of NTO, NQ, and DNAN from six IMX-101 particles as a function of rainfall amount. NTO is indicated in *green*, NQ in *burgundy*, and DNAN in *blue*.



Dissolution of NTO and NQ was also quicker initially followed by slower dissolution over time (Figures 23 and 24). This is explained by higher solubility and consequently fast dissolution of these compounds as they are first exposed to rainfall followed by slower dissolution later due to access to these compounds being restricted by the DNAN matrix.

RDX and DNAN dissolved much slower, and patterns of their dissolution were similar (Figures 23, 24, and 25) and linearly related to cumulative rainfall. The plots of DNAN and RDX concentration vs. cumulative rainfall did not overlap though, as size and surface area of each particle was different, but it was similar for similarly sized particles.

For most constituents, there was a negative nonlinear relationship between the amount of rainfall and the solution concentrations (not shown), possibly due to kinetic limitation on dissolution during high-intensity rainfall. This would indicate that climates where high-intensity rains are predominate would have less explosives dissolved per rainfall amount. This is supported by data so far collected in Arizona.

Figure 24. Dissolution of NTO, RDX, and DNAN from six IMX-104 particles as a function of rainfall amount. NTO is indicated in *green*, NQ in *burgundy*, and DNAN in *blue*.

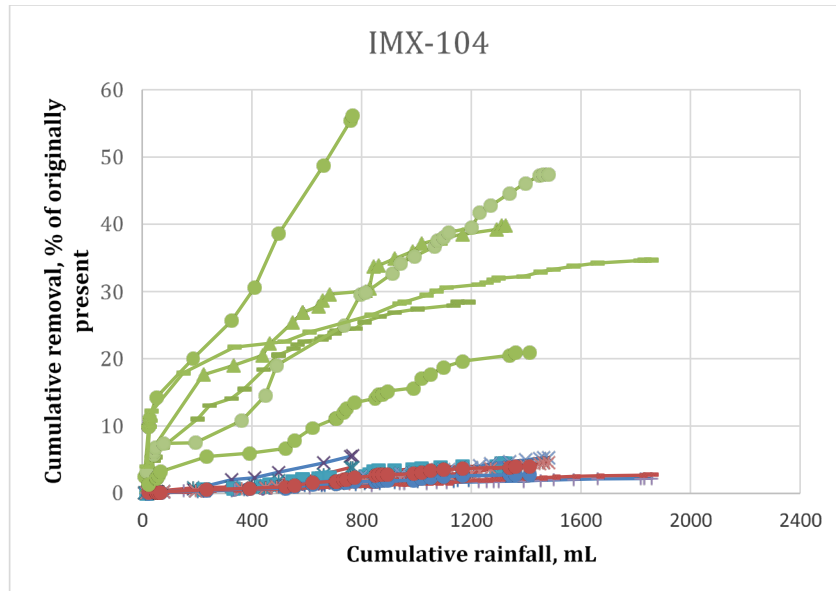
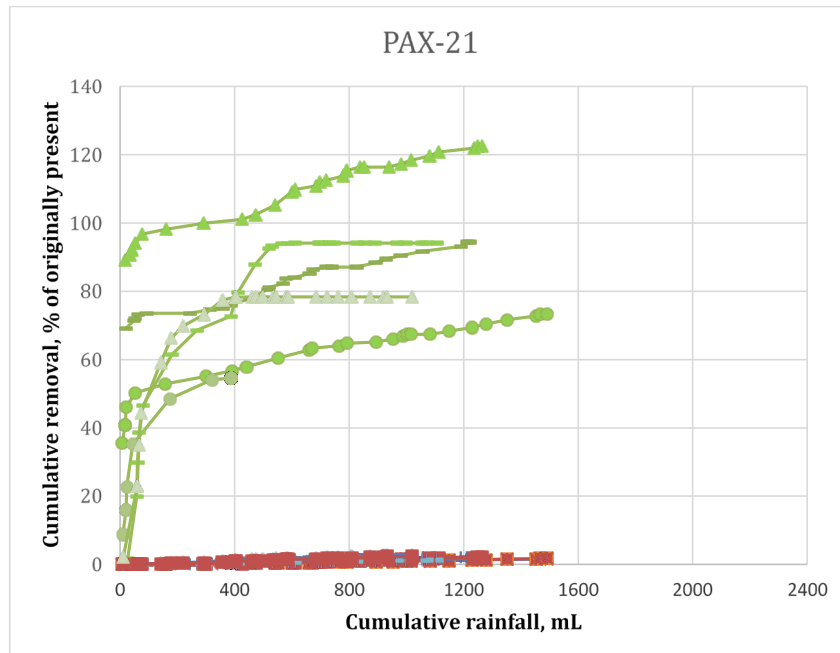


Figure 25. Dissolution of ClO_4^- , RDX, and DNAN from six PAX-21 particles as a function of rainfall amount. NTO is indicated in *green*, NQ in *burgundy*, and DNAN in *blue*.



Over 390 days of the experiment, $53.8 \pm 5.5\%$ of NTO dissolved from IMX-101 particles and $43.9 \pm 10.3\%$ from IMX-104 (Table 7) likely due to differences in NTO crystal size (Taylor et al. 2013). Similarly, more RDX was

removed from IMX-104 than from PAX-21 ($4.39 \pm 0.78\%$ vs. $1.66 \pm 0.30\%$) because the crystal size of RDX in IMX-104 is smaller (Taylor et al. 2013).

Table 7. Removal of munitions constituents in solution as percent of original mass in the particle.

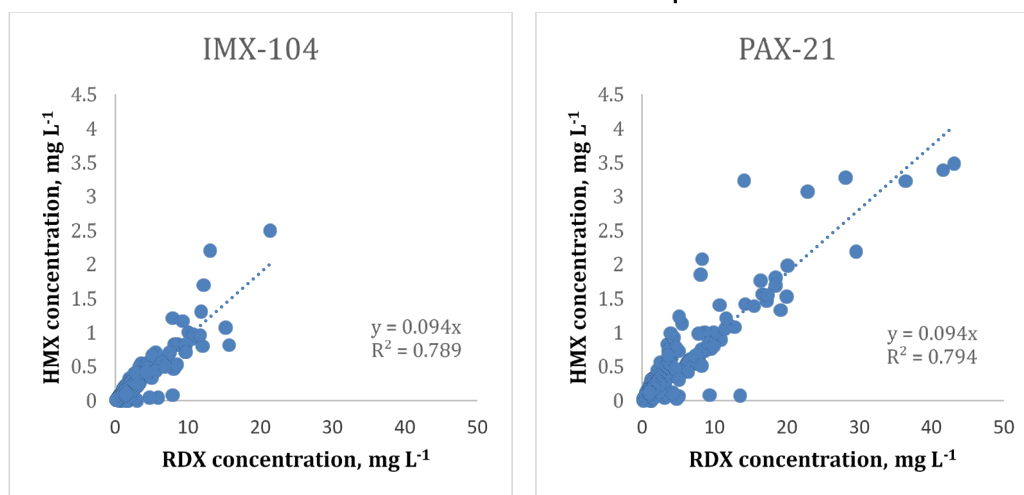
Sample Name	IMX-101			IMX-104			PAX-21		
	DNAN	NQ	NTO	DNAN	RDX	NTO	DNAN	RDX	ClO ₄ ⁻
MA	3.13	18.78	73.90	10.54	7.89	91.84	1.62	1.83	73.28
MB	3.66	34.40	64.80	1.85	2.49	28.40	2.09	2.07	94.46
MC	2.32	24.64	50.74	2.75	4.38	39.85	1.67	2.03	122.60
FA	2.43	15.05	40.81	5.26	4.64	47.42	0.53	0.35	54.56
FB	1.26	9.10	39.17	2.21	2.84	34.70	1.45	1.32	94.11
FC	2.71	16.98	53.27	2.77	4.07	20.90	2.79	2.33	78.37
Average	2.58	19.83	53.78	4.23	4.39	43.85	1.69	1.66	86.23
Standard Error	0.33	3.57	5.53	1.35	0.78	10.30	0.30	0.30	9.46

In IMX-101, less NQ ($19.8 \pm 3.6\%$) was dissolved than NTO ($53.8 \pm 5.5\%$), consistent with an order of magnitude higher solubility of NTO and the presence of smaller NTO crystals in the mixture. However, in IMX-104 and PAX-21, similar percentages of RDX and DNAN were recovered in solutions despite higher water solubility of DNAN. Comparisons between different IM constituents described above are based on dissolution values normalized to the content of each compound in the formulation; unnormalized concentrations had similar relationships between compounds to normalized ones for IMX-101 and PAX-21 and higher concentrations of DNAN than RDX in IMX-104. Whether particles were new or resulted from low-order detonations had no significant effect on recovery of IM constituents.

We detected HMX in solutions resulting from dissolution of formulations containing RDX, IMX-104, and PAX-21, consistent with the presence of HMX in technical grade RDX. While released HMX concentrations were different due to different amounts of RDX present in each formulation (15% in IMX-104 and 36% in PAX-21), they were highly correlated to RDX concentrations (p -value equal to 2.50×10^{-72} and 2.64×10^{-64} for IMX-104 and PAX-21, respectively) for both formulations. The slopes of the lines were not statistically different (0.094 ± 0.005 for IMX-104 and 0.094 ± 0.006 for PAX-21) and agreed with the known percent of HMX in RDX (Figure 26). Because differences in formulation total composition and particle size of RDX crystals did not affect the ratio of HMX to RDX in

solution, we think that both compounds dissolve from the formulations together and are not affected by differences in their solubilities.

Figure 26. Correlation between concentrations of HMX and RDX in solutions resulting from dissolution of IMX-101 and PAX-21 particles.



We also observed products of DNAN transformation, 2-ANAN and its isomer 4-ANAN, in collected solutions, possibly due to contamination of the particles with microbial communities as a result of dust deposition. Greater concentrations of 2-ANAN than 4-ANAN were measured, indicating regioselectivity of the transformation reaction (Hawari et al. 2015; Arthur et al. 2017). A sum of these products in solution averaged $1.27 \pm 0.16\%$ of DNAN concentrations in IMX-101, $1.12 \pm 0.12\%$ in IMX-104, and $3.50 \pm 0.33\%$ in PAX-21 but varied with time. Samples collected in the first 150 days of exposure, when there was little rain (Figure 19), accumulated larger percentages of DNAN transformation products. No change in concentration of constituents and no products of DNAN transformation were detected in the control vessels that were left outside but protected from sun within the experimental box. The results indicate that transformation occurred only on the sun-exposed explosive particles.

We also detected ammonium and nitrate, products of NTO biotransformation (Krzmarzick et al. 2015; Madeira et al. 2017) in solutions resulting from dissolution of IMX-101 and IMX-104. Both nitrate and ammonium have also been shown to result from DNAN photolysis in solution (Hawari et al. 2015), and nitrate was detected during RDX photolysis (Bedford et al. 1996; Taylor et al. 2010). However, we cannot definitely attribute them to transformation of IM constituents in these experiments due to concurrent detection of these ions in blank samples without the particles. After

removal of several outliers with ammonium concentrations above 30 mg L^{-1} (1/27 in blank, 5/162 in IMX-101, and 3/162 in IMX-104), the average concentration over 390 days of the experiment for blank samples was $4.0 \pm 1.9 \text{ mg L}^{-1}$ (mean \pm confidence interval) for ammonium and $2.2 \pm 0.9 \text{ mg L}^{-1}$ for nitrate, while results for IMX-101 were $2.99 \pm 0.43 \text{ mg L}^{-1}$ for ammonium and $3.24 \pm 1.75 \text{ mg L}^{-1}$ for nitrate. For IMX-104, it was $3.09 \pm 0.39 \text{ mg L}^{-1}$ for ammonium and $3.35 \pm 0.72 \text{ mg L}^{-1}$ for nitrate, not significantly different from blanks without explosives for both ions. We explain the presence of these ions in blank samples by atmospheric deposition in natural rainfall and dust; and since they were not different from IM samples, we have to conclude that transformation of IM constituents was not the source of nitrogen-containing inorganic ions. However, the ratio of nitrate to ammonium was different between blank and IMX samples. There was a strong relationship between ammonium and nitrate concentrations for blank, IMX-101, and IMX-104 samples (p -value of 1.98×10^{-6} , 2.30×10^{-47} , and 1.43×10^{-55} , respectively); and while slopes of these relationships were not statistically different between IMX-101 and IMX-104, they were significantly lower for blank samples (Figure 27).

We observed that the pH of solutions resulting from dissolution of IMX-101 and IMX-104 particles were related to their NTO concentrations (Figure 28), consistent with previous observations in the lab and outdoor dissolution experiments for IM formulations (Taylor et al. 2015a). The relationship was similar across the two studied formulations that contained NTO: IMX-101 and IMX-104. However, there was considerable scatter in the data likely due to contamination with high pH dust that is prevalent in the Southwest.

Figure 27. The relationship between ammonium and nitrate concentrations in solutions of IMX-101 and IMX-104 and blank samples without explosives.

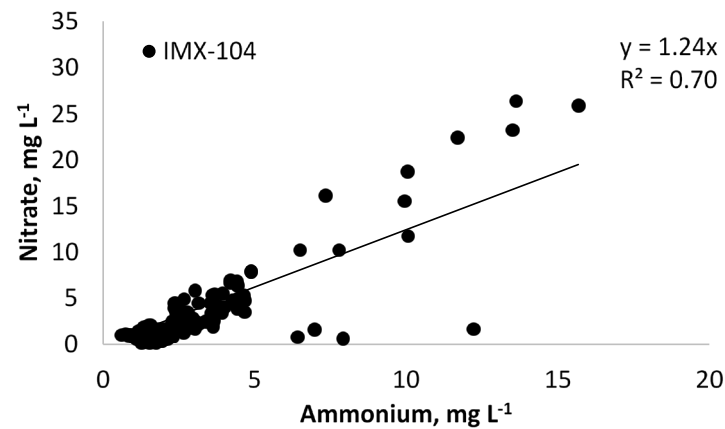
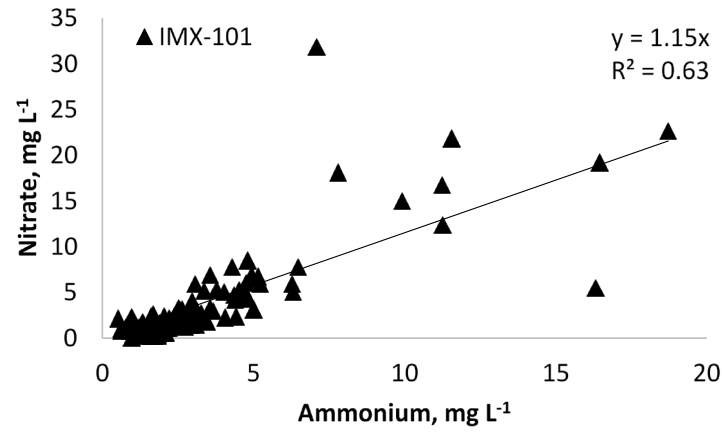
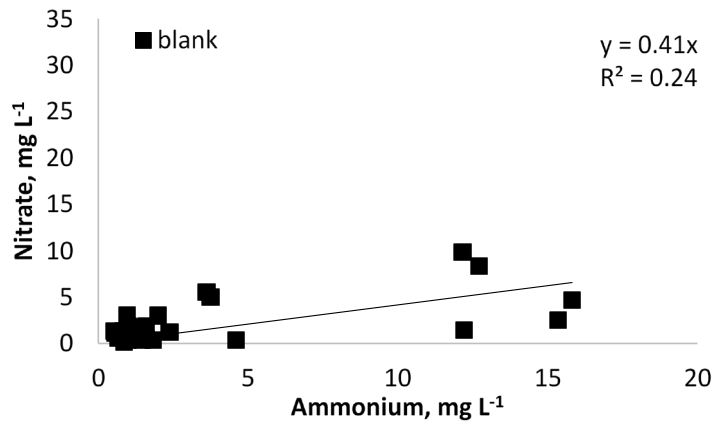
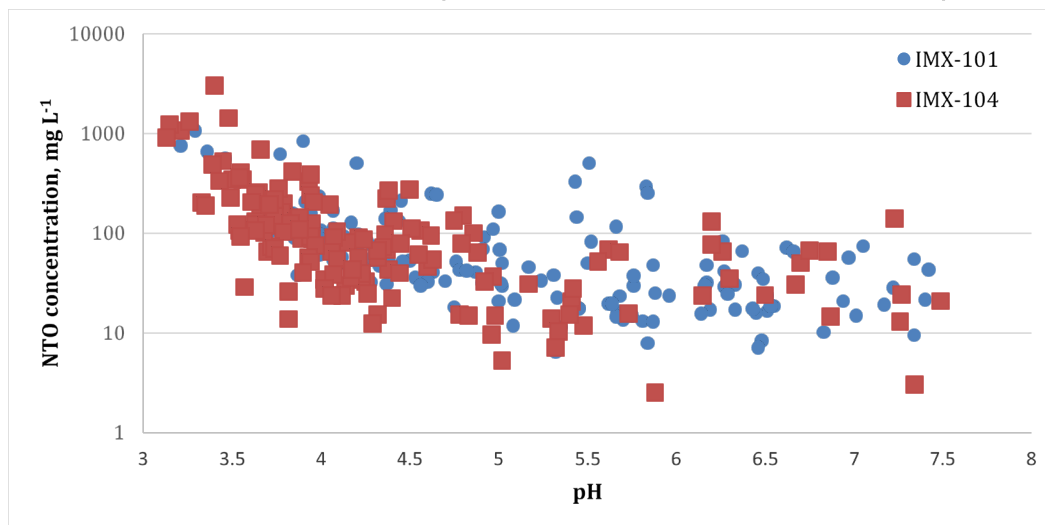


Figure 28. The relationship between pH and NTO concentrations for solutions resulting from dissolution of IMX-101 and IMX-104 particles. Data was combined for all studied particles.



3.3.4 Mass balance

The weight of IM formulation particles decreased with time and rainfall. Lab dissolution studies for traditional munitions (Taylor et al. 2009) and IMX-101, IMX-104, and PAX-21 (Taylor et al. 2015a) showed good mass balance with all mass loss for the particles recovered in solution. However, in outdoor experiments in New Hampshire for both traditional munitions and IM, while there was a linear relationship between mass loss in the particles and recovery in solution, the slope was less than one, indicating that there was some amount of energetics that was lost from the particle but not recovered in solution by HPLC analysis (Chapter 1). This mass loss was attributed to phototransformation of energetics and formation of volatile and unknown products of phototransformation. In New Hampshire for the traditional munitions, on average $83.5 \pm 4.4\%$ of the original mass lost from the particle was not recovered in solution (Chapter 1) while the IM munitions percent was lower ($18.7 \pm 3.7\%$) due to higher solubility and faster dissolution of IM components, such as NTO, NQ, and AP (Chapter 1). In Arizona, the percent of IM explosives not recovered was higher at $22.8 \pm 17.8\%$ but not significantly different than in New Hampshire (Table 8). In addition, in New Hampshire there was no difference between formulations in amount of IM components that were not recovered.

Table 8. Removal of IM constituents in solution, percent of original present in the particle, after 390 days of exposure to sunlight and rainfall outdoors.

Sample Name	Initial mass (g)	Final mass (g)	Difference (g)	Dissolved Mass (g)	Missing Mass (g)	Dissolved Mass/Difference
IMX-101 MA	0.7764	0.3190	0.4574	0.1808	0.2766	0.40
IMX-101 MB	0.4783	0.3237	0.1546	0.1305	0.0241	0.84
IMX-101 MC	0.3985	0.2983	0.1002	0.0808	0.0194	0.81
IMX-101 FA	0.6943	0.5028	0.1915	0.1039	0.0876	0.54
IMX-101 FB	2.6151	2.2553	0.3598	0.3079	0.0519	0.86
IMX-101 FC	0.6396	0.4903	0.1493	0.1159	0.0334	0.78
Mean						0.70
CI ^a						0.15
IMX-104 MA ^b	0.2036	0.1214	0.0822	0.0741	0.0081	0.90
IMX-104 MB	0.7192	0.5639	0.1553	0.1157	0.0396	0.74
IMX-104 MC	0.1718	0.1200	0.0518	0.0391	0.0127	0.75
IMX-104 FA	0.8688	0.4544	0.4144	0.2398	0.1746	0.58
IMX-104 FB	0.9744	0.3144	0.6600	0.1907	0.4693	0.29
IMX-104 FC	0.8604	0.4858	0.3746	0.1089	0.2657	0.29
Mean						0.59
CI						0.20
PAX-21 MA	0.3345	0.2533	0.0812	0.0780	0.0032	0.96
PAX-21 MB	0.3089	0.2520	0.0569	0.0925	-0.0356	1.63
PAX-21 MC	0.3360	0.2565	0.0795	0.1284	-0.0489	1.61
PAX-21 FA ^c	1.1052	0.6808	0.4244	0.1845	0.2399	0.43
PAX-21 FB	2.2643	1.4603	0.8040	0.6624	0.1416	0.82
PAX-21 FC	0.9270	0.5633	0.3637	0.2359	0.1278	0.65
Mean						1.02
CI						0.40

^a Confidence interval

^b The sample was damaged, and the last weight measurement was taken on day 223.

^c The sample was damaged, and the last weight measurement was taken on day 148.

Taylor et al. (2010) demonstrated for the traditional formulations that the largest particles lose the most mass, but small chunks lose a larger percentage of their initial mass due to a larger ratio of surface area to mass. Using data collected by Dr. Taylor, we observed a significant linear relationship between mass loss and initial particle mass ($p = 0.00238$) and significant negative correlation between mass loss as a fraction of the original mass (normalized mass loss) and original mass ($p = 0.00444$), though power function better described the second trend (Figure 29a and b). The linear relationship between mass loss and original mass was also observed for IM in New Hampshire (Taylor et al. 2015a) and Arizona ($p =$

3.89×10^{-10} and 2.71×10^{-7} for New Hampshire and Arizona, respectively) (Figure 29c and f). However, the slopes were 9 to 20 times larger than for traditional munitions, indicating larger mass loss (faster dissolution and transformation). The relationship between normalized mass loss and original mass was weaker for IMs (Figure 29d and g); there was a significant negative correlation for New Hampshire data ($p = 0.0430$), but the relationship was not significant for Arizona data ($p = 0.948$). The patterns were similar across all three IM formulations studied in Arizona. The slope for mass loss vs. original mass was significantly higher for New Hampshire (0.67 ± 0.06) than for Arizona (0.30 ± 0.07), indicating a greater amount of mass loss. The difference can probably be explained by the shorter duration of the experiment (13 vs. 29 months) as the ratios between time of exposure and slopes between the two locations are almost identical ($29 \text{ months} / 13 \text{ months} = 2.23$ and $0.67/0.30 = 2.23$).

In experiments conducted in Arizona, we also observed that there was a linear relationship between particle mass loss and energetics concentrations in solutions for each particle (Figure 30) as demonstrated by Taylor et al. (2010) for traditional munitions in New Hampshire. It was not possible to develop the same relationship for IMs in New Hampshire due to the fragility of the particles. However, by placing particles in the mesh cradles in Arizona experiments, we were able to weight them without disturbing them. Results showed that the slope of this relationship between particle mass loss and energetics recovery in solutions was smaller than one, 0.70 ± 0.16 for IMX-101, 0.79 ± 0.12 for IMX-104, and 0.86 ± 0.28 for PAX-21, much higher than for traditional munitions, which varied between 0.16 and 0.40. There was not a significant difference between IM formulations.

Figure 29. The relationship between particle size and mass loss of the particles for outdoor dissolution of traditional and insensitive munitions in New Hampshire and Arizona. Data for traditional munitions is from Taylor et al. (2010) and for IMs from Taylor et al. (2015a).

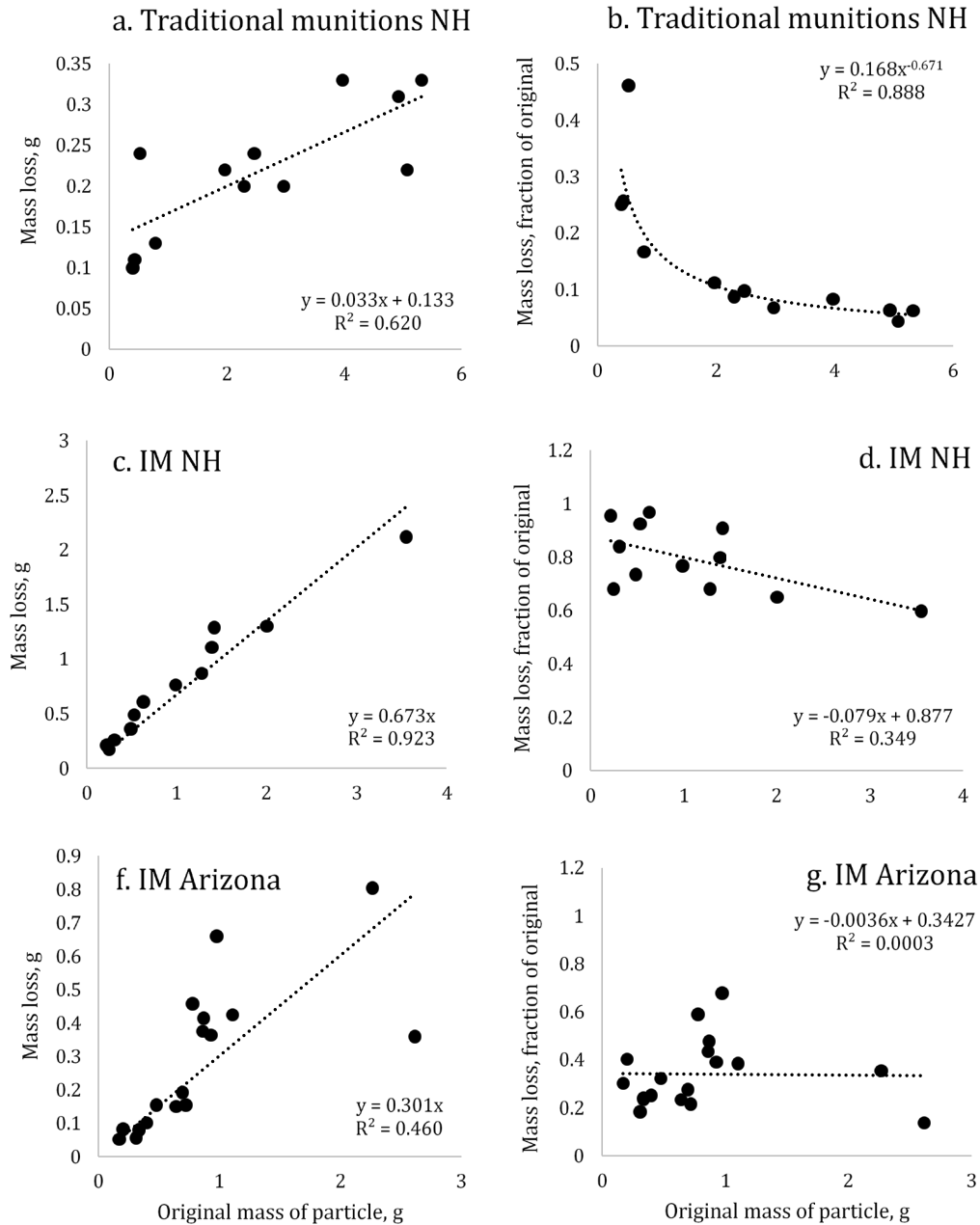
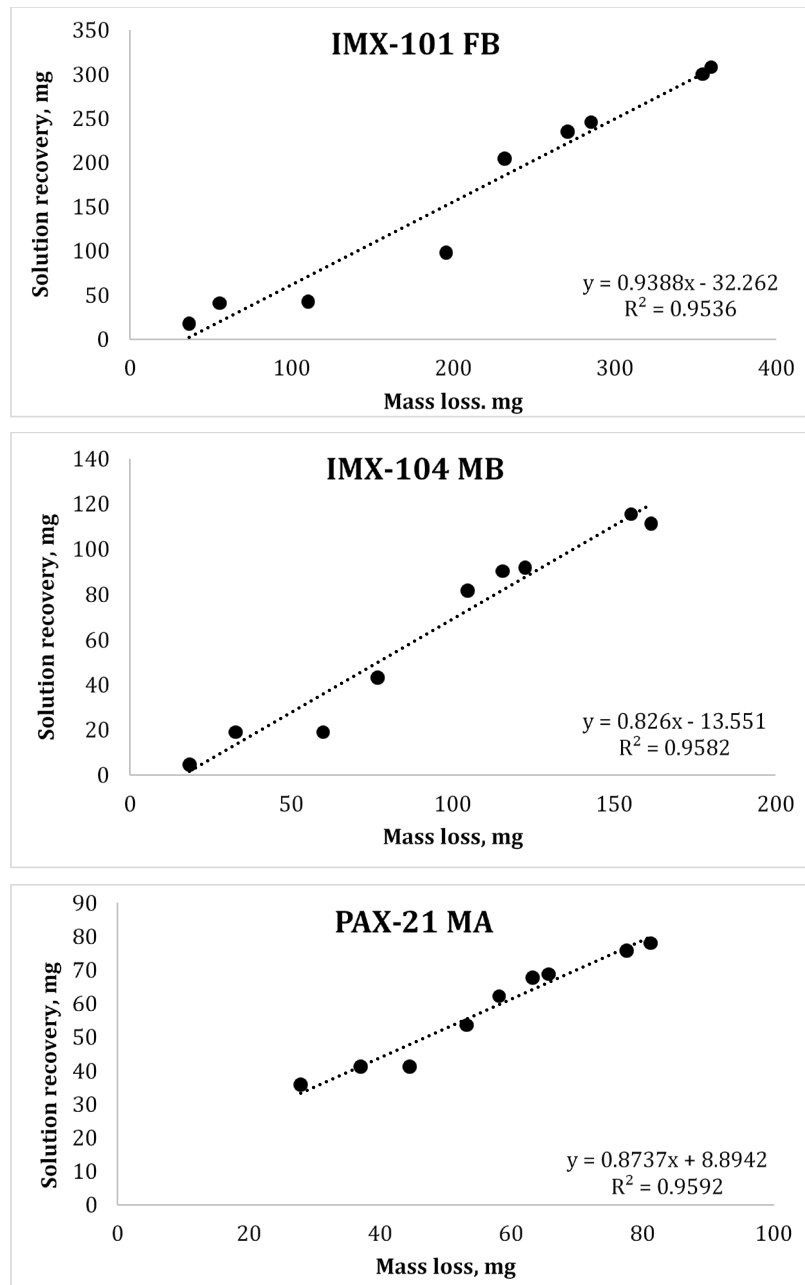


Figure 30. The relationship between mass loss during particle dissolution and phototransformation and recovery of products of dissolution and phototransformation in solution analyzed by HPLC, using IMX-101 FB, IMX-104 MB, and PAX-21 MA particles as examples.



3.4 Conclusions

We conducted outdoor dissolution and phototransformation experiments for particles (as manufactured and resulting from low-order detonations) of IMX-101, IMX-104, and PAX-21 formulations. We observed the release of formulation constituents in solution and mass loss of the particles as a

result of dissolution and phototransformation. IM constituents dissolved in order of their solubility, with the most soluble compounds dissolving first. NTO dissolved first from IMX-101 followed by NQ and DNAN; in IMX-104, NTO was followed by DNAN and RDX; and in PAX-21, AP was followed by DNAN and RDX in about the same concentrations. Comparison between different formulations and compounds indicated that, in addition to solubility, a factor that apparently influenced dissolution was crystal size of the constituents. Presence of smaller crystals with larger specific surface area resulted in greater dissolution relative to the amount in the formulation. Constituents with high solubility, NTO, NQ, and AP, exhibited nonlinear increase with cumulative rainfall that particles were exposed to, with faster initial dissolution when crystals on the particle surface were dissolving. Over time, as surface crystals were removed and crystals deeper within the particle were dissolving, release of these compounds into solution slowed down due to time needed for these constituents to diffuse to the particle surface. This trend is different from what was previously observed for the traditional munitions and more similar to behavior of propellants because of the large difference in solubilities of the DNAN matrix and NTO, NQ, and AP explosive fill. DNAN and RDX exhibited linear dissolution with rainfall. There was a trend for decrease in concentration of dissolving compounds in solution with increase in rainfall intensity. That would indicate that small intensity rains spread over time would dissolve more of IM constituents compared to few large rainfall events of the same total volume.

The mass of the particles decreased with time, but mass loss was not recovered completely in collected solution when analyzed by HPLC. Larger particles lost more mass; but unlike traditional munitions, when normalized to the original mass, the amount lost was not inversely related to particle size. More mass relative to the original was lost in the experiment conducted in New Hampshire than in the current experiment, but the difference was consistent with the shorter duration of the Arizona experiment. There was also a significant positive correlation between the amount lost and recovery of the constituents and their known transformation products in solution. The slope was larger (higher recovery) than was measured for traditional explosives, likely due to faster dissolution of IM compounds. There was no difference in this relationship between the three studied formulations.

We recovered products of DNAN transformation: 2-ANAN and 4-ANAN. Their percentage relative to DNAN changed over time but was between one and two percent of DNAN concentrations on average for all three formulations. We also detected HMX present in IMX-104 and PAX-21 formulations as an admixture in RDX. HMX recovery was similar for the two formulations and was consistent with the known content of HMX in technical-grade RDX. We also measured inorganic nitrogen ions, nitrate and ammonium, which are possible products of NTO and DNAN transformation, but could not attribute them positively to explosives transformation due to their presence in blank solutions without any explosives.

This study further examined dissolution and transformation of IM munitions when exposed to rainfall and sunlight outdoors, simulating behavior of IM residues during use on training grounds. Obtained data and established relationships between measured parameters help predict the release of IM energetics and the impact of IM deposition on contamination of the environment.

4 Dissolution and Transport of Insensitive Munitions Formulations IMX-101 and IMX-104 in Saturated Soil Columns

By Jennifer D. Arthur, Noah W. Mark, Susan Taylor, Jiri Šimůnek, Mark L. Brusseau, and Katerina M. Dontsova⁹

4.1 Introduction

As particles of IM dissolve in rain water, solutions of IM constituents enter the soil. Here, they can be adsorbed and transformed, resulting in their natural attenuation. Fate of munition compounds in the soils may depend on their concentration and their pattern of dissolution. We have previously examined adsorption and transformation of IM constituents in batch and column studies and developed relationships between soil properties and transport parameters for NTO and DNAN (Dontsova et al. 2014; Mark et al. 2016, 2017; Arthur et al. 2017). However, we need to determine if solutions resulting from dissolution of IM formulations would exhibit the same behavior in soils as solution of pure NTO and DNAN.

The objective of our study was to examine the dissolution and fate (adsorption and mass loss) of IMX-101 and IMX-104 in two soils collected from military training ranges in Camp Swift, Texas, and Camp Guernsey, Wyoming. The results are assessed and compared to the individual compounds that are part of the IM formulations; and we discuss the implications of correlations between dissolution, fate, and transport parameters and soil properties for IMX-101 and IMX-104.

4.2 Method

4.2.1 Soils

Camp Swift (Bergstrom sandy clay loam, mixed, superactive, thermic Cumulic Haplustolls) and Camp Guernsey (Keeline-Turnercrest loam, mixed, superactive, calcareous, mesic Ustic Torriorthents) were the soils used for this experiment. These two soils were previously used in batch and column transport experiments conducted with NTO and DNAN (Dontsova et al.

⁹ This material is a part of the dissertation defended by Jennifer Arthur as one of the requirements for her PhD degree.

2014; Mark et al. 2016, 2017; Arthur et al. 2017). We selected these soils for their low organic matter content to provide a conservative estimate of soil attenuation of IM compounds. Soil samples were collected to a depth of 30 cm at Camp Swift, Texas, and Camp Guernsey, Wyoming, with the location used as the soil name. Soils were air-dried and sieved (<2 mm) prior to being analyzed for pH, electrical conductivity, cation exchange capacity, organic carbon (OC) content, and clay mineralogy (Mark et al. 2016) (Table 9). Both soils had high pH and low OC content but differed in their particle size. Camp Swift has high clay content, and Camp Guernsey is a sandy soil.

Table 9. Measured physical and chemical properties of soils used in dissolution and transport studies with IMX-101 and IMX-104 (Mark et al. 2016).

Soil	Texture	Clay (%)	Silt (%)	Sand (%)	pH ^a	EC ^b ($\mu\text{S cm}^{-1}$)	SSA ^c ($\text{m}^2 \text{g}^{-1}$)	OC ^d (%)	CEC ^{8.2e} (cmol kg^{-1})	Mineralogy ^f
Camp Swift	sandy clay loam	23.7	20.8	55.6	7.83	203	15.1	0.34	6.5	K,M,S,Q
Camp Guernsey	loam	4.1	12.5	83.4	8.21	477	3.9	0.77	2.9	S,M,K,C,Q

^a In 1:1 soil:water

^b EC = Electrical conductivity

^c SSA = specific surface area

^d OC = organic carbon

^e CEC^{8.2} = cation exchange capacity at pH 8.2

^f Mineralogy is listed in order of decreasing content: C = chlorite, K = kaolinite, M = mica, Q = quartz, S = smectite.

4.2.2 Column experiments

We conducted saturated flux-controlled flow column experiments under steady-state and transient conditions to measure dissolution and transport behavior of IMX-101 and IMX-104. We used Supelco (Belfonte, PA) glass columns with an internal diameter of 1.18 cm and 7 cm length. Columns were packed with Camp Guernsey and Camp Swift soils. Small increments of soil were added to each column during packing to ensure even distribution and to minimize preferential flow. Glass wool was placed on the top and bottom of the soil profile to prevent soil movement. The average packed bulk density (ρ_b) was $1.61 \pm 0.05 \text{ g cm}^{-3}$ for Camp Guernsey soil and $1.51 \pm 0.04 \text{ g cm}^{-3}$ for Camp Swift soil. The bulk density was determined from the dry mass of the soil used to pack the glass columns of known volume.

Columns were saturated from bottom to top with 0.005 M CaCl_2 background solution for 1 hr to avoid air entrapment. Pore volume of the

columns was determined by the volume of solution necessary to fill the packed column. After this, about 50 mg of undetonated and detonated IMX-101 and IMX-104 were placed on top of the column on a layer of glass wool (Figure 31). Technical grade IMX-101 and IMX-104 used in the experiments (undetonated samples) were provided by the US Army Armament Research, Development, and Engineering Center (ARDEC), Picatinny Arsenal, while detonated samples were residues of low-order detonations.

Figure 31. Image of IMX-101 on top of the soil profile during dissolution experiments.



PTFE caps sealed the tops of the columns, and Tygon microbore tubing connected PTFE caps with the Cole-Parmer (Vernon Hills, IL) Masterflex peristaltic pump, which supplied solution. Columns were connected to the pump on the top, and flow was started. Pump flow rate was calibrated for a target flow rate of 0.01 mL min^{-1} or 0.55 cm hr^{-1} before the start of the experiments. The measured average flow rate was $0.008 \pm 0.001 \text{ mL min}^{-1}$ with Darcy flux of $0.42 \pm 0.05 \text{ cm hr}^{-1}$. After 3–5 pore volumes for IMX-101 (5–8 pore volumes for IMX-104), depending on the soil, IM particles were removed, and flow was switched to background solution (0.005 M CaCl_2) that was applied for another 3–5 pore volumes to monitor the elution of the explosives from the soil. In addition, we conducted flow interruption studies where flow was stopped for 24 hr to allow the explosives to equilibrate with the soil. This technique is used to differentiate between mechanisms responsible for sorption nonequilibrium (Brusseau et al. 1989, 1997).

Effluent samples were collected continuously into 4 mL amber vials using a Teledyne ISCO (Lincoln, NE) Foxy 200 Fraction collector with a 200-vial capacity. Conservative tracer, Br^- , in the effluent was analyzed using IC

(Dionex ICS 5000 with diode array) to determine the longitudinal dispersivity (λ) and to observe for preferential flow for each soil, while HPLC was used to quantify eluting IM components as described below. Once experiments ended, columns were subdivided into thirds (top, middle, and bottom), and soil extractions were performed using acetonitrile. A 1:2 soil to acetonitrile suspension was agitated for 24 hr, centrifuged and filtered using a 0.45 μm Millex-HV PVDF filter (EMD Millipore Darmstadt, Germany) (US Environmental Protection Agency 1994) followed by HPLC analysis.

Eight columns were used for each continuous flow dissolution study experiment with two replicate experiments for each explosive treatment. A total of twenty-four columns were packed with either Camp Swift or Camp Guernsey soil.

4.2.3 Analytical method

Column effluent was analyzed for energetic compounds and their transformation products using Dionex Ultimate 3000 HPLC equipped with a diode array detector (ThermoFisher, MA). The running method for NTO was adapted from Le Campion et al. (1999a). The parameters used for analyzing NTO samples were mobile phase ratio of acetonitrile: deionized water (75:25) with 0.1% TFA run isocratically at 1 mL min⁻¹. Oven temperature was set at 32°C. NTO and its transformation products were separated using a Thermo Scientific Hypercarb Column. NTO was detected at approximately 2.8 min using a 315 nm wavelength. The UV detector was set at 220 nm to monitor for the presence of ATO (Le Campion et al. 1999a). No ATO was detected. The operational method for DNAN, RDX, NQ, HMX, and DNAN transformation products was adapted from Olivares et al. (2013). To analyze these samples, we used a mobile phase ratio of 43:57 methanol and water, the Thermo Scientific Acclaim reversed phase column C-18 with 5 μm particle size, and a flow rate of 1 mL min⁻¹. The wavelengths used for detection and quantification were 300 nm for DNAN and NQ; 254 nm for 2-ANAN, 4-ANAN, RDX, and HMX; and 210 nm for DAAN. The retention times for each compound on HPLC were for DNAN approximately 21 min, 11 min for 2-ANAN, 6 min for 4-ANAN, 8 min for RDX, 5 min for HMX, and 3 min for NQ. Detection limits were 0.015 mg L⁻¹ for DNAN, 2-ANAN, 4-ANAN, NQ, RDX, and HMX and 0.020 mg L⁻¹ for NTO.

4.2.4 Numerical analysis

We analyzed all experiments by using the HYDRUS-1D code for simulating the one-dimensional movement of water, heat, and multiple solutes in variably saturated porous media (Šimůnek et al. 2008; Šimůnek and van Genuchten 2008). The software was used in the inverse mode to analyze breakthrough curves (BTCs) obtained in the column experiments. HYDRUS-1D was modified to also estimate dissolution rate of explosive materials in solid form. Previous studies (Dontsova et al. 2006, 2008, 2009; Taylor et al. 2012) have used this modification to estimate the dissolution rates of energetic materials—explosives and propellants. Our analysis of BTCs used the advection-dispersion equation for the Br⁻ tracer and the equilibrium sorption model (with decay) for explosives and their transformation products.

4.2.4.1 Nonreactive solute

The advection-dispersion equation can best describe the transport behavior of the Br⁻ tracer. The equation describes the constant water content, dispersion coefficient, and flux density:

$$\partial C / \partial t = D(\partial^2 C / \partial z^2) - \partial q C / \partial z, \quad (1)$$

where

- C = the concentration of the solution (M L⁻³);
- z = the spatial coordinate (l); and
- D = the dispersion coefficient, which accounts for both hydrodynamic and molecular dispersion (l² T⁻¹), which is represented in equation 2.

$$D = \lambda v + D^*, \quad (2)$$

where

- q = the volumetric fluid flux density (l T⁻¹) evaluated by Darcy–Buckingham law,
- v = the average linear velocity (l T⁻¹),
- λ = the longitudinal dispersivity (l), and
- D^* = the effective diffusion coefficient (l² T⁻¹).

4.2.4.2 Dissolution

For explosive materials in this study, the DNAN, NTO, NQ, HMX, and RDX dissolution rate, Y , was defined as

$$Y = \max(Y_{max}e^{-\chi t}, aY_{max}), \quad (3)$$

where

- Y_{max} = the initial dissolution rate ($\text{mg L}^{-1} \text{hr}^{-1}$),
- χ = the decay constant (T^{-1}),
- a = the dimensionless constant that defines the minimum dissolution rate or steady-state dissolution rate (aY_{max}) as a fraction of the initial or maximum dissolution rate (Y_{max}), and
- t = time (T).

If $Y_{max}e^{-\chi t} > aY_{max}$, then $Y_{max}e^{-\chi t}$ is used in the equation. If $Y_{max}e^{-\chi t} < aY_{max}$, then aY_{max} is used in the equation. Results of the dissolution rates are calculated relative to the mass of the IMX-101 or IMX-104 added to the column (Taylor et al. 2012).

4.2.4.3 Reactive transport

The transport of explosives was best described by equilibrium sorption with decay. Sorption, S (MM^{-1}), is assumed to be instantaneous and is defined as

$$S = K_d C, \quad (4)$$

where K_d is the linear adsorption coefficient ($\text{l}^3 \text{M}^{-1}$). The transport equation is then as follows for flux density, constant water content, dispersion coefficient, bulk density, and distribution coefficient:

$$\frac{\partial \theta C}{\partial t} = D * \left(\frac{\partial^2 C}{\partial z^2} \right) - \frac{\partial q C}{\partial z} - \frac{\rho b \partial S}{\partial t} - \varphi - + Y \theta, \quad (5)$$

where φ is the sink/source term, which accounts for zero, first-order, and other reactions ($\text{M l}^{-3} \text{T}^{-1}$). In this model, φ is the first-order rate constant for the solution only ($\text{M l}^{-3} \text{T}^{-1}$):

$$\varphi = k \theta C, \quad (6)$$

where

- k = the mass-loss rate coefficient due to transformation and/or irreversible adsorption (T^{-1}),
- θ = the volumetric water content ($l^3 l^{-3}$),
- γ = the dissolution rate as described in equation 2 ($mg L^{-1} hr^{-1}$),
and
- ρ_b = the bulk density ($g cm^{-3}$).

C was defined previously.

4.2.4.4 Parameter estimation

We performed numerical analysis of the experimental data by first using the nonreactive tracer bromide (Br^-) to estimate the longitudinal dispersivity, λ (cm). The equilibrium sorption with decay model was used to analyze explosive BTCs. The dispersivity was then a fixed value determined for the tracer. We estimated the following parameters for explosives: K_d ($L kg^{-1}$) and dissolution parameters, Y_{max} , Y_{min} ($mg L^{-1} hr^{-1}$), and χ . The mass-loss-rate coefficient for the dissolved phase, k (hr^{-1}) (degradation rate), was set to be equal to one determined from batch studies for DNAN (Arthur et al. 2017) and NTO (Mark et al. 2016) and derived from literature for NQ, RDX, and HMX. It was estimated by HYDRUS-1D for 2-ANAN and 4-ANAN. The 95% confidence intervals and R^2 values for fitted parameters were obtained by analyzing the observed and predicted breakthrough concentrations. Parameter estimates were considered significant if they were different from zero. Mass-balance calculations were performed for all IM components by integrating each BTC, performing soil extractions, and extracting the remaining IM particles.

4.3 Results

4.3.1 Breakthrough curves

Measured Br^- BTCs were all symmetrical and well described using the advection-dispersion transport model (Figures 32, 33, 35, and 36). Longitudinal dispersivity was slightly larger for the coarser Camp Guernsey soil (0.57 ± 0.57 cm) than for the finer Camp Swift soil (0.20 ± 0.23), but differences were not significant (Tables 11 and 12). BTCs for the conservative tracer occurred at 1 pore volume (~ 420 min), which indicates a lack of preferential flow or air entrapment or both within the column.

All IMX-101 components, NTO, NQ, and DNAN, as well as 2-ANAN and 4-ANAN, transformation products of DNAN, were observed in the effluent from both detonated and undetonated IMX-101 (Figure 32). The 2-ANAN and 4-ANAN, which were not detected in batch experiments, were observed before in DNAN column experiments (Arthur et al. 2017). Behavior of NTO, NQ, and DNAN was consistent with previously determined NQ (Haag et al. 1990; Dontsova et al, 2007; Taylor et al, 2012), DNAN (Arthur et al.2017), and NTO (Mark et al. 2016) fate and transport parameters and agreed with patterns of IMX dissolution observed in laboratory drip studies (Taylor et al. 2013, 2015b). The IM constituents BTCs followed a general pattern of a high initial peak in effluent concentration followed by fast decrease and relatively steady-state (though still decreasing) concentrations after that. This pattern was very pronounced for NTO and NQ while DNAN effluent concentrations were relatively constant once breakthrough occurred.

For NTO, we observed breakthrough with the tracer for all IMX-101 experiments, detonated and undetonated, with and without flow interruption (Figures 32 and 33). NTO also had the highest maximum outflow concentrations in all experiments despite representing only 19.7% of the total mass of IMX-101. The high concentrations of NTO seen in the effluent are consistent with its high solubility and with laboratory drip studies (Taylor et al. 2013, 2015b). The arrival of NTO on the BTC was at the same time as the nonreactive tracer Br^- (Figures 32, 33, 35, and 36). This indicated that NTO was not adsorbing to the soil. In solution, NTO is in its deprotonated form and is negatively charged at environmentally relevant pHs (Smith and Cliff 1999). Previous research conducted on soil adsorption of NTO showed high mobility and low sorption (Braidia et al. 2012; Hawari et al. 2012; Richard and Weidhaas 2014; Mark et al. 2016). NTO K_d 's were not significantly different from zero in HYDRUS-1D simulations for IMX-101 and therefore were set to zero (Table 10).

Figure 32. Breakthrough curves for individual explosives for detonated IMX-101 in Camp Swift soil: NTO, 3-nitro-1, 2, 4-triazol-5-one; NQ, nitroguanidine; DNAN, 2, 4-dinitroanisole; 2-ANAN, 2-amino-4-nitroanisole; and 4-ANAN, 4-amaino-2- nitroanisole. The *vertical gray solid line* indicates a switch to background solution.

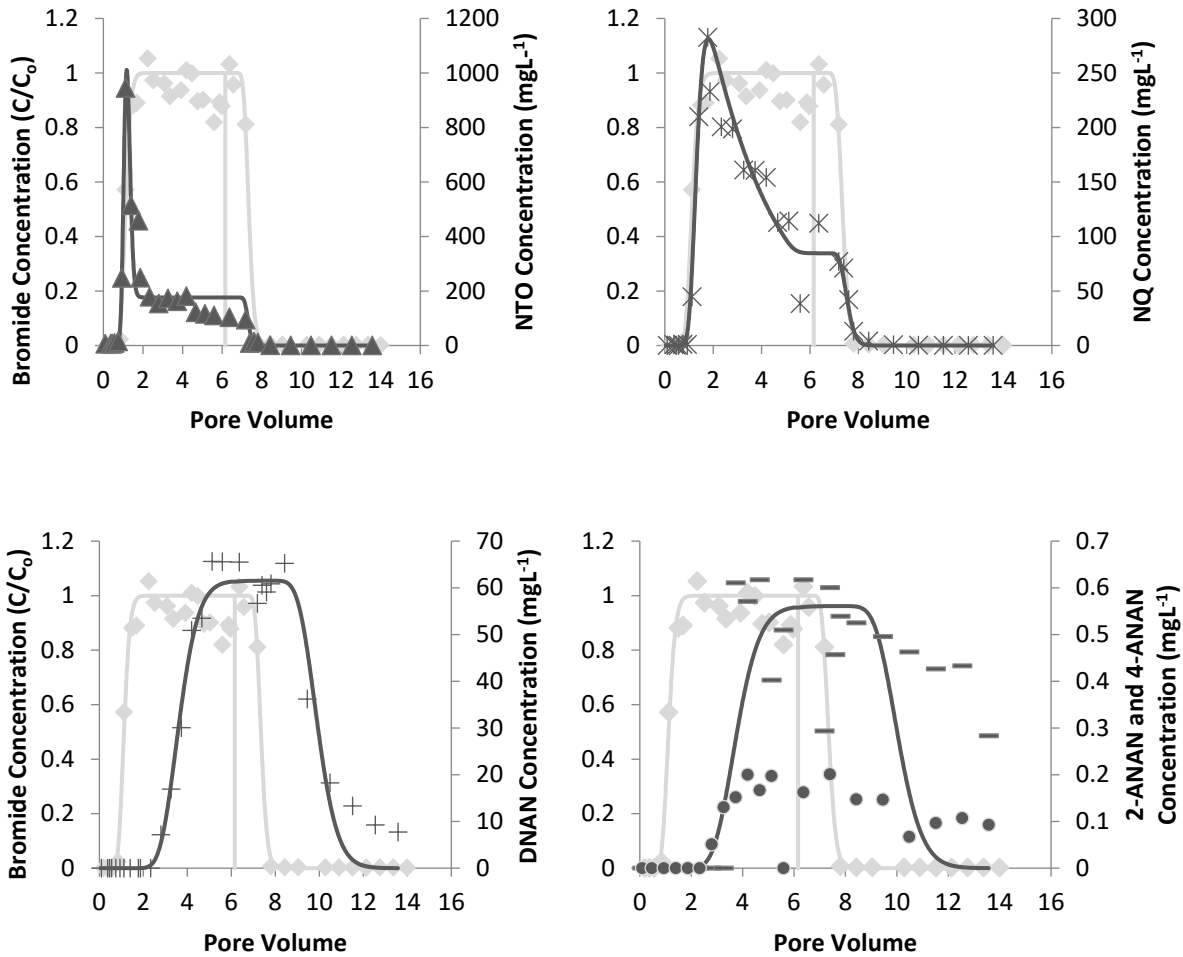


Table 10. The Y_{max} , χ , and Y_{min} estimates obtained from Taylor et al. 2015b for IMX-101 and IMX-104.

Formulation	Compound	$Y_{max}(\text{mg L}^{-1} \text{ hr}^{-1} \text{ mg}^{-1})$	$\chi(\text{hr}^{-1})$	$Y_{min}(\text{mg L}^{-1} \text{ hr}^{-1} \text{ mg}^{-1})$
IMX-101	NTO	0.1180	0.0001	0.0028
	NQ	0.0793	0.0000	0.0048
	DNAN	0.2973	0.0000	0.0585
IMX-104	RDX	0.465	0.000	0.131
	HMX	0.065	0.000	0.010
	DNAN	1.121	0.000	0.234
	NTO	0.416	0.003	0.000

NQ was the second compound to break through (Figure 32). It is similar to NTO in that it is a relatively inert compound in soil environments. NQ also arrived with the nonreactive tracer Br^- on the BTC (Figure 33), indicating that NQ was not adsorbing to the soil. Previous research has indicated limited adsorption of NQ to soil and little degradation/transformation (Haag et al. 1990; Dontsova et al. 2007, 2008; Taylor et al. 2012). IMX-101 is composed of 36.8% NQ; however, the initial peak concentrations of NQ were lower than those of NTO. The solubility of NTO is four times higher than NQ (Table 1), explaining higher concentrations of NTO over NQ. K_d 's were very low compared to the range of 0.15 to 0.43 L kg^{-1} reported by Pennington et al. (2004) and 0.14 to 0.61 L kg^{-1} reported by Taylor et al. (2012) but were consistent with the Haag et al. (1990) value, which was less than 0.1 L kg^{-1} .

DNAN was the last compound to break through (Figure 32). The curve was symmetrical and indicated retardation. DNAN also had the lowest effluent concentrations. Previous research has shown that DNAN adsorbs to soil (Hawari et al. 2015; Arthur et al. 2017), and the adsorption is heavily influenced by the organic carbon and clay content in the soil. DNAN also is reduced, forming 2-ANAN and 4-ANAN (Arthur et al. 2017). K_d values estimated by HYDRUS-1D (Table 10) were closer to batch experiment K_d 's ($0.60 \pm 0.20 \text{ L kg}^{-1}$) for Camp Swift soil than estimated column experiment K_d values ($1.2 \pm 0.08 \text{ L kg}^{-1}$) (Arthur et al. 2017). The 2-ANAN and 4-ANAN were detected in column effluent and also exhibited retardation (Figure 32). They both appeared at the same time as DNAN on the BTCs for detonated and undetonated IMX-101. The 2-ANAN concentrations in the effluent were about an order of magnitude lower than DNAN concentrations. Additionally, 4-ANAN concentrations were smaller than 2-ANAN concentrations, indicating regioselectivity of DNAN amino-transformation (Hawari et al. 2015). Tailing occurred at the end of the experiments for 2-ANAN and 4-ANAN. K_d values estimated for 2-ANAN were similar to the values determined in column transport study of pure DNAN (0.43–1.93 L kg^{-1}) (Arthur et al. 2017). Estimated mass loss rates for 2-ANAN were similar to the estimated mass loss rate determined for 2-ANAN in Camp Swift soil in column transport studies ($0.03 \pm 0.04 \text{ hr}^{-1}$) (Arthur et al. 2017).

Flow interruption experiments were conducted for detonated IMX-101 only. After resuming flow after 24 hr, effluent NTO and NQ concentrations increased in both soils and then returned to steady-state values consistent

with continuing dissolution of IM particles while flow is interrupted (Figure 33). For DNAN, no clear decrease or increase in concentration was observed after flow interruption; but concentrations of its transformation products, 2-ANAN and 4-ANAN, increased immediately after flow was resumed, indicating continued transformation. Absence of a corresponding decrease in DNAN concentration was explained by a low transformation rate. DNAN also did not experience an increase in concentration following flow resumption like NTO and NQ due to the relatively slow dissolution rate of DNAN. The 2-ANAN exhibited tailing on the elution curve; however, 4-ANAN decreased in concentration (Figure 33). There were no significant differences between undetonated and detonated IMX-101 K_d values for all constituents. Furthermore, there were no significant differences between K_d values in the two soils. Transformation rates of DNAN were fixed in HYDRUS-1D simulations at the values determined in batch studies (Arthur et al. 2017) and were not allowed to change. However, good agreement between simulated and measured BTCs for experiments with flow interruption indicates that these values described observed patterns well.

The following mechanism explains the shape of the BTCs. Initially, there is dissolution of the IM constituents on the external surfaces of the IM particles, faster for more soluble components and slower for less soluble ones. It is followed by slower dissolution of constituents within the matrix, where it is limited by diffusion from the particle interior. Similar dissolution patterns have been described for propellant constituents in insoluble nitrocellulose matrix (Dontsova et al. 2009; Taylor et al. 2011, 2012) but have not previously been observed for explosive formulations (Dontsova et al. 2006). While constituent concentrations in solution and estimated dissolution parameters differed between individual columns (Table 11), HYDRUS-1D simulated Y_{max} dissolution rates had a highly significant correlation between individual components in the IMX-101 formulation, NTO and DNAN (Figure 34, $p = 0.000423$), indicating a link between dissolution of constituents from the IM particles. The Thompson tau method was used to determine outliers within the data set. Y_{max} , Y_{min} , and χ for NTO and NQ undetonated were higher than detonated (Table 11); but differences were not significant. The χ and Y_{max} for DNAN were higher, but the Y_{min} was lower in undetonated IMX-101 than detonated. Parameter estimates for IMX-101 from Taylor et al. (2015b) underestimated the dissolution in this study, possibly due to larger size and therefore lower specific surface area of the particles they used (Table 10).

Figure 33. Breakthrough curves for individual explosives for detonated IMX-101 flow interruption in Camp Swift soil: NTO, 3-nitro-1, 2, 4-triazol-5-one; NQ, nitroguanidine; DNAN, 2, 4-dinitroanisole; 2-ANAN, 2-amino-4-nitroanisole; 4-ANAN, 4-amino-2-nitroanisole. The *vertical dashed line* indicates the start of 24 hr flow interruption. The *vertical gray solid line* indicates a switch to background solution.

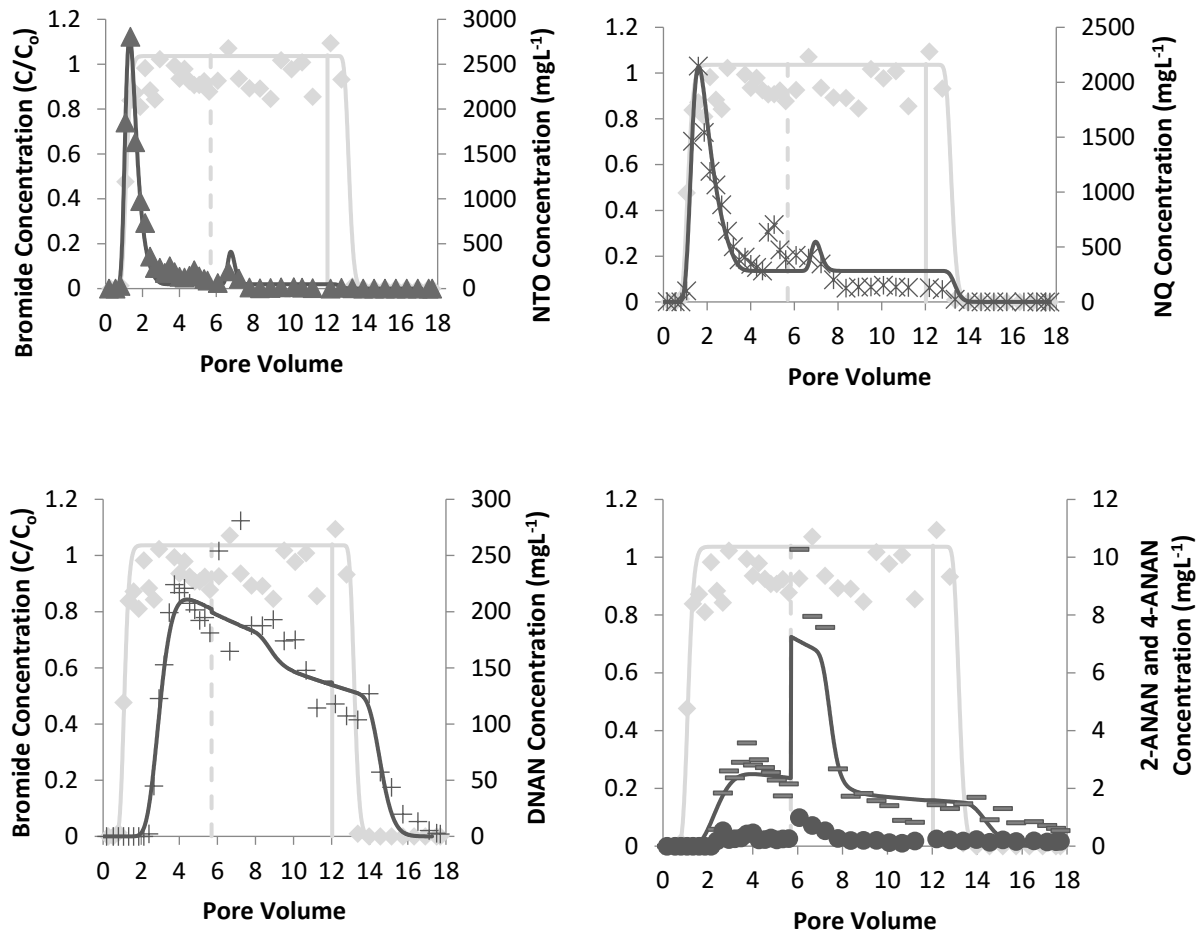


Table 11. Dissolution and transport parameters obtained by HYDRUS-1D for saturated column experiments involving Br⁻ tracer and IMX-101 (19.7% NTO, 36.8% NQ, and 43.5% DNAN) in Camp Swift and Camp Guernsey soils. λ was estimated from Br⁻ breakthrough, whereas K_d , χ , Y_{max} , Y_{min} , and mass-loss rate coefficient, k , were estimated from explosives breakthrough curves. FI = flow interruption for 24 hr, D = detonated, UD = undetonated, and NA= not applicable and K_d fixed to zero.

Soils, Treatment	Bromide			NTO								
	λ	95% CI	R^2	K_d (L kg ⁻¹)	95% CI	χ	95% CI	Y_{max} (mg L ⁻¹ hr ⁻¹ mg ⁻¹)	95 % CI	Y_{min} (mg L ⁻¹ hr ⁻¹ mg ⁻¹)	95 % CI	R^2
Camp Swift D	0.20	0.28	0.97	NA	NA	0.90	0.17	673.92	53.52	23.95	8.21	0.98
Camp Swift D	0.13	0.08	0.99	NA	NA	0.63	0.13	285.1	41.07	15.26	8.85	0.94
Camp Guernsey D	0.21	0.13	0.97	NA	NA	0.15	0.01	300.53	17.14	0.00	0.00	0.98
Camp Guernsey D	0.42	0.34	0.97	NA	NA	0.94	0.53	140.4	83.91	1.98	1.91	0.92
Mean and std. dev				NA	NA	0.66	0.36	349.99	227.68	10.30	11.34	
Camp Swift UD	0.28	0.26	0.94	NA	NA	1.34	0.50	704.13	222.19	15.03	8.15	0.97
Camp Swift UD	0.18	0.11	0.98	NA	NA	0.00	0.02	1.93	0.84	0.19	0.00	0.57
Camp Guernsey UD	0.11	0.10	0.97	NA	NA	0.28	0.06	301.66	28.43	10.84	5.61	0.99
Camp Guernsey UD	0.16	0.15	0.97	NA	NA	2.54	1.04	1333.27	472.96	19.53	6.94	0.97
Mean and std. dev				NA	NA	1.04	1.15	585.25	575.71	11.40	8.27	
Camp Swift D FI	0.92	1.80	0.71	NA	NA	0.47	0.28	941.61	491.07	2.63	9.96	0.86
Camp Swift D FI	0.11	0.13	0.98	NA	NA	0.27	0.13	1027.88	387.69	4.25	19.36	0.84
Camp Guernsey D FI	1.83	4.04	0.87	NA	NA	0.42	0.16	1240.18	319.03	3.40	17.78	0.92
Camp Guernsey D FI	0.55	0.43	0.96	NA	NA	0.20	0.02	497.14	20.92	2.25	3.60	0.98
Mean and std. dev				NA	NA	0.39	1.12	926.70	312.65	3.13	7.31	

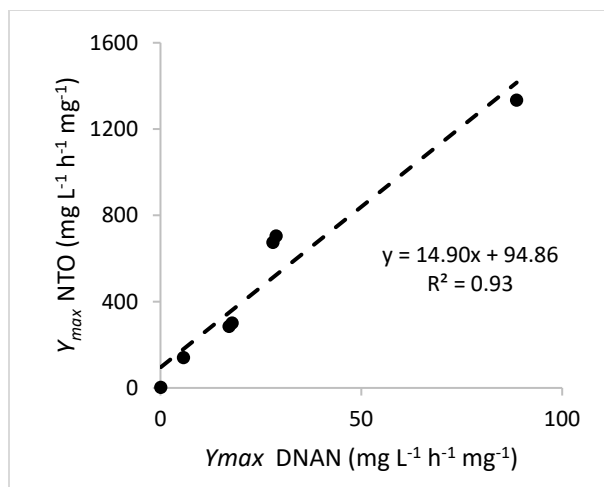
Table 11 (cont.). Dissolution and transport parameters obtained by HYDRUS-1D for saturated column experiments involving Br⁻ tracer and IMX-101 in Camp Swift and Camp Guernsey soils. λ was estimated from Br⁻ breakthrough, whereas K_d , χ , Y_{max} , Y_{min} , and mass-loss rate coefficient, k , were estimated from explosives breakthrough curves. FI = flow interruption for 24 hr, D = detonated, UD = undetonated, and NA= not applicable and K_d fixed to zero.

Soils, Treatment	NQ								
	K_d (L kg ⁻¹)	95% CI	χ	95% CI	Y_{max} (mg L ⁻¹ hr ⁻¹ mg ⁻¹)	95% CI	Y_{min} (mg L ⁻¹ hr ⁻¹ mg ⁻¹)	95% CI	R^2
Camp Swift D	0.12	0.05	0.73	1.24	303.25	439.41	18.01	26.47	0.98
Camp Swift D	0.05	0.02	0.06	0.01	37.79	2.01	9.22	2.60	0.98
Camp Guernsey D	0.10	0.09	0.32	0.69	289.77	402.78	48.86	73.14	0.96
Camp Guernsey D	0.12	0.14	1.94	14.32	77.63	610.57	0.51	4.07	0.97
Mean and std. dev	0.10	0.03	0.86	0.83	177.11	138.94	19.15	21.06	
Camp Swift UD	0.07	0.17	0.67	3.26	294.57	1278.94	12.48	73.60	0.94
Camp Swift UD	0.06	0.25	6.59	324.11	14.66	899.45	0.16	10.71	0.43
Camp Guernsey UD	0.10	0.02	0.27	0.10	186.23	40.05	8.40	4.78	0.98
Camp Guernsey UD	0.01	0.03	0.10	0.05	79.97	14.99	13.56	4.63	0.97
Mean and std. dev	0.06	0.04	1.91	3.13	143.86	122.86	8.65	6.08	
Camp Swift D FI	0.00	0.13	0.10	0.05	247.11	311.46	16.41	13.78	0.72
Camp Swift D FI	0.04	0.02	0.18	0.04	393.78	39.63	31.22	7.93	0.96
Camp Guernsey D FI	0.02	0.16	0.47	0.88	1264.35	2066.28	1.05	30.73	0.94
Camp Guernsey D FI	0.02	0.03	0.06	0.01	260.51	13.1	38.73	13.78	0.96
Mean and std. dev	0.02	0.02	0.20	0.19	541.44	486.47	21.85	16.68	

Table 11 (cont.). Dissolution and transport parameters obtained by HYDRUS-1D for saturated column experiments involving Br⁻ tracer and IMX-101 in Camp Swift and Camp Guernsey soils. λ was estimated from Br⁻ breakthrough, whereas K_d , χ , Y_{max} , Y_{min} , and mass-loss rate coefficient, k , were estimated from explosives breakthrough curves. FI = flow interruption for 24 hr, D = detonated, UD = undetonated, and NA= not applicable and K_d fixed to zero.

Soils, Treatment	DNAN									2-ANAN			
	K_d (L kg ⁻¹)	95% CI	χ	95% CI	Y_{max} (mg L ⁻¹ hr ⁻¹ mg ⁻¹)	95% CI	Y_{min} (mg L ⁻¹ hr ⁻¹ mg ⁻¹)	95% CI	R^2	K_d (L kg ⁻¹)	95% CI	k (hr ⁻¹)	95% CI
Camp Swift D	0.72	0.05	0.05	0.01	28.03	4.07	5.89	4.37	0.97	0.74	4.43	0.02	0.35
Camp Swift D	0.60	0.02	11.07	0.00	17.11	0.00	6.79	0.00	0.98	0.63	5.89	0.04	0.47
Camp Guernsey D	0.53	0.09	0.09	0.09	17.85	2.47	3.8	0.00	0.98	4.24	48.76	0.07	0.61
Camp Guernsey D	0.42	0.14	0.14	0.14	5.76	3.54	2.34	1.65	0.96	1.52	4.91	0.05	0.34
Mean and std. dev	0.57	0.13	2.84	5.49	17.19	9.10	4.71	2.01		1.78	1.69	0.05	0.02
Camp Swift UD	0.38	0.10	9.78	6189.11	31.52	19598.33	0.01	4.27	0.86	0.63	12.69	0.01	0.77
Camp Swift UD	1.14	0.20	131.63	0.00	0.11	0.00	0.02	0.02	0.55	1.99	26.65	0.00	0.22
Camp Guernsey UD	0.65	0.09	0.96	4.90	107.87	132.46	5.15	6.40	0.97	1.85	24.31	0.11	1.43
Camp Guernsey UD	0.61	0.06	1.48	8.64	88.67	633.87	7.86	56.28	0.94	1.44	12.03	0.10	0.90
Mean and std. dev	0.70	0.06	35.96	63.91	57.04	49.92	3.26	3.91		1.46	0.61	0.05	0.06
Camp Swift D FI	0.53	0.12	0.00	0.00	17.81	2.81	1.60	0.00	0.94	0.14	1.85	0.00	0.20
Camp Swift D FI	0.42	0.03	0.01	0.00	25.28	1.83	12.77	2.14	0.96	0.15	1.25	0.00	0.18
Camp Guernsey D FI	0.52	0.10	15.23	0.00	43.88	0.00	26.68	0.00	0.9	0.22	2.61	0.05	0.20
Camp Guernsey D FI	0.43	0.12	0.74	14.61	53.76	596.08	14.83	163.64	0.91	0.10	0.56	0.00	0.07
Mean and std. dev	0.48	0.04	4.00	7.50	35.18	16.54	13.97	10.28		0.15	0.05	0.01	0.03

Figure 34. Correlation between simulated Y_{max} of individual components in IMX-101 formulation from continuous flow experiments: NTO, 3-nitro-1, 2, 4-triazol-5-one, and DNAN, 2,4-dinitroanisole. The Thompson Tau method was used to reject one outlier in the data set.



IMX-104 contains 53.0% NTO, 15.3% RDX, and 31.7% DNAN, 33.3% more NTO and 11.8% less DNAN than IMX-101. The behavior of NTO was similar to that of NTO in IMX-101; however, it was retarded slightly more in both Camp Swift and Camp Guernsey soils. Similar to patterns observed for IMX-101, NTO arrived before all other IM constituents in the IMX-104 and had the highest peak and steady-state concentrations (Figure 35). NTO K_d 's ranged from 0 to 0.23 L kg^{-1} (Table 12), which in some cases was higher than K_d values obtained for NTO in the IMX-101 dissolution studies and K_d values obtained in batch study experiments performed by Mark et al. (2016). RDX was the second IM compound to break through (Figure 36). RDX exhibited retardation due to sorption, as demonstrated by the delay in RDX breakthrough relative to the conservative tracer. K_d values obtained for RDX ranged between 0.20 and 0.85 L kg^{-1} (Table 12). These values fell within the range of 0 to 8.2 L kg^{-1} RDX K_d values reported by Brannon et al. (2002) but were higher than the reported K_d values by Dontsova et al. (2006). Another propellant in the effluent was HMX. HMX is present in the original formulation as a contaminant in RDX (about 10% of the RDX amount). Concentrations of HMX in solution were smaller than those of RDX. HMX K_d 's ranged from 0.36 to 1.27 L kg^{-1} (Table 12). These values were consistent with HMX K_d values reported by Brannon et al. (2002) (<1 L kg^{-1}) and Dontsova et al. (2006) (0.22–0.36 L kg^{-1}). HMX is more strongly adsorbed by soils than RDX, DNAN, 2-ANAN, and 4-ANAN (Figure 35). Breakthrough for DNAN, 2-ANAN, and 4-ANAN occurred at about

3 pore volumes (Figure 35). All curves were asymmetrical. The arrival curve of DNAN, 2-ANAN, and 4-ANAN appeared at the same time; however, as DNAN decreased on elution, 2-ANAN exhibited tailing and 4-ANAN increased then decreased. DNAN K_d 's ranged from 0.58 to 1.47 L kg⁻¹ (Table 12) and were similar to results of batch kinetic and column transport studies of DNAN. DNAN K_d values in Camp Swift and Camp Guernsey soils were 0.60 ± 0.20 L kg⁻¹ and 0.90 ± 0.10 L kg⁻¹, respectively, and 1.2 ± 0.08 L kg⁻¹ in column studies for Camp Swift soil (Arthur et al. 2017). The 2-ANAN K_d values ranged from 0.40 to 4.88 L kg⁻¹ (Table 12).

We conducted flow interruption experiments with detonated IMX-104. Flow interruption had no effect on NTO in Camp Swift soil (Figure 36). RDX and HMX exhibited greater attenuation to the soil than did NTO. The breakthrough for RDX occurred around 2 pore volumes whereas for HMX it was at 4 pore volumes (Figure 36). HMX concentrations were lower than RDX concentrations. RDX and HMX concentrations first decreased and then increased after flow resumption. Predicted BTCs showed a smaller range of both decrease and increase, indicating that used RDX transformation rate (Brannon and Pennington 2002), as well as dissolution rate calculated using it, were lower than observed. DNAN, 2-ANAN and 4-ANAN also adsorbed to the soil as indicated by the delay in the BTC (Figure 37). Before flow interruption, DNAN and 2-ANAN concentrations decreased with time on the arrival wave. After resuming flow, DNAN concentrations slightly decreased, and 2-ANAN and 4-ANAN concentrations increased, indicating transformation in Camp Swift soil.

There were no significant correlations of K_d values between undetonated and detonated IMX-104 nor were there differences in K_d values between the two soils used in the experiments. Significant or highly significant correlations existed between estimated HYDRUS-1D values for Y_{min} NTO and Y_{min} RDX ($p = 0.0061$), Y_{max} NTO and Y_{max} DNAN ($p = 0.010$), and Y_{min} HMX and Y_{min} DNAN ($p = 0.018$) (Figure 37). The Y_{max} NTO and Y_{max} DNAN correlation was also seen in the IMX-101 studies. When comparing estimated dissolution parameters between treatments, we found that minimum dissolution rates and decay constants of NTO were lower for detonated IMX-104 than in undetonated IMX-104. The maximum dissolution rate was higher for NTO in detonated IMX-104. All three estimated parameters were higher in undetonated IMX-104 than in detonated IMX-104 for RDX. The estimated minimum dissolution rate and decay constant were higher for HMX in detonated IMX-104. The maximum dissolution

rate was higher in undetonated IMX-104. Lastly, DNAN's maximum and minimum dissolution rates were high for detonated IMX-104, and the decay constants were similar for both treatments (Table 12).

We compared these dissolution parameters to those found by Taylor et al. (2015b) and found the former to be higher. This may be due to the different size of the particles dissolved in the two studies.

Figure 35. Breakthrough curves for individual explosives for the detonated IMX-104 particle in Camp Swift soil: NTO, 3-nitro-1, 2, 4-triazol-5-one; RDX, hexahydro-1,3,5-trinitro-1,3,5-triazine; HMX, octahydro-1,3,5,7-tetranitro-1,3,5,7-tetrazocine; DNAN, 2, 4- dinitroanisole; 2-ANAN, 2-amino-4-nitroanisole; and 4-ANAN, 4-amino-2-nitroanisole. The *vertical gray solid line* indicates a switch to the background solution.

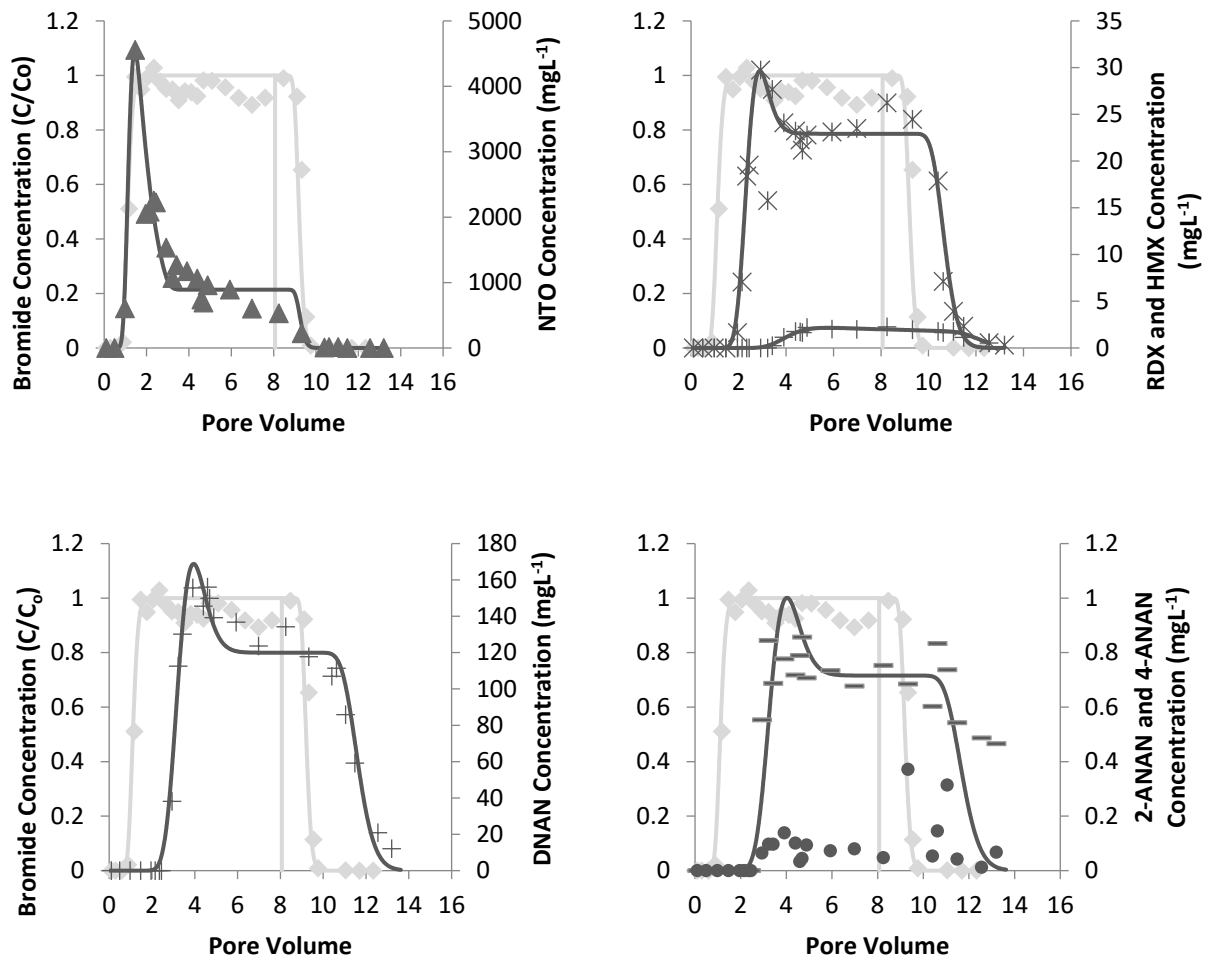


Figure 36. Flow interruption breakthrough curves for individual explosives for detonated IMX-104 particle in Camp Swift soil: NTO, 3-nitro-1, 2, 4-triazol-5-one; RDX, hexahydro-1,3,5-trinitro-1,3,5-triazine; HMX, octahydro-1,3,5,7-tetranitro-1,3,5,7-tetrazocine; DNAN, 2, 4- dinitroanisole; 2-ANAN, 2-amino-4-nitroanisole; and 4-ANAN, 4-amino-2-nitroanisole. The *vertical dashed gray line* indicates the start of 24 hr flow interruption. The *vertical solid gray line* indicates a switch to the background solution.

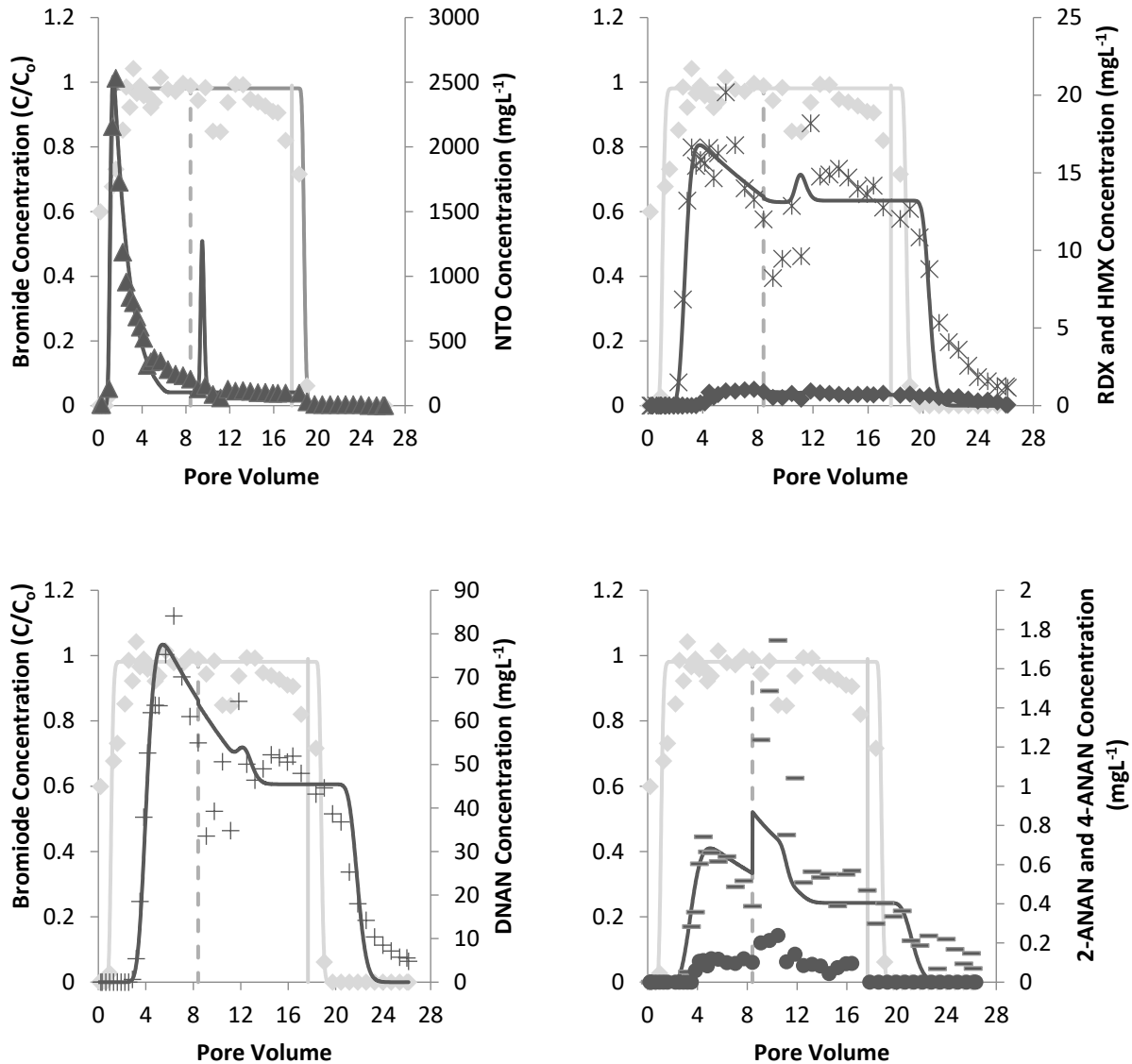


Table 12. Solute transport and dissolution parameters obtained by HYDRUS-1D for column-saturated experiments involving Br⁻ and IMX-104 (53.0% NTO, 15.3% RDX, and 31.7% DNAN) in Camp Swift and Camp Guernsey soils. λ was estimated from Br⁻ BTCs, whereas K_d , Y_{max} , Y_{min} , and mass-loss rate coefficient, k , were estimated from explosives. D = detonated, UD = undetonated, and NA = *not applicable and K_d fixed to zero.*

Soils, Treatment	Bromide			NTO								
	λ	95% CI	R^2	K_d (L kg ⁻¹)	95% CI	χ	95% CI	Y_{max} (mg L ⁻¹ hr ⁻¹ mg ⁻¹)	95% CI	Y_{min} (mg L ⁻¹ hr ⁻¹ mg ⁻¹)	95% CI	R^2
Camp Swift D	0.05	0.05	0.97	0.10	0.02	0.05	0.01	176.64	10.94	8.71	0.00	0.92
Camp Swift D	0.10	0.10	0.95	0.02	0.02	0.18	0.04	921.53	81.15	117.77	30.92	0.97
Camp Guernsey D	0.08	0.04	0.99	0.09	0.01	0.05	0.01	224.85	19.51	18.95	0.00	0.94
Camp Guernsey D	1.42	2.84	0.9	0.23	0.49	0.00	0.01	2662.67	3867.89	0.00	0.01	0.71
Mean and std. dev				0.11	0.04	0.12	0.08	996.42	1161.79	38.64	58.84	
Camp Swift UD	0.15	0.18	0.94	NA	NA	0.21	0.06	260.21	27.39	49.07	9.68	0.94
Camp Swift UD	0.10	0.10	0.96	NA	NA	0.31	0.11	953.29	157.13	64.71	73.83	0.74
Camp Guernsey UD	0.12	0.12	0.94	0.16	0.03	0.05	0.01	230.62	23.55	3.68	0.00	0.92
Camp Guernsey UD	0.50	0.42	0.97	0.11	0.08	0.24	0.27	815.38	631.54	57.18	66.66	0.88
Mean and std. dev				0.14	0.04	0.20	0.11	564.88	287.87	43.66	27.41	
Camp Swift D FI	0.07	0.09	0.94	NA	NA	0.12	0.02	447.25	34.55	14.12	7.87	0.96
Camp Swift D FI	0.12	0.17	0.96	NA	NA	0.14	0.02	1067.54	60.22	2.58	16.68	0.96
Camp Guernsey D FI	0.47	1.17	0.7	NA	NA	0.21	0.04	725.15	89.94	29.39	13.9	0.9
Camp Guernsey D FI	0.96	0.75	0.94	NA	NA	0.18	0.04	661.42	76.96	35.56	10.67	0.93
Mean and std. dev				NA	NA	0.16	0.04	725.34	257.24	20.41	14.92	

Table 12 (cont.). Solute transport and dissolution parameters obtained by HYDRUS-1D for column-saturated experiments involving Br⁻ and IMX-104 in Camp Swift and Camp Guernsey soils. λ was estimated from Br⁻ BTCs, whereas K_d , Y_{max} , Y_{min} , and mass-loss rate coefficient, k , were estimated from explosives. D = detonated, UD = undetonated, and NA = *not applicable and K_d fixed to zero.*

Soils, Treatment	RDX								
	K_d (L kg ⁻¹)	95% CI	χ	95%CI	Y_{max} (mg L ⁻¹ hr ⁻¹ mg ⁻¹)	95 % CI	Y_{min} (mg L ⁻¹ hr ⁻¹ mg ⁻¹)	95 % CI	R^2
Camp Swift D	0.85	0.09	0.04	0.02	5.61	2.04	0.03	0.00	0.81
Camp Swift D	0.37	0.06	0.49	0.17	15.06	5.08	3.03	1.04	0.95
Camp Guernsey D	0.20	0.03	0.18	57.97	0.93	26.05	0.83	21.39	0.96
Camp Guernsey D	0.40	0.20	0.00	0.02	2.80	1.44	0.01	0.00	0.90
Mean and std. dev	0.46	0.07	0.18	0.22	6.10	6.28	0.98	1.42	
Camp Swift UD	0.41	0.05	0.31	0.41	6.67	6.10	1.07	0.95	0.98
Camp Swift UD	0.40	0.03	0.42	0.66	10.67	9.10	2.99	2.70	0.98
Camp Guernsey UD	0.32	0.03	0.01	0.01	0.98	0.09	0.65	0.19	0.98
Camp Guernsey UD	0.32	0.18	0.11	0.04	535.97	457.84	144.14	153.40	0.96
Mean and std. dev	0.36	0.07	0.21	0.31	138.57	226.40	37.21	76.07	
Camp Swift D FI	0.40	0.04	0.01	0.01	2.46	0.38	1.82	0.32	0.90
Camp Swift D FI	0.46	0.06	0.07	0.15	6.92	4.79	4.15	3.01	0.94
Camp Guernsey D FI	0.44	0.13	0.39	9.25	6.75	64.21	2.79	27.78	0.85
Camp Guernsey D FI	0.56	0.19	0.15	0.93	1.28	3.04	0.57	1.47	0.83
Mean and std. dev	0.47	0.07	0.16	4.46	4.35	30.79	2.33	13.14	

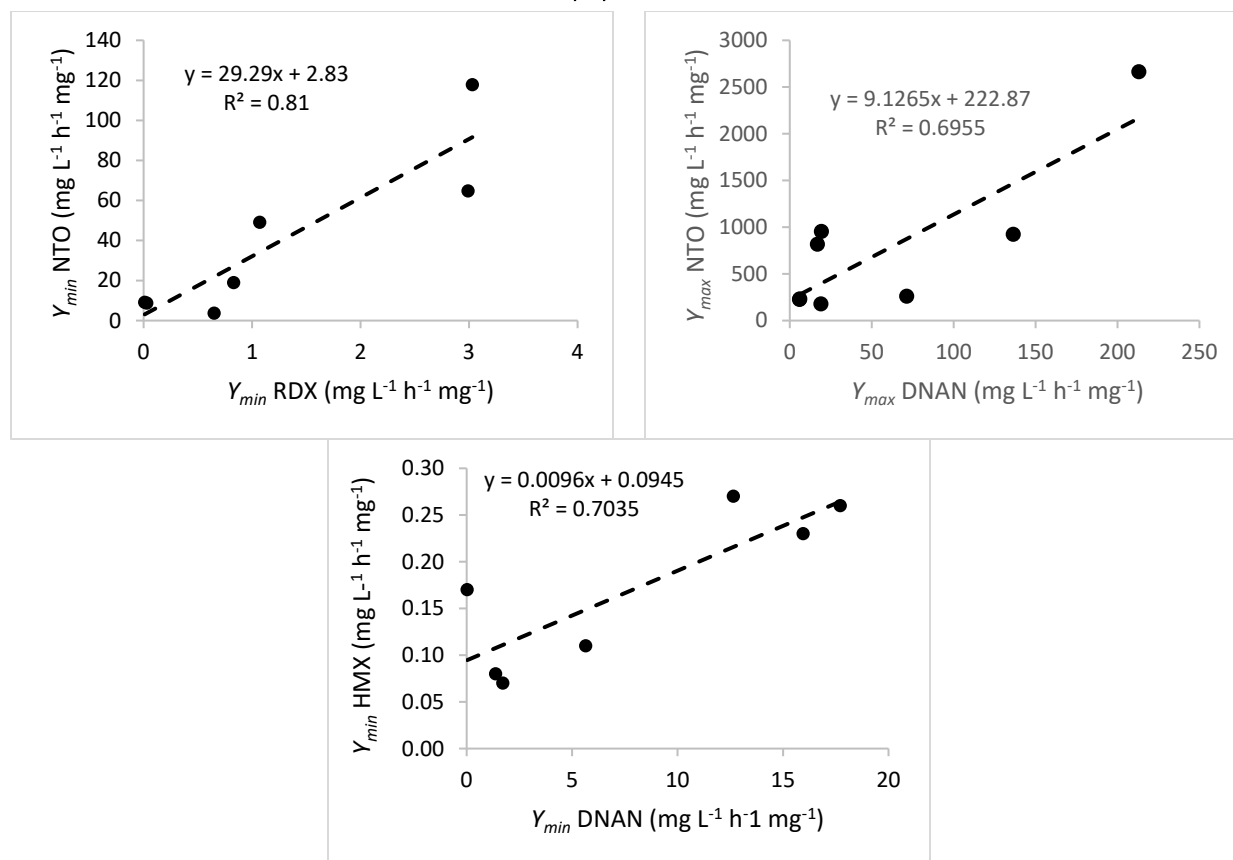
Table 12 (cont.). Solute transport and dissolution parameters obtained by HYDRUS-1D for column-saturated experiments involving Br⁻ and IMX-104 in Camp Swift and Camp Guernsey soils. λ was estimated from Br⁻ BTCs, whereas K_d , Y_{max} , Y_{min} ; and mass-loss rate coefficient, k , were estimated from explosives. D = detonated, UD = undetonated, and NA = *not applicable and K_d fixed to zero.*

Soils, Treatment	HMX								
	K_d (L kg ⁻¹)	95% CI	χ	95%CI	Y_{max} (mg L ⁻¹ hr ⁻¹ mg ⁻¹)	95 % CI	Y_{min} (mg L ⁻¹ hr ⁻¹ mg ⁻¹)	95 % CI	R^2
Camp Swift D	0.82	0.05	149.90	0.00	2.03	0.00	0.26	0.00	0.92
Camp Swift D	0.75	0.05	0.91	0.01	0.31	0.05	0.23	0.05	0.98
Camp Guernsey D	0.36	0.06	78.50	0.00	16.25	0.00	0.08	0.00	0.89
Camp Guernsey D	0.50	0.05	106.86	0.00	16.73	0.00	0.17	0.00	0.90
Mean and std. dev	0.61	0.21	84.04	62.72	8.83	8.87	0.19	0.08	
Camp Swift UD	1.16	0.52	1.95	7.12	16.53	250.79	0.11	1.63	0.79
Camp Swift UD	0.80	0.19	2.18	3.90	19.98	172.29	0.27	2.32	0.89
Camp Guernsey UD	0.68	0.05	1.24	2.41	24.21	33.51	0.07	0.12	0.90
Camp Guernsey UD	1.11	0.51	0.01	10.17	31.35	118.79	0.10	0.34	0.95
Mean and std. dev	0.94	0.23	1.35	0.98	23.02	6.38	0.14	0.09	
Camp Swift D FI	0.84	0.05	0.01	0.01	0.14	0.02	0.10	0.03	0.84
Camp Swift D FI	1.27	0.09	0.02	0.01	0.50	0.12	0.24	0.06	0.92
Camp Guernsey D FI	0.83	0.13	0.15	2.17	0.47	2.05	0.22	1.16	0.90
Camp Guernsey D FI	0.81	0.16	0.01	0.00	0.12	0.00	0.16	0.00	0.73
Mean and std. dev	0.94	0.22	0.05	0.07	0.31	0.21	0.18	0.06	

Table 12 (cont.). Solute transport and dissolution parameters obtained by HYDRUS-1D for column-saturated experiments involving Br⁻ and IMX-104 in Camp Swift and Camp Guernsey soils. λ was estimated from Br⁻ BTCs, whereas K_d , Y_{max} , Y_{min} ; and mass-loss rate coefficient, k , were estimated from explosives. D = detonated, UD = undetonated, and NA = *not applicable and K_d fixed to zero.*

Soils, Treatment	DNAN									2-ANAN			
	K_d (L kg ⁻¹)	95% CI	χ	95% CI	Y_{max} (mg L ⁻¹ hr ⁻¹ mg ⁻¹)	95 % CI	Y_{min} (mg L ⁻¹ hr ⁻¹ mg ⁻¹)	95 % CI	R^2	K_d (L kg ⁻¹)	95% CI	K (hr ⁻¹)	95% CI
Camp Swift D	0.58	0.06	0.52	0.00	19.10	0.00	17.72	0.00	0.94	0.59	19.97	0.10	3.09
Camp Swift D	0.60	0.04	0.42	0.11	136.54	45.55	15.96	5.17	0.99	0.63	6.11	0.08	0.73
Camp Guernsey D	0.60	0.03	0.01	0.01	6.01	1.01	1.38	0.00	0.95	0.49	2.75	0.13	0.60
Camp Guernsey D	1.47	0.49	0.16	0.15	213.15	297.93	0.03	0.00	0.92	4.88	40.63	0.04	0.44
Mean and std. dev	0.81	0.44	0.28	0.23	93.70	98.92	8.77	9.36		1.64	2.16	0.09	0.04
Camp Swift UD	0.74	0.08	0.90	1.07	71.50	63.80	5.65	4.97	0.97	0.79	4.61	0.00	0.31
Camp Swift UD	0.61	0.03	0.01	0.01	19.46	1.45	12.65	1.70	0.98	0.61	6.87	0.05	0.68
Camp Guernsey UD	0.96	0.04	0.03	0.01	6.23	0.82	1.72	0.00	0.97	0.94	1.49	0.06	0.15
Camp Guernsey UD	0.74	0.08	0.03	0.01	16.94	3.42	3.84	0.00	0.97	2.56	43.38	0.13	2.17
Mean and std. dev	0.76	0.15	0.24	0.44	28.53	29.21	5.97	4.74		1.23	0.90	0.06	0.05
Camp Swift D FI	0.73	0.03	0.01	0.00	12.03	0.60	6.32	0.62	0.96	0.40	4.03	0.06	0.41
Camp Swift D FI	0.70	0.03	0.01	0.00	24.90	2.61	14.70	1.71	0.96	0.70	6.47	0.06	0.43
Camp Guernsey D FI	0.60	0.06	0.20	20.93	14.46	258.95	11.36	179.89	0.96	1.18	3.16	0.04	0.09
Camp Guernsey D FI	1.03	0.10	0.01	0.00	16.87	1.91	6.48	1.57	0.95	0.62	1.61	0.05	0.09
Mean and std. dev	0.77	0.19	0.05	0.10	17.07	5.58	9.72	4.06		0.73	0.33	0.05	0.01

Figure 37. Correlations between simulated Y_{max} and Y_{min} of individual propellants in IMX-104 formulation from continuous flow experiments: NTO, 3-nitro-1, 2, 4-triazol-5-one; RDX, hexahydro-1,3,5-trinitro-1,3,5-triazine; HMX, octahydro-1,3,5,7-tetranitro-1,3,5,7-tetrazocine; and DNAN, 2, 4- dinitroanisole.



For both IMX-101 and IMX-104, we found maximum and minimum dissolution rates between some individual compounds within the IMX formulations to be related. Dissolution rates are affected by the solubility of the compound, temperature, particle size and surface area, and agitation. We maintained a constant temperature during our experiments, thus it was not a factor influencing the dissolution rate. Additionally, the solid IMX particle was stationary on top of the soil profile, so the dissolution rate may have been affected by the particle size and surface area and the solubility of the compounds. Table 1 lists the solubility of each compound. NTO is highly soluble followed by NQ, DNAN, and RDX.

IMX-101 and IMX-104 are made by meltcasting. During production, NTO, NQ, and RDX crystals are added to the molten DNAN. Two different studies conducted by Taylor et al. (2013, 2015a, 2015b) on the dissolution of IMX-101 and IMX-104 demonstrated that the compounds dissolved in order of their solubilities. They found that in IMX-101, NTO and NQ

dissolved faster than DNAN and that more NTO dissolved from each particle than NQ. These findings were also supported by Richard et al. (2014).

Tables 11 and 12 list the dissolution parameters estimated by HYDRUS-1D. For IMX-101, NTO has the highest maximum and minimum dissolution rates, followed by NQ and DNAN. For IMX-104, NTO again has the highest maximum dissolution rate, followed by DNAN, RDX, and HMX. IMX-101 and IMX-104 both contain NTO and DNAN in their formulations; however, IMX-104 contains 2.6 times more NTO than IMX-101 and 1.4 times less DNAN. The maximum and minimum dissolution rates are higher for NTO in IMX-101 than IMX-104. NTO could be shielded by DNAN, RDX, and HMX, which are less soluble, resulting in lower dissolution rates of NTO in IMX-104.

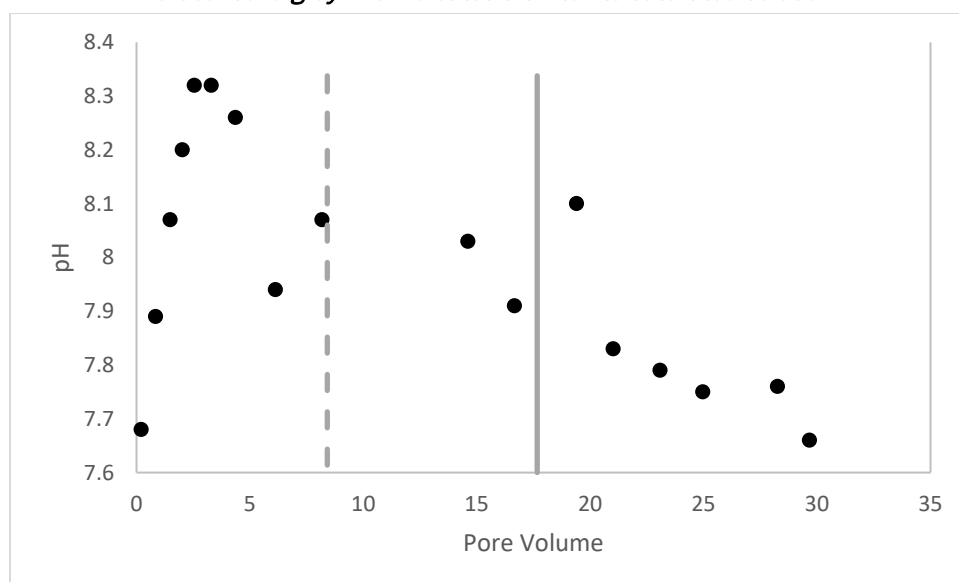
When comparing the maximum and minimum dissolution for DNAN, we found that the dissolution rates of DNAN in IMX-101, when normalized for its percent in the formulation, are lower than the rates in IMX-104. This could be the result of how accessible DNAN is to the simulated rainfall. The small particle could have NTO and NQ on the outside and DNAN on the inside. The compounds would need to dissolve before the water could access DNAN, resulting in lower dissolution rates. The shrinking core model gives a good description of the dissolution behavior of the IMX particles. It describes how reactions occur first on the outer skin of the particle. The zone of the reaction then moves into the solid, leaving behind inert (in our case, less soluble) materials and exposing another layer of the reactant (e.g., Levenspiel 1999, 569–570). NTO has the highest solubility. When NTO dissolves from the outside of the particle, the reaction front moves deeper. This process continues; and thus the unreacted core of the particle, where NTO remains, shrinks. Taylor et al. (2013) examined the physical changes undergone by IM particles during dissolution. They confirmed that for IMX-101, NTO and NQ dissolved from the outside of the particles, leaving behind thin bridges of DNAN, which dissolves slower. The resulting IMX porous material allowed access of water to NTO and NQ in the particle interior, promoting their dissolution, followed by diffusion to the particle exterior.

4.3.2 pH of the insensitive munitions solutions

The pH of effluent solutions of IMX-101 and IMX-104 was measured after the water interacted with the explosives and soil column. In solution, NTO is acidic and has a pK_a of 3.67–3.76 (Lee et al. 1987; Smith and Cliff 1999).

NTO acts as a weak acid as a result of the N-H bond dissociation. Taylor et al. (2015a) showed that the pH of NTO solutions is inversely related to their concentrations and can reach pH values as low as 2–3. In our column experiments, NTO solutions were buffered by reactions with the soil, and as a result, the average pH of the effluent solution for IMX-101 was 8.44 ± 0.19 and for IMX-104 8.27 ± 0.26 . However, several pore volumes collected when NTO concentrations were the highest also had lower pH values (Figure 38).

Figure 38. The pH of samples collected during analysis for IMX-104 flow interruption experiments. The *vertical dashed gray line* indicates the start of 24 hr flow interruption. The *vertical solid gray line* indicates a switch to saturated solution.



Based on effluent pH, the deprotonated form of NTO was present predominantly in the effluent solutions of IMX-101 and IMX-104 (Smith and Cliff 1999). Measuring the pH of the solutions can help indicate which form of NTO is likely to be present in the field, as well as its behavior in soils. Mark et al. (2016) found a highly significant inverse relationship between NTO soil adsorption coefficients and soil pH.

4.3.3 Mass balance

IMX-101 (NTO, NQ, and DNAN) and IMX-104 (NTO, RDX, and DNAN) constituents were recovered in column effluent, soil extracts, and residual particle extracts. In addition to parent compound recoveries, DNAN transformation products 2-ANAN and 4-ANAN were recovered. HMX was also recovered in IMX-104 studies. Mass-balance calculations (Table 13) indicate the majority of the individual compounds were recovered in effluent

solution as well as in the residual particle. There were no significant differences in solution recoveries of individual compounds in detonated vs. undetonated IMX-101 nor between continuous flow vs. flow interruption experiments for detonated samples except for NQ ($p = 0.0048$). In soil recoveries, there was only a significant difference for NTO ($p = 0.031$) and 2-ANAN ($p = 0.012$) in detonated samples between continuous flow and flow interruption. NTO had the highest recoveries in solution followed by NQ, DNAN, 2-ANAN, and 4-ANAN (Table 13). DNAN had the highest recovery in soil followed by NTO, NQ, 2-ANAN, and 4-ANAN.

For IMX-104, there were no significant differences in soil recoveries of individual IM components for undetonated vs. detonated IMX-104 samples nor in continuous flow vs. flow interruption experiments. There was a significant difference between the solution recoveries of 2-ANAN in undetonated vs. detonated samples ($p = 0.028$) and continuous and flow interruption for detonated particles ($p = 0.015$). NTO had the highest recoveries in effluent solution followed by DNAN, RDX, 2-ANAN, 4-ANAN, and HMX (Table 13). DNAN had the highest recovery in soil followed by RDX, NTO, 4-ANAN, 2-ANAN, and HMX (Table 13). DNAN, 2-ANAN, 4-ANAN, RDX, and HMX all adsorbed to the soil as shown by the delay in their BTCs (Figure 36).

Recoveries of the explosive compounds from the soil were small (Table 13). The experiments design encouraged the majority of munitions constituents to be desorbed from the soils and eluted by the time the experiment was finished and the soils extracted with acetonitrile. However, it is possible that some of the energetics were strongly adsorbed where they would not be desorbed with water. Previous research has shown limited desorption of NTO and DNAN from soil with water and with acetonitrile (Richard and Weidhaas 2014; Mark et al. 2016; Arthur et al. 2017). NQ has also shown limited desorption from soil. Williams et al. (1989) showed that recoveries of NQ from soil were directly dependent on the amount of organic matter present in the soil; as the organic matter increased, the percent recovery decreased (Williams et al. 1989). For our studies, the amount of organic matter present in the soils was <1 % (Table 9). However, a minimal amount of NQ was extracted from the soil. Though, acetonitrile has been found to be a good solvent for extracting RDX and HMX from soil (Jenkins and Grant 1987), we had poor recoveries of RDX and HMX in our study when using acetonitrile (Table 13), possibly as a result of irreversible adsorption or transformation (Yaron et al. 2012). Transformation products

were not detected for NTO, RDX, HMX, or NQ. However, the transformation products of DNAN, 2-ANAN and 4-ANAN, were detected and recovered in solution and soil extractions for DNAN, which Arthur et al. (2017) also reported. Lower recoveries of explosive compounds in solution for several columns with IMX-101 likely resulted because the particles were not wetted consistently by the simulated rainfall.

4.4 Conclusion

This study examined the dissolution, fate, and transport behavior of IMX-101 and IMX-104 in two soils. IM compounds dissolved in order of aqueous solubility as indicated by earlier dissolution studies without soils. Estimated dissolution rates were higher for explosive compound with higher aqueous solubilities. Initial elution of the high concentration pulse of highly soluble NTO and NQ was followed by lower concentrations later, while DNAN had generally lower and more constant concentrations. The sorption of NTO and NQ was low, while RDX, HMX, and DNAN all adsorbed to the soils. We also observed that DNAN transformed in soils with formation of amino-reduction products, 2-ANAN and 4-ANAN. This indicates that under flow conditions, DNAN, RDX, and HMX show potential for natural attenuation, even in the low organic matter soils like ones selected for this study. Estimated adsorption coefficients from HYDRUS-1D for each explosive compound were similar to those of pure NTO, NQ, DNAN, RDX, and HMX. Therefore, using distribution coefficients from batch studies or column studies of pure explosives in solution can estimate transport of the IM formulations.

Table 13. Mass recoveries of IMX-101 and IMX-104 constituents in effluent and soil and extractions of remaining IM particles during dissolution column transport studies. FI = flow interruption for 24 hr, D = detonated, UD = undetonated, and na = data not available.

Soils, Treatment	IMX-101												
	Solution Recoveries					Soil Recoveries					IMX Particle Recoveries		
	NTO (%)	NQ (%)	DNAN (%)	2-ANAN (%)	4-ANAN (%)	NTO (%)	NQ (%)	DNAN (%)	2-ANAN (%)	4-ANAN (%)	NTO (%)	NQ (%)	DNAN (%)
Camp Swift D	53.49	19.58	32.65	0.18	0.06	0.85	0.21	1.14	0.20	0.01	63.85	63.40	33.22
Camp Swift D	34.14	12.56	4.55	0.07	0.02	0.78	0.20	0.91	0.19	0.01	43.97	40.24	23.82
Camp Guernsey D	88.17	43.02	6.75	0.08	0.17	0.92	0.22	1.34	0.40	0.01	23.93	37.06	32.64
Camp Guernsey D	8.33	1.12	1.70	0.08	0.03	5.12	0.25	2.00	0.36	0.01	na	na	na
Mean	46.03	19.07	11.41	0.10	0.07	1.92	0.22	1.35	0.29	0.01	43.92	46.90	29.90
95% CI	32.96	17.33	14.02	0.05	0.07	2.09	0.02	0.46	0.11	0.00	30.94	29.67	17.60
Camp Swift UD	35.23	14.15	6.00	0.28	0.02	0.83	0.21	1.53	0.23	0.01	81.42	69.54	27.22
Camp Swift UD	3.85	0.32	0.05	0.02	0.00	0.83	0.20	1.08	0.09	0.00	86.63	74.49	133.98
Camp Guernsey UD	55.36	17.42	4.22	0.07	0.03	1.00	0.26	1.17	0.37	0.00	70.77	69.09	96.39
Camp Guernsey UD	43.08	19.77	62.37	0.47	0.03	0.90	0.21	0.96	0.28	0.00	63.38	55.14	79.48
Mean	34.38	12.91	18.16	0.21	0.02	0.89	0.22	1.18	0.25	0.00	75.55	67.06	84.27
95%CI	21.54	8.53	28.99	0.20	0.01	0.08	0.03	0.24	0.11	0.00	10.25	8.15	43.44
Camp Swift D FI	60.60	76.51	31.92	0.77	0.08	0.02	0.01	0.21	0.01	0.00	4.39	3.56	67.02
Camp Swift D FI	49.35	90.75	36.06	1.06	0.11	0.03	0.03	0.19	0.01	0.01	3.92	16.20	59.73
Camp Guernsey D FI	84.65	33.60	36.56	2.45	0.26	0.06	0.00	0.65	0.03	0.01	8.33	9.42	42.69
Camp Guernsey D FI	99.12	121.17	23.98	5.81	0.52	0.16	0.29	0.44	0.03	0.04	4.38	14.09	42.12
Mean	73.43	80.51	32.13	2.52	0.25	0.07	0.08	0.37	0.02	0.01	5.25	10.82	52.89
95%CI	22.13	35.67	5.70	2.26	0.20	0.06	0.14	0.21	0.01	0.02	2.02	5.50	12.22

Table 13 (cont.). Mass recoveries of IMX-101 and IMX-104 constituents in effluent and soil and extractions of remaining IM particles during dissolution column transport studies. FI = flow interruption for 24 hr, D = detonated, UD = undetonated, and na = data not available.

Soils, Treatment	IMX-104															
	Solution Recoveries						Soil Recoveries						IMX Particle Recoveries			
	NTO (%)	DNAN (%)	2-ANAN (%)	4-ANAN (%)	RDX (%)	HMX (mg)	NTO (%)	DNAN (%)	2-ANAN (%)	4-ANAN (%)	RDX (%)	HMX (mg)	NTO (%)	DNAN (%)	RDX (%)	HMX (mg)
Camp Swift D	57.99	23.90	0.14	0.01	7.30	0.05	0.02	0.50	0.02	0.01	0.04	0.00	17.77	44.53	90.73	0.47
Camp Swift D	52.82	21.21	2.01	0.02	7.88	0.06	0.02	0.49	0.02	0.07	0.04	0.01	9.26	34.18	48.26	0.29
Camp Guernsey D	52.20	4.24	0.15	0.04	1.74	0.01	0.03	0.24	0.03	0.03	0.05	0.01	34.52	37.61	44.61	0.25
Camp Guernsey D	38.12	13.27	0.18	0.05	4.68	0.04	0.02	0.38	0.03	0.00	0.06	0.00	3.19	43.02	30.72	0.18
Mean	50.28	15.66	0.62	0.03	5.40	0.04	0.03	0.40	0.02	0.03	0.04	0.01	16.18	39.83	53.58	0.30
95% CI	8.34	8.67	0.91	0.01	2.75	0.02	0.00	0.12	0.01	0.03	0.01	0.01	13.34	4.70	25.37	0.12
Camp Swift UD	42.14	7.65	0.14	0.01	3.04	0.04	0.05	0.22	0.02	0.01	0.03	0.00	41.73	48.47	11.27	0.65
Camp Swift UD	63.21	17.94	0.18	0.02	7.78	0.06	0.04	0.40	0.01	0.02	0.02	0.00	32.72	38.01	8.84	0.06
Camp Guernsey UD	58.06	3.10	0.23	0.06	1.27	0.02	0.03	0.22	0.01	0.02	0.02	0.01	33.45	48.70	13.40	0.08
Camp Guernsey UD	62.64	8.80	0.11	0.06	5.05	0.03	0.03	0.29	0.02	0.00	0.03	0.00	37.84	91.66	109.12	0.69
Mean	56.51	9.37	0.16	0.04	4.28	0.04	0.04	0.28	0.02	0.01	0.03	0.00	36.43	56.71	35.66	0.37
95% CI	9.66	6.10	0.05	0.02	2.74	0.02	0.01	0.08	0.00	0.01	0.00	0.00	4.11	23.35	48.03	0.34
Camp Swift D FI	73.05	19.31	0.37	0.05	10.85	0.05	0.00	0.33	0.01	0.01	0.08	0.00	18.26	52.67	52.36	0.28
Camp Swift D FI	105.14	54.11	0.55	0.08	26.49	0.14	0.01	0.47	0.00	0.02	0.16	0.01	1.39	41.46	31.24	0.21
Camp Guernsey D FI	97.50	26.63	0.00	0.22	14.99	0.09	0.18	0.20	0.01	0.03	0.01	0.00	6.08	63.99	60.75	0.33
Camp Guernsey D FI	109.98	26.37	1.67	0.24	3.63	0.08	0.37	1.15	0.02	0.11	1.13	0.01	5.54	43.80	34.40	0.21
Mean	79.07	26.50	0.53	0.12	11.74	0.07	0.12	0.45	0.01	0.04	0.28	0.01	7.07	45.05	45.36	0.27
95% CI	16.07	15.07	0.70	0.10	9.38	0.04	0.17	0.41	0.01	0.04	0.52	0.01	7.12	10.02	13.90	0.06

5 Predicting Dissolution and Transport of IMX-101 and IMX-104 Constituents Using HYDRUS-1D

By Jennifer D. Arthur, Noah W. Mark, Susan Taylor, Jiri Šimůnek, Mark L. Brusseau, and Katerina M. Dontsova¹⁰

5.1 Introduction

There is no direct field information about the behavior of new explosive formulations used in IM in the environment. However, it is important to be able to predict if constituents in IM formulations would travel through soils to the groundwater where they can be transported off military training bases. This is particularly critical because NTO and NQ, and to a smaller degree DNAN, are more soluble than either TNT or RDX and have been shown to have some human and environmental toxicity.

We have accumulated a body of knowledge regarding dissolution and transport of constituents in IM formulations under controlled conditions. Here we are applying this knowledge to three different locations across the United States to estimate if dissolution of particles of IM formulations, IMX-101 and IMX-104, would result in groundwater contamination over 25 years.

5.2 Methods

HYDRUS-1D, software that can simulate dissolution, was used to model the dissolution, fate, and transport of NTO, NQ, and DNAN in IMX-101 and NTO, DNAN, RDX, and HMX in IMX-104 in three soils, Plymouth, Camp Swift, and Camp Guernsey. We simulated transport to a 20 cm depth over a year and transport to the groundwater level for a 1 year, 10 years, and 25 years for a fully saturated soil profile receiving precipitation characteristic of the location of soil collection. Fully saturated conditions present a conservative estimate of the time needed for an explosive profile to propagate down; the time would be longer under unsaturated conditions.

¹⁰ Portions of this material are part of the dissertation defended by Jenifer Arthur as one of the requirements for her PhD degree.

The depth to the groundwater was determined for each soil as the lowest value for the well closest to the soil collection. Rainfall intensity and distribution through the year for each soil were determined using the mean precipitation record for each location. We assumed that no precipitation occurred when the rainfall amount per day was lower than 1.27 cm (0.5 in.). For the days that the rainfall amount was above this, we assumed that total rainfall for the year was uniformly distributed over the days when it rained. The flow rate was assumed to be equal to the precipitation rate.

The dissolution and transport parameters we used for forward simulations, maximum dissolution rate (Y_{max}), minimum dissolution rate (Y_{min}), decay constant (χ), linear adsorption coefficient (K_d), and mass-loss rate coefficient (k), were determined in Arthur et al. (2017, 2018) and the dissolution and transport experiments described in this report (Chapter 3). NQ K_d and k were determined from Mirecki et al. (2006). RDX and HMX K_d and k were selected from a summary of published parameters using percent clay, percent organic carbon, and cation exchange capacity (Branon and Pennington 2002). Dissolution rates were calculated for a 50 mg source of IMX-101 or IMX-104 as used in column experiments.

While in long simulations energetics in such small particles will soon be completely dissolved, in the field conditions a variety of particle sizes are present, and larger particles would continue to dissolve over longer time periods. Here we assumed that dissolution rates for particles of different sizes would be similar and that the particles will never dissolve completely (assumed to be a constant source). While this is a simplification, developing a relationship between particle size and dissolution rate and linking it to the particulate size distribution during energetic deposition resulting from low-order detonations and frequency of low-order detonations was outside the scope of this project. The assumptions we made provide a conservative estimate for potential groundwater contamination.

The bulk density (ρ_b) was obtained from the US Department of Agriculture soil web survey, and porosity (n) was calculated from the ρ_b . The longitudinal dispersivity (λ) was determined using soil texture, depth, and flow boundary condition (Vanderborght et al. 2001). Tables 14 and 15 list all input parameters used for forward simulations. Forward simulations for transport of NQ in Camp Swift and Plymouth soil and HMX in Camp Guernsey soil assumed constant input of these compounds over time at the solubility limit because dissolution simulations indicated that their concentrations do not go below solubility under simulated conditions.

Table 14. Dissolution and transport parameters used for forward simulation of energetic compounds in IMX-101: 3-nitro-1,2,4-triazol-5-one (NTO); nitroguanidine (NQ); 2,4-dinitroanisole (DNAN); and DNAN product, 2-amino-4-nitroanisole (2-ANAN).

Soil	Explosive Compound	Depth to Groundwater (cm)	λ (cm)	ρ_b (g cm ⁻³)	n	Flow Rate (cm hr ⁻¹)	Total 1-Year Rainfall (cm)	K_d (L kg ⁻¹)	k (hr ⁻¹)	χ	Y_{max} (mg L ⁻¹ hr ⁻¹)	Y_{min} (mg L ⁻¹ hr ⁻¹)
Camp Guernsey	NTO	2562	21.7	1.30	0.51	0.00927	35.0	0.02	0.0007	0.66	17499.00	525
Camp Guernsey	NQ	2562	21.7	1.30	0.51	0.00927	35.0	0.10	0.000	0.86	8885.00	889
Camp Guernsey	DNAN	2562	21.7	1.30	0.51	0.00927	35.0	0.90	0.0033	2.84	859.50	232
Camp Guernsey	2-ANAN	2562	21.7	1.30	0.51	0.00927	35.0	1.78	0.05			
Camp Swift	NTO	6155	36.2	1.40	0.47	0.01228	92.7	0.04	0.0007	0.66	17499	525
Camp Swift	NQ	6155	36.2	1.40	0.47	0.01228	92.7	0.1	0.000	0.86	8885	889
Camp Swift	DNAN	6155	36.2	1.40	0.47	0.01228	92.7	0.60	0.0006	2.84	859.5	232
Camp Swift	2-ANAN	6155	36.2	1.40	0.47	0.01228	92.7	1.78	0.05			
Plymouth	NTO	783	15.7	1.53	0.42	0.01495	120.9	0.5	0.0041	0.66	17499	525
Plymouth	NQ	783	15.7	1.53	0.42	0.01495	120.9	0.1	0.000	0.86	8885	889
Plymouth	DNAN	783	15.7	1.53	0.42	0.01495	120.9	4.4	0.0068	2.84	859.5	232
Plymouth	2-ANAN	783	15.7	1.53	0.42	0.01495	120.9	1.78	0.05			

Table 15. Dissolution and transport parameters used for forward simulation of IMX-104 compounds: 3-nitro-1,2,4-triazol-5-one (NTO); 2,4-dinitroanisole (DNAN); hexahydro-1,3,5-trinitro-1,3,5-triazine (RDX); octahydro-1,3,5,7-tetranitro-1,3,5,7-tetrazocine (HMX); and DNAN product, 2-amino-4-nitroanisole (2-ANAN).

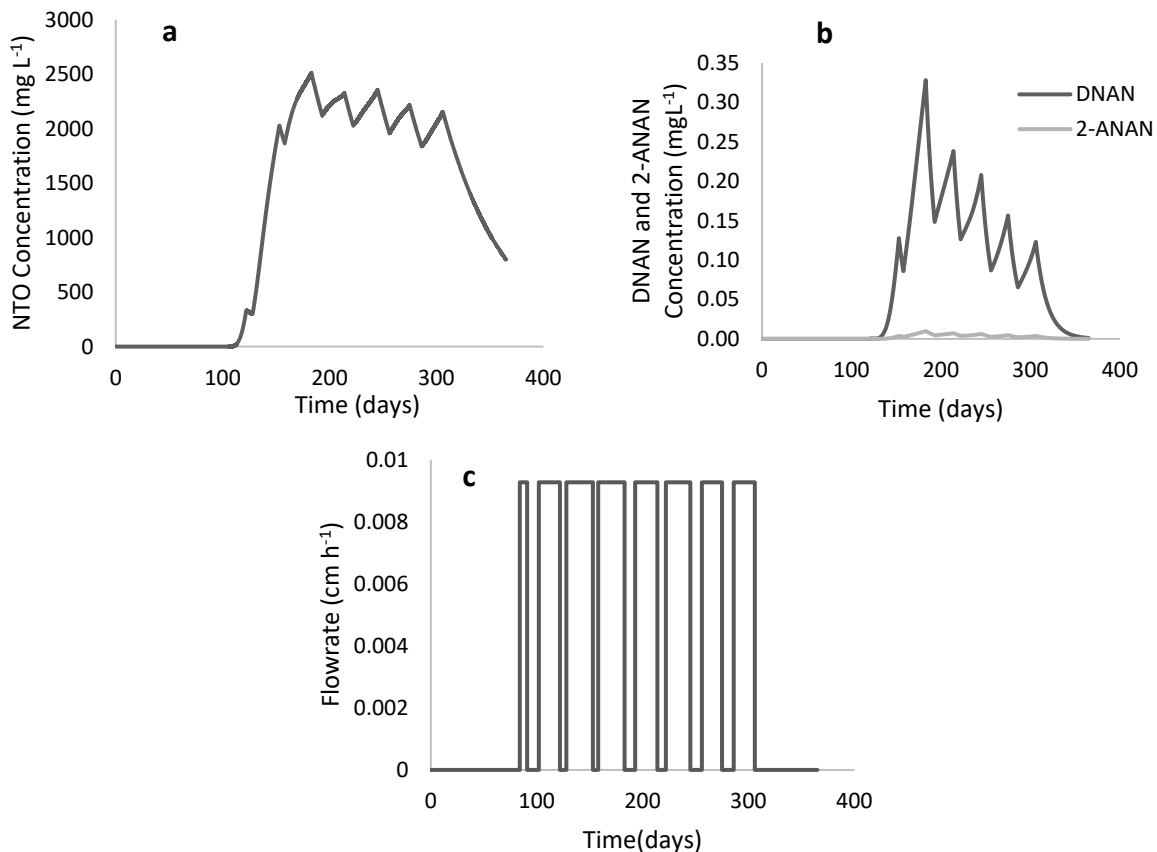
Soil	Explosive Compound	Depth to Groundwater (cm)	λ (cm)	ρ_b (g cm ⁻³)	n	Flow Rate (cm hr ⁻¹)	Total 1-Year Rainfall (cm)	K_d (L kg ⁻¹)	k (hr ⁻¹)	χ	Y_{max} (mg L ⁻¹ hr ⁻¹)	Y_{min} (mg L ⁻¹ hr ⁻¹)
Camp Guernsey	NTO	2562	21.7	1.30	0.51	0.00927	35.0	0.02	0.0007	0.12	49821	1495
Camp Guernsey	RDX	2562	21.7	1.30	0.51	0.00927	35.0	0.16	0.000	0.18	305	49
Camp Guernsey	HMX	2562	21.7	1.30	0.51	0.00927	35.0	0.30	0.000	0.19	441.5	8.8
Camp Guernsey	DNAN	2562	21.7	1.30	0.51	0.00927	35.0	0.90	0.0033	0.23	4687.5	422
Camp Guernsey	2-ANAN	2562	21.7	1.30	0.51	0.00927	35.0	1.6	0.09			

5.3 Results

5.3.1 IMX-101 dissolution and transport to a 20 cm depth in Camp Guernsey and Plymouth soils

Figure 39 shows the results of the forward simulations of dissolution and soil transport of explosive compounds comprising IMX-101 at a depth of 20 cm in Camp Guernsey soil with 1 year of rainfall, as well as a plot of rainfall. NTO and DNAN BTCs had the same patterns observed in dissolution and transport laboratory studies: NTO was the first compound to break through at 129 days, followed by DNAN at 141 days and 2-ANAN, a product of DNAN transformation, at 174 days. NTO had higher concentrations than DNAN; and DNAN transformed, producing a small amount of 2-ANAN. The pattern observed for all BTCs was an increase in energetics concentrations over time during flow periods, followed by a decrease when there was no infiltration due to in situ transformation.

Figure 39. Breakthrough curves of NTO, DNAN, and 2-ANAN in Camp Guernsey soil at a 20 cm depth with 1 year of rainfall (*a* and *b*). Plot of flow rate vs. time (*c*). Zero flow rate indicates periods of no flow.



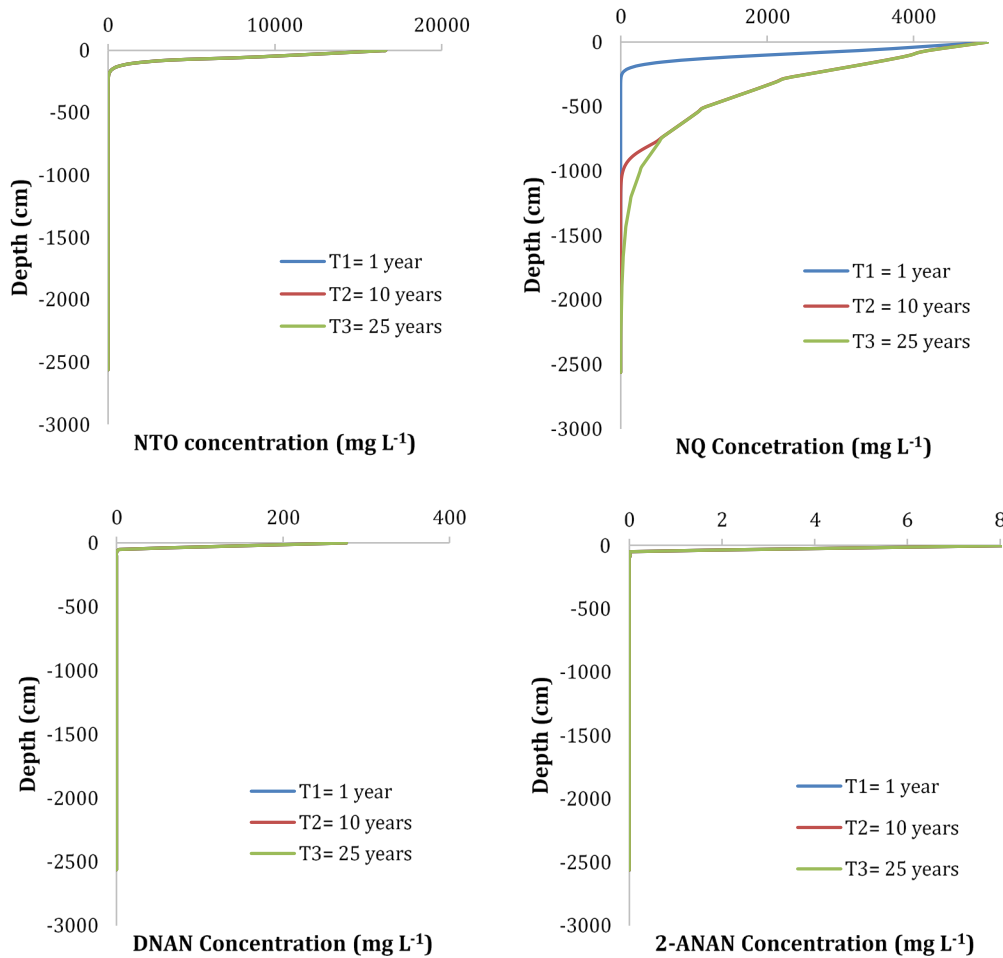
5.3.2 IMX-101 dissolution and transport to groundwater in Camp Guernsey soil

Figure 40 shows forward simulations of NTO, NQ, and DNAN dissolution and transport in Camp Guernsey soil with 1 year, 10 years, and 25 years of rainfall. The depth to groundwater level for Camp Guernsey soil is 2562 cm, and the average flow rate is $0.00927 \text{ cm hr}^{-1}$, similar to flow rates used in column experiments. After 1 year of rainfall on a 50 mg particle of IMX-101, NTO breakthrough (depth at half max concentration) was at a 51.24 cm depth, but low concentrations of NTO reached a depth of 358 cm due to dispersion and diffusion. NTO concentrations decreased with depth. The 1-year line shifting to the left indicates that NTO is degrading in the soil. The NTO depth profiles for 10- and 25-year simulations overlapped with the 1-year profile, indicating that NTO completely degrades in Camp Guernsey soil each year during a prolonged period of no flow. We do not account for changes in soil temperature and potential freezing, which would decrease transformation rates. However, freezing would also prevent NTO dissolution, so the effects of temperature on dissolution and transformation may counterbalance each other. NTO does not reach groundwater in Camp Guernsey soil over a 25-year period of average rainfall.

Because of the lack of transformation and adsorption in soils, NQ was more mobile in Camp Guernsey soil than NTO was. After 1 year of rainfall at 0.025 mg L^{-1} , NQ breakthrough occurred at a depth of 77 cm; and some NQ was reaching the depth of 385 cm. After 10 years of rainfall, NQ reached a depth of 1384 cm at a concentration of 0.01 mgL^{-1} , but not groundwater; and after 25 years of rainfall on the particle, NQ reached groundwater level but at a very low concentration (0.05 mg L^{-1}). The breakthrough of NQ after 10 years and 25 years occurred at a depth of 256 cm.

DNAN, the last compound in IMX-101, adsorbs to and degrades in the soil and is not as mobile as NTO and NQ (Figure 40). After 1 year of rainfall, it reached a depth of 51.25 cm. All three time periods overlap in Camp Guernsey soil, indicating, as was observed for NTO, that a long annual period of no flow removes all DNAN from the soil profile each year. The 2-ANAN, one of the known transformation products of DNAN, exhibited the same behavior as DNAN in Camp Guernsey soil, except the concentrations were smaller. The 2-ANAN reached a maximum depth of 77 cm. DNAN and 2-ANAN have not reached the groundwater level in Camp Guernsey soil in 25-year simulation.

Figure 40. Forward simulations of NTO, NQ, DNAN, and 2-ANAN in Camp Guernsey soil with rainfall over 1 year, 10 years, and 25 years. Note that the depth profiles for NTO, DNAN, and 2-ANAN for the three time periods overlap.

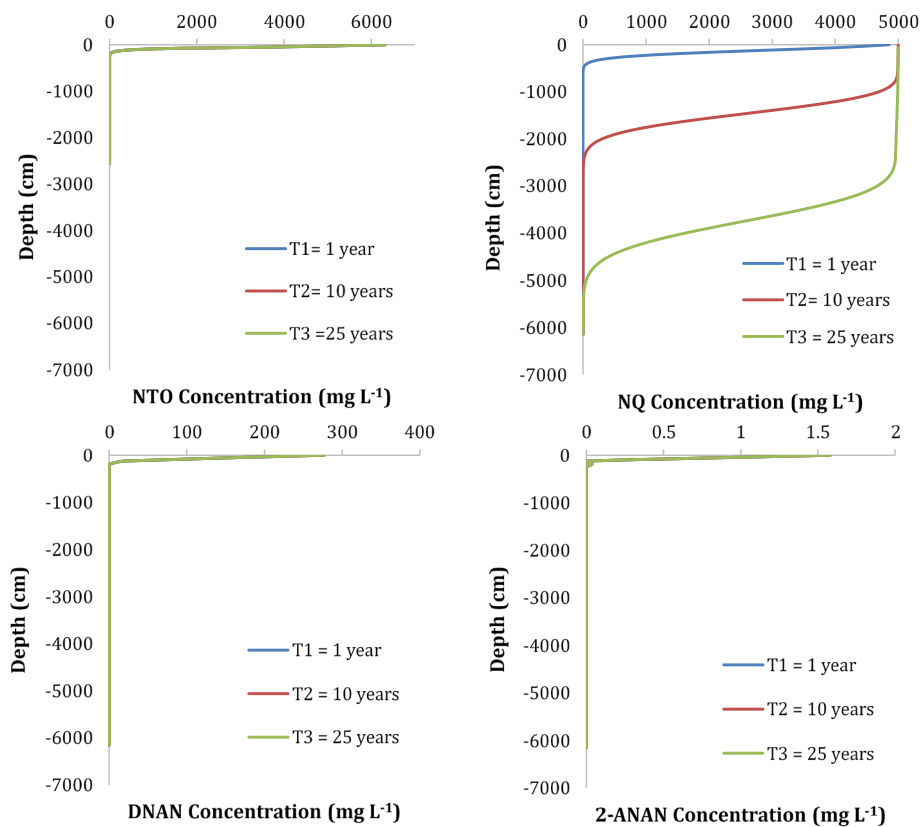


5.3.3 IMX-101 dissolution and transport to groundwater in Camp Swift Soil

The next soil used for forward simulation was Camp Swift. The groundwater level in Camp Swift soil is at 6156 cm. We simulated NTO, NQ, and DNAN with the same time periods as for Camp Guernsey. The average flow rate in Camp Swift soil was 0.01228 cm hr⁻¹. After 1 year of rainfall on a 50 mg particle of IMX-101, NTO surface concentrations were lower than the NTO concentrations in Camp Guernsey soil, consistent with the higher flow rate for this soil (Figure 41). The behavior of NTO in Camp Swift soil was similar to NTO behavior in Camp Guernsey soil (Figure 40); it had little adsorption but degraded in soil and was relatively mobile. After 1 year of rainfall, NTO breakthrough occurred at a depth of 51 cm, and small concentrations reached a depth of 122 cm. NTO did not reach the groundwater level in the simulated 25 years.

NQ again was more mobile than NTO in this soil as it was in Camp Guernsey soil. After 1 year of rainfall, NQ breakthrough occurred at a depth of 123 cm, and NQ reached a depth of 784 cm at 0.03 mg L^{-1} . After 10 years, NQ breakthrough occurred at a depth of 1477 cm. NQ at 0.01 mg L^{-1} concentration could be detected at a 3201 cm depth. After 25 years of rainfall, NQ breakthrough occurred at a depth of 3755 cm and was observed at groundwater depth (6156 cm) at a concentration of 0.04 mg L^{-1} .

Figure 41. Forward simulations of NTO, NQ, DNAN, and 2-ANAN in Camp Swift soil with rainfall over 1 year, 10 years, and 25 years. Note that the depth profiles for NTO, DNAN, and 2-ANAN for the three time periods overlap.

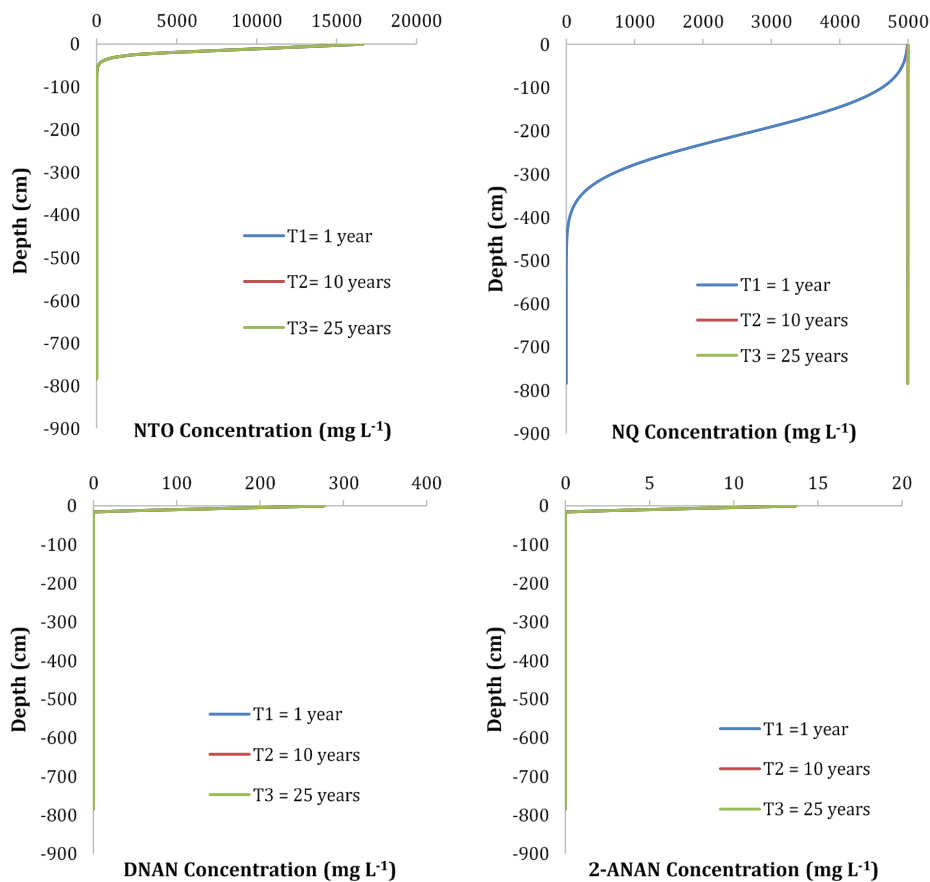


DNAN initial concentrations were smaller, and it was not as mobile as NTO and NQ. DNAN adsorbed and degraded in the soil and reached a depth of 308 cm with a concentration of 0.01 mg L^{-1} . Profiles over 1, 10, and 25 years overlapped. The same behavior was observed for 2-ANAN. The 2-ANAN concentrations were smaller than DNAN concentrations, and 2-ANAN reached a depth of 185 cm. DNAN and 2-ANAN did not reach groundwater in the simulated 25 years.

5.3.4 IMX-101 dissolution and transport to groundwater in Plymouth soil

Plymouth soil was the last soil used for forward simulation analysis of compounds in IMX-101 (Figure 42). The groundwater level in Plymouth soil is at 783 cm, and the average flow rate was $0.01495 \text{ cm hr}^{-1}$. NTO adsorbed and degraded in the soil. After 1, 10, and 25 years of rainfall on a 50 mg particle of IMX-101, NTO breakthrough occurred at a depth of 16 cm. NTO travelled to a depth of 125 cm with concentrations of 0.01 mg L^{-1} .

Figure 42. Forward simulations of NTO, NQ, DNAN, and 2-ANAN in Plymouth soil with rainfall over 1 year, 10 years, and 25 years. Note that the depth profiles for NTO, DNAN, and 2-ANAN for the three time periods overlap.



NQ, again, was more mobile in the soil than NTO. It did not reach groundwater after 1 year; but after 10 and 25 years of rainfall, it reached groundwater at solubility limit concentrations due to lack of adsorption or transformation.

DNAN was not as mobile as NQ and adsorbed and degraded in the soil. After 1 year of rainfall, DNAN concentrations were less than 0.0001 mg L^{-1} , reaching a depth of 31 cm. After 10 and 25 years of rainfall, DNAN concentrations reached a depth of 16 cm with a concentration of 0.01 mg L^{-1} .

DNAN transforms to 2-ANAN, and 2-ANAN concentrations were predicted to be about two orders of magnitude smaller than DNAN concentrations in Plymouth soil. The 2-ANAN also was not mobile in the soil, and DNAN and 2-ANAN travelled to a depth of only 16 cm, not reaching the groundwater after 25 years of precipitation.

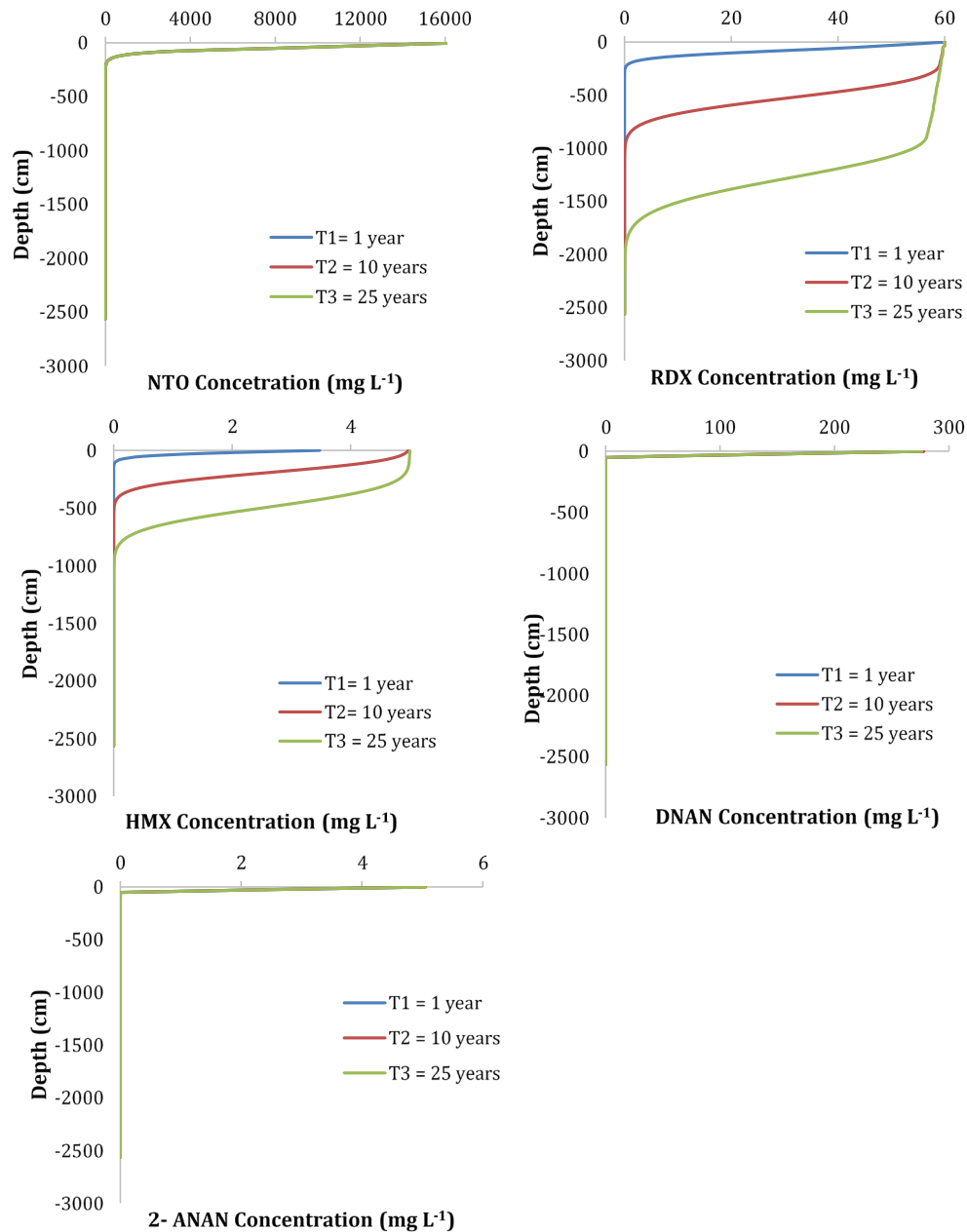
5.3.5 IMX-104 dissolution and transport to groundwater in Camp Guernsey soil

Forward dissolution and transport simulations were also done for Camp Guernsey soil with explosive compounds NTO, RDX, and DNAN that make up IMX-104 (Figure 43). The depth to groundwater level for Camp Guernsey soils is 2562 cm, and the average flow rate is 0.00927 cm hr⁻¹. NTO displayed the same behavior observed in the IMX-101 simulations. After 1, 10, and 25 years of rainfall, NTO was slightly mobile, traveling to a depth of 256 cm. NTO breakthrough occurred at a depth of 51.24 cm. NTO adsorbed to the soil and degraded in the soil in all three time periods of rainfall observed. NTO did not reach groundwater level over the simulated 25 years.

RDX was mobile in this soil (Figure 43). After 1 year of rainfall was applied to the 50 mg particle of IMX-104, RDX breakthrough occurred at a depth of 77 cm. RDX breakthrough occurred at a depth of 538 cm after 10 years of rainfall and at a depth of 1281 cm after 25 years of rainfall. After one year of rainfall, RDX traveled to a maximum depth of 307 cm with a concentration of 0.01 mg L⁻¹; after 10 years to a depth of 1102 cm with a concentration of 0.01 mg L⁻¹; and after 25 years to a depth of 1051 cm with a concentration of 0.03 mg L⁻¹. Small concentrations of RDX reached a depth of 2050 cm but not groundwater level.

A small amount of HMX, an impurity in technical-grade RDX, also appears in IMX-104 formulations. HMX concentrations were smaller than RDX concentrations. After 1 year of rainfall was applied to the 50 mg IMX-104 particle, HMX, which adsorbs to the soil, travelled to a maximum depth of 102 cm with a concentration of 0.03 mg L⁻¹. HMX breakthrough occurred at a depth of 26 cm. HMX breakthrough occurred at a depth of 205 cm after 10 years of rainfall and at 487 after 25 years of rainfall. After 10 years of rainfall, HMX traveled to a maximum depth of 436 cm with a concentration of 0.04 mg L⁻¹; after 25 years of rainfall, it traveled to a depth of 974 cm with a concentration of 0.01 mg L⁻¹. However, HMX never reached groundwater level in 25 years.

Figure 43. Forward simulations of NTO, RDX, HMX, DNAN, and 2-ANAN in Camp Guernsey soil with rainfall over 1 year, 10 years, and 25 years. The depth profiles for NTO, DNAN, and 2-ANAN for the three time periods overlap.



Only a small concentration of DNAN (0.21 mg L⁻¹) was observed at a depth of 51 cm over the three different time periods of rainfall. All three lines overlapped (Figure 43). There was no 2-ANAN predicted in the soils after 1, 10, and 25 years of rainfall. Neither DNAN nor 2-ANAN ever reached groundwater level.

5.4 Conclusions

NTO, DNAN, and 2-ANAN released during dissolution of IM were either adsorbed or degraded or both by the three soils used in the simulations. They did not reach groundwater in any of the scenarios simulated. While NTO and DNAN will naturally attenuate in soil, NQ, RDX, and HMX were more mobile in the simulated cases as years of rainfall continued. NQ is the most mobile explosive compound of those simulated. Therefore, NQ, RDX, and HMX should be monitored for risk of contaminating groundwater.

6 Summary

We characterized detonation residues of IM formulations, IMX-101, IMX-104, and PAX-21, using light and electron microscopy, as well as X-ray tomography and Raman spectroscopy. Additionally, we exposed them to either simulated rainfall in the lab or to natural rainfall and sunshine outside at two locations, one in New Hampshire and one in Arizona. Indoor particles were again examined using X-ray tomography following exposure to water to quantify changes to their three-dimensional structure as they dissolve. Solution concentrations of NTO, NQ, DNAN, RDX, HMX, and AP were also measured to calculate the amount of IM constituents dissolved into solution. The photodegradation of DNAN and NTO in solid (outdoors) and aqueous (in the lab) form was measured to determine if these compounds degrade in sunlight either before or after dissolution. Transport of products of dissolution of IM particles was studied in several soils collected on training facilities. Results helped to determine how DNAN and NTO interact with the soils. Together, obtained dissolution and transport parameters were used in HYDRUS-1D, a software package for simulating water, heat, and solute movement in one-dimensional variably saturated media, to predict the environmental fate of IM explosives for several locations.

Both outdoor and indoor dissolution experiments indicated that IM constituents dissolve sequentially as predicted by solubility, NTO, followed by NQ and DNAN in IMX-101 and DNAN and RDX in IMX-104. Fast dissolution of most soluble components resulted in porous particles that broke easily. High initial concentrations of NTO caused significant decrease of pH for rainwater in contact with IM formulations. Phototransformation of outdoor IM was evident, but its relative contribution is smaller than for traditional explosives due to faster dissolution of IM compounds. Solution-phase NTO phototransformation was influenced by pH and enhanced in the presence of dissolved organic matter while DNAN phototransformation rates increased with temperature.

NTO adsorption in soils was very low and further decreased with increasing soil pH, while DNAN was adsorbed and its adsorption positively correlated with soil organic matter and clay. Both NTO and DNAN were transformed in soils, and products of DNAN transformation, 2-ANAN (2-amino-4-nitroanisole) and 4-ANAN (4-amino-2-nitroanisole) were observed. Exposing explosive residues to water resulted in an initial high peak in concentration for NTO and NQ which then tailed off. DNAN in

solution, on the other hand, had low but fairly constant concentrations. High release of NTO and its low adsorption in soils indicate higher risk of its transport to the ground and surface waters, while DNAN's slower dissolution and TNT-like behavior in soils indicates lower potential for off-site transport. However, numerical simulations indicate that both NTO and DNAN would be transformed in soils, preventing them from reaching groundwater.

Both the experimental and modeling results, coupled with the mass of IM formulations scattered on a range, will allow us and others to estimate the dissolved IM mass loads, their subsequent transport and fate, and their likelihood of reaching groundwater.

References

- Ahn, S. C., D. K. Cha, B. J. Kim, S.-Y. Oh. 2011. "Detoxification of PAX-21 Ammunitions Wastewater by Zero-Valent Iron for Microbial Reduction of Perchlorate." *Journal of Hazardous Materials* 192:909–914.
- Arnett, C. M., G. Rodriguez, and S. W. Maloney. 2009. "Analysis of Bacterial Community Diversity in Anaerobic Fluidized Bed Bioreactors Treating 2,4-Dinitroanisole (DNAN) and n-Methyl-4-Nitroaniline (MNA) Using 16S rRNA Gene Clone Libraries." *Microbes and Environments* 24:72–75.
- Arthur, J. D., N. W. Mark, S. Taylor, J. Šimůnek, M. L. Brusseau, and K. M. Dontsova. 2017. "Batch Soil Adsorption and Column Transport Studies of 2,4-Dinitroanisole (DNAN) in Soils." *Journal of Contaminant Hydrology* 199:14–23.
- Arthur, J. D., N.W. Mark, S. Taylor, J. Šimůnek, M. L. Brusseau, and K. M. Dontsova. 2018. "Dissolution and Transport of Insensitive Munitions Formulations IMX-101 and IMX-104 in Saturated Soil Columns." *Science of the Total Environment* 624:758–768.
- Bedford, C. D., P. S. Carpenter, and M. P. Nadler. 1996. *Solid-State Photodecomposition of Energetic Nitramines (RDX and HMX)*. NAWCWPNS TP 8271. China Lake, CA: Naval Air Warfare Center Weapons Division.
<http://www.dtic.mil/dtic/tr/fulltext/u2/a310064.pdf>.
- Boddu, V. M., K. Abburi, S. W. Maloney, and R. Damavarapu. 2008. "Thermophysical Properties of an Insensitive Munitions Compound, 2,4-Dinitroanisole." *Journal of Chemical Engineering and Data* 53:1120–1125.
- Boyer, I., J. K. Miller, R. E. Watson, J. DeSesso II, and C. M. Vogel. 2007. *Comparison of the Relative Risks of CL-20 and RDX*. Falls Church, VA: Noblis Center for Science and Technology.
- Braida, W. J., M. Wazne, A. Ogundipe, G. Sen Tuna, J. Pavlov, and A. Koutsospyros. 2012. "Transport of Nitrotriazolone (NTO) in Soil Lysimeters." In *Proceedings of Protection and Restoration of the Environment XI*, Thessaloniki, Greece.
- Brannon, J. M., and J. C. Pennington. 2002. *Environmental Fate and Transport Process Descriptors for Explosives*. ERDC/EL TR-02-10. Vicksburg, MS: US Army Engineer Research and Development Center.
- Brusseau, M. L., Q. Hu, and R. Srivastava. 1997. "Using Flow Interruption to Identify Factors Causing Nonideal Contaminant Transport." *Journal of Contaminant Hydrology* 24 (3–4): 205–219.
- Brusseau, M. L., P. S. C. Rao, R. E. Jessup, and J. M. Davidson. 1989. "Flow Interruption: A Method for Investigating Sorption Nonequilibrium." *Journal of Contaminant Hydrology* 4:223–240.

- Burrows, E. P., D. H. Rosenblatt, W. R. Mitchell, and D. L. Parmer. 1989. *Organic Explosives and Related Compounds: Environmental and Health Considerations*. Frederick, MD: Fort Detrick, Army Biomedical Research & Development Laboratory. <http://www.dtic.mil/dtic/tr/fulltext/u2/a210554.pdf>.
- Burton, D. T., S. D. Turley, and G. T. Peters. 1993. *Toxicity of Nitroguanidine, Nitroglycerin, Hexahydro-1,3,5-Trinitro-1,3,5-Triazine (RDX) and 2,4,6-Trinitrotoluene (TNT) to Selected Freshwater Aquatic Organisms*. Queenstown, MD: University of Maryland System, Wye Research and Education Center. <http://www.dtic.mil/dtic/tr/fulltext/u2/a267467.pdf>.
- Chen, P.-Y. 1977. *Table of Key Lines in X-Ray Powder Diffraction Patterns of Minerals in Clays and Associated Rocks*. Geological Survey Occasional Paper 21. Bloomington, IN: Indiana Geological Survey.
- Cuddy, M. F., A. R. Poda, and M. A. Chappell. 2014. "Estimations of Vapor Pressures by Thermogravimetric Analysis of the Insensitive Munitions IMX-101, IMX104, and Individual Components." *Propellants, Explosives, Pyrotechnics* 39 (2): 236–242.
- Dave, G., E. Nilsson, and A. S. Wernersson. 2000. "Sediment and Water Phase Toxicity and UV-Activation of Six Chemicals Used in Military Explosives." *Aquatic Ecosystem Health and Management* 3:291–299.
- Davies P. J., and A. Provas. 2006. *Characterization of 2,4-Dinitroanisole: An Ingredient for Use in Low Sensitivity Melt Cast Formulations*. DSTO-TR-1904. Edinburgh, Australia: Defence Science and Technology Organization, Weapons Systems Division. <http://www.dtic.mil/dtic/tr/fulltext/u2/a458880.pdf>.
- Deeter, D. P. 2000. *Occupational Health (Textbook of Military Medicine—Part 3, Disease and the Environment)*. Falls Church, VA: US Department of the Army. <http://www.dtic.mil/dtic/tr/fulltext/u2/a278721.pdf>.
- Dodard S. G., M. Sarrazin, J. Hawari, L. Paquet, G. Ampleman, S. Thiboutot, and G. I. Sunahara. 2013. "Ecotoxicological Assessment of a High Energetic and Insensitive Munitions Compound: 2,4-Dinitroanisole (DNAN)." *Journal of Hazardous Materials* 262:143–150.
- Doll, D. W., J. M. Hanks, A. G. Allred, and J. B. Niles. 2006. Reduced Sensitivity, Melt-pourable TNT Replacements. United States Patent 7,067,024 B2, filed 27 June 2001 and issued 27 June 2006.
- Dontsova, K., S. Taylor, R. Pesce-Rodriguez, M. Brusseau, J. Arthur, N. Mark, M. Walsh, J. Lever, and J. Šimůnek. 2014. *Dissolution of NTO, DNAN, and Insensitive Munitions Formulations and Their Fates in Soils*. ERDC/CRREL TR-14-23. Hanover, NH: US Army Engineer Research and Development Center.
- Dontsova, K. M., M. Chappell, J. Šimůnek, and J. C. Pennington. 2008. "Dissolution and Transport of Nitroglycerin, Nitroguanidine and Ethyl Centralite from M9 and M30 Propellants in Soils." In *Characterization and Fate of Gun and Rocket Propellant Residues on Testing and Training Ranges: Final Report*. ERDC TR-08-1. Vicksburg, MS: US Army Engineer Research and Development Center. <http://hdl.handle.net/11681/8575>.

- Dontsova, K. M., C. Hayes, J. Šimůnek, J. C. Pennington, and C. W. Williford. 2009. "Dissolution and Transport of 2,4-DNT and 2,6-DNT from M1 Propellant in Soil." *Chemosphere* 77:597–603.
- Dontsova, K. M., J. C. Pennington, S. Yost, and C. Hayes. 2007. "Transport of Nitroglycerin, Nitroguanidine and Diphenylamine in Soils." In *Characterization and Fate of Gun and Rocket Propellant Residues on Testing and Training Ranges: Interim Report 1*. ERDC TR-07-1. Vicksburg, MS: US Army Engineer Research and Development Center. <http://hdl.handle.net/11681/8516>.
- Dontsova, K. M., S. L. Yost, J. Šimůnek, J. C. Pennington, and C. W. Williford. 2006. "Dissolution and Transport of TNT, RDX, and Composition B in Saturated Soil Columns." *Journal of Environmental Quality* 35:2043–2054.
- Etnier, E. L. 1986. *Water Quality Criteria for Hexahydro-1,3,5-Trinitro-1,3,5-Triazine (RDX). Final Report*. ORNL-6178. Oak Ridge, TN: Oak Ridge National Laboratory.
- Fedoroff, B. T., H. A. Aaronson, E. F. Reese, O. E. Sheffield, and G. D. Clift. 1960. *Encyclopedia of Explosives and Related Items*, Volume 1, A-448. Picatinny, NJ: US Army Research and Development Command.
- Fida, T. T., S. Palamuru, G. Pandey, and J. C. Spain. 2014. "Aerobic Biodegradation of 2,4-Dinitroanisole by *Nocardioideis* Sp. Strain JS1661." *Applied Environmental Microbiology* 80:7725–7731.
- Fung, V., J. Morris, D. Price, N. Tucker, E. LeClaire, and A. Carrillo. 2010. *Further Development and Optimization of IM Ingredients at Holston Army Ammunition Plant*. Paper for the 2010 Insensitive Munitions and Energetic Materials Technology Symposium, Munich, Germany. https://imemg.org/wp-content/uploads/IMEMTS%202010/papers/Fung-10504_Further%20Development%20and%20Optimization%20of%20IM%20Melt-pour%20Ingredients%20at%20Holston%20Army%20Ammunition_IMEMTS2010-Paper.pdf.
- Glover, D., and J. Hoffsommer. 1973. "Thin-Layer Chromatographic Analysis of HMX in Water." *Bulletin of Environmental Contamination and Toxicology* 10:302–304.
- Haag, W. R., R. Spanggord, T. Mill, R. T. Podoll, T.-W. Chou, D. S. Tse, and J. C. Harper. 1990. "Aquatic Environmental Fate of Nitroguanidine." *Environmental Toxicology and Chemistry* 9:1369–1367.
- Haderlein, S. B., K. W. Weissmahr, and R. P. Schwarzenbach. 1996. "Specific Adsorption of Nitroaromatic Explosives and Pesticides to Clay Minerals." *Environmental Science and Technology* 30:612–622.
- Hastings, S. H., and F. A. Matsen. 1948. "The Photodecomposition of Nitrobenzene." *Journal of the American Chemistry Society* 70:3514–3515.
- Hawari, J., F. Monteil-Rivera, N. N. Perreault, A. Halasz, L. Paquet, Z. Radovic-Hrapovic, S. Deschamps, S. Thiboutot, and G. Ampleman. 2015. "Environmental Fate of 2,4-Dinitroanisole (DNAN) and Its Reduced Products." *Chemosphere* 119:16–23.

- Hawari, J., N. Perreault, A. Halasz, L. Paquet, Z. Radovic, D. Manno, G. I. Sunahara, S. Dodard, M. Sarrazin, S. Thiboutot, G. Ampleman, S. Brochu, E. Diaz, A. Gagnon, and A. Marois. 2012. *Environmental Fate and Ecological Impact of NTO, DNAN, NQ, FOX-7, and FOX-12 Considered as Substitutes in the Formulations of Less Sensitive Composite Explosives*. Annual Report 2010–2011, NRC# 53363. National Research Council Canada.
- Hoyt, N., M. Brunell, K. Kroeck, M. Hable, L. Crouse, A. O'Neill, and D. I. Bannon. 2013. "Biomarkers of Oral Exposure to 3-Nitro-1,2,4-Triazol-5-One (NTO) and 2,4-Dinitroanisole (DNAN) in Blood and Urine of Rhesus Macaques (*Macaca mulatta*)."
Biomarkers 18:587–594.
- Jenkins, T. F., and C. L. Grant. 1987. "Comparison of Extraction Techniques for Munitions Residues in Soil."
Analytical Chemistry 59:1326–1331.
- Jenkins, T. F., J. C. Pennington, T. A. Ranney, T. E. Berry Jr., P. H. Miyares, M. E. Walsh, A. D. Hewitt, N. M. Perron, L. V. Parker, C. A. Hayes, and E. G. Wahlgren. 2001. *Characterization of Explosives Contamination at Military Firing Ranges*. ERDC TR-01-5. Hanover, NH: US Army Engineer Research and Development Center.
- Koch, R. L., E. J. T. Chrystal, B. Beaulieu Jr., and P. Goldman. 1979. "Acetamide—A Metabolite of Metronidazole Formed by the Intestinal Flora."
Biochemical Pharmacology 28:3611–3615.
- Krzmarzick, M. J., R. Khatiwada, C. I. Olivares, L. Abrell, R. Sierra-Alvarez, J. Chorover, and J. A. Field. 2015. "Biotransformation and Degradation of the Insensitive Munitions Compound, 3-Nitro-1,2,4-Triazol-5-One, by Soil Bacterial Communities."
Environmental Science and Technology 49:5681–5688.
- Le Champion L., M. T. Adeline, and J. Ouazzani. 1997. "Separation of NTO Related 1,2,4-Triazole-3-One Derivatives by High Performance Liquid Chromatography and Capillary Electrophoresis."
Propellants, Explosives, Pyrotechnics 22:233–237.
- Le Champion, L., C. Giannotti, and J. Ouazzani. 1999a. "Photocatalytic Degradation of 5-Nitro-1,2,4-Triazol-3-One NTO in Aqueous Suspension of TiO₂. Comparison with Fenton Oxidation."
Chemosphere 38:1561–1570.
- Le Champion, L., A. Vandais, and J. Ouazzani. 1999b. "Microbial Remediation of NTO in Aqueous Industrial Wastes."
FEMS Microbiology Letters 176:197–203.
- Lee, K.-Y., L. B. Chapman, and M. D. Cobura. 1987. "3-Nitro-1,2,4-Triazol-5-One, a Less Sensitive Explosive."
Journal of Energetic Materials 5:27–33.
- Levenspiel, O. 1999. *Chemical Reaction Engineering*. 3rd ed. New York: John Wiley & Sons.
- Lever, J. H., S. Taylor, L. Perovich, K. Bjella, and B. Packer. 2005. "Dissolution of Composition B Detonation Residuals."
Environmental Science and Technology 39:8803–8811.
- Liang, J., C. Olivares, J. A. Field, and R. Sierra-Alvarez. 2013. "Microbial Toxicity of the Insensitive Munitions Compound, 2,4-Dinitroanisole (DNAN), and Its Aromatic Amine Metabolites."
Journal of Hazardous Materials 262:281–287.

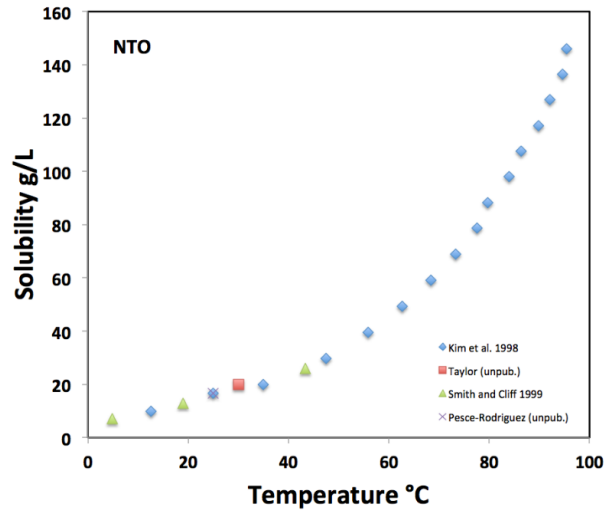
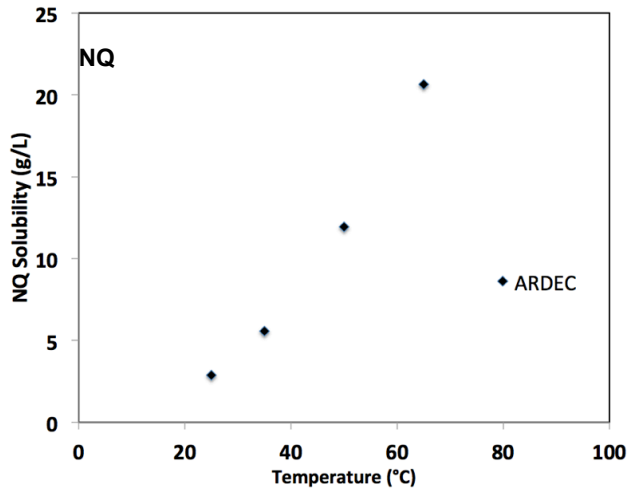
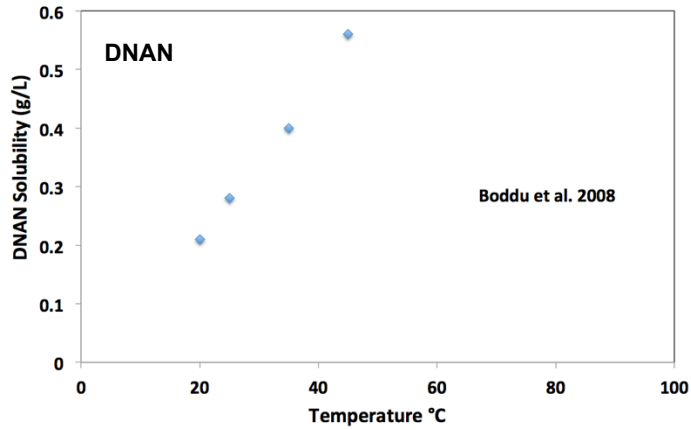
- London J. O., and D. M. Smith. 1985. *A Toxicological Study of NTO*. LA-10533-MS. Los Alamos, NM: Los Alamos National Laboratory.
<https://permalink.lanl.gov/object/tr?what=info:lanl-repo/lareport/LA-10533-MS>.
- Madeira, C. L., S. A. Speet, C. A. Nieto, L. Abrell, J. Chorover, R. Sierra-Alvarez, and J. A. Field. 2017. "Sequential Anaerobic-Aerobic Biodegradation of Emerging Insensitive Munitions Compound 3-Nitro-1,2,4-Triazol-5-One (NTO)." *Chemosphere* 167:478–484.
- Mark, N., J. Arthur, K. Dontsova, M. Brusseau, and S. Taylor. 2016. "Adsorption and Attenuation Behavior of 3-Nitro-1,2,4-Triazol-5-One (NTO) in Eleven Soils." *Chemosphere* 144:1249–1255.
- Mark, N., J. Arthur, K. Dontsova, M. Brusseau, S. Taylor, and J. Šimůnek. 2017. "Column Transport Studies of 3-Nitro-1,2,4-Triazol-5-One (NTO) in Soils." *Chemosphere* 171:427–434.
- McCormick, N. G., F. E. Feeherry, and H. S. Levinson. 1976. "Microbial Transformation of 2,4,6-Trinitrotoluene and Other Nitroaromatic Compounds." *Applied and Environmental Microbiology* 31 (6): 949–958.
- Mirecki, J. E., B. Porter, and C. A. Weiss. 2006. *Environmental Transport and Fate Process Descriptors for Propellant Compounds*. ERDC/EL TR-06-7. Vicksburg, MS: US Army Engineer Research and Development Center.
- Olivares, C. I., J. Liang, L. Abrell, R. Sierra-Alvarez, and J. A. Field. 2013. "Pathways of Reductive 2,4-Dinitroanisole (DNAN) Biotransformation in Sludge." *Biotechnology and Bioengineering* 110:1595–1604.
- Olivares, C. I., L. Abrell, R. Khatiwada, J. Chorover, R. Sierra-Alvarez, and J. A. Field. 2016. "(Bio)transformation of 2,4-Dinitroanisole (DNAN) in Soils." *Journal of Hazardous Materials* 304:214–221.
- Pennington, J.C., T. F. Jenkins, G. Ampleman, and S. Thiboutot. 2004. *Distribution and Fate of Energetics on DoD Test and Training Ranges: Interim Report 4*. TR-04-4. Vicksburg, MS: US Army Engineer Research and Development Center.
<http://hdl.handle.net/11681/8551>.
- Perreault, N. N., D. Manno, A. Halasz, S. Thiboutot, G. Ampleman, and J. Hawari. 2012. "Aerobic Biotransformation of 2,4-Dinitroanisole in Soil and Soil *Bacillus* sp." *Biodegradation* 23:287–295. doi:10.1007/s10532-011-9508-7.
- Pichtel, J. 2012. "Distribution and fate of military explosives and propellants in soil: A review." *Applied and Environmental Soil Science* 2012. doi: 10.1155/2012/617236.
- Platten, W. E., D. Bailey, M. T. Suidan, and S. W. Maloney. 2010. "Biological Transformation Pathways of 2,4-Dinitroanisole and N-Methylparanitroaniline in Anaerobicfluidized-Bed Bioreactors." *Chemosphere* 81:1131–1136.
- Rao, B., W. Wang, Q. Cai, T. Anderson, and B. Gu, 2013. "Photochemical Transformation of the Insensitive Munitions Compound 2,4-Dinitroanisole." *Science of the Total Environment* 443:692–699. <https://doi.org/10.1016/j.scitotenv.2012.11.033>.

- Richard, T., and J. Weidhaas. 2014. "Biodegradation of IMX-101 Explosive Formulation Constituents: 2,4-Dinitroanisole (DNAN), 3-Nitro-1,2,4-Triazol-5-One (NTO), and Nitroguanidine." *Journal of Hazardous Materials* 280:372–379.
- Rugge, K., T. B. Hofstetter, S. B. Haderlein, P. L. Bjerg, S. Knudsen, C. Zraunig, H. Mosbaek, and T. H. Christensen. 1998. "Characterization of Predominant Reductants in an Anaerobic Leachate-Contaminated Aquifer by Nitroaromatic Probe Compounds." *Environmental Science and Technology* 32:23–31.
- Salter-Blanc, A. J., E. J. Bylaska, J. J. Ritchie, and P. G. Tratnyek. 2013. "Mechanisms and Kinetics of Alkaline Hydrolysis of the Energetic Nitroaromatic Compounds 2,4,6-Trinitrotoluene (TNT) and 2,4-Dinitroanisole (DNAN)." *Environmental Science and Technology* 47:6790–6798. doi: 10.1021/es304461t.
- Schroer, H. W., K. L. Langenfeld, X. Li, H.-J. Lehmler, and C. L. Just. 2015. "Stable Isotope-Enabled Pathway Elucidation of 2,4-Dinitroanisole Metabolized by *Rhizobium litchii*." *Environmental Science and Technology Letters* 2:362–366. doi: 10.1021/acs.estlett.5b00278.
- Schwarzenbach, R. P., R. Stierli, B. R. Folsom, and J. Zeyer. 1988. "Compound Properties Relevant for Assessing the Environmental Partitioning of Nitrophenols." *Environmental Science and Technology* 22:83–92.
- Šimůnek, J., M. Šejna, H. Saito, M. Sakai, and M. T. van Genuchten. 2008. *The HYDRUS-1D Software Package for Simulating the Movement of Water, Heat, and Multiple Solutes in Variably Saturated Media*. Version 4.0. HYDRUS Software Series 3. Riverside, CA: Department of Environmental Sciences, University of California Riverside.
- Šimůnek, J., and M. T. van Genuchten. 2008. "Modeling Nonequilibrium Flow and Transport Processes Using HYDRUS." *Vadose Zone Journal* 7 (2): 782–797.
- Singh, J., S. D. Comfort, L. S. Hundal, and P. J. Shea. 1998. "Long-Term RDX Sorption and Fate in Soil." *Journal of Environmental Quality* 27:572–577.
- Smith, M. W., and M. D. Cliff. 1999. *NTO Based Explosive Formulations: A Technology Review*. DSTO-TR-0796. Salisbury, Australia: Aeronautical and Maritime Research Laboratory, Weapons Systems Division. <http://www.dtic.mil/dtic/tr/fulltext/u2/a364083.pdf>.
- Sokkalingam, N., J. J. Potoff, V. M. Boddu, and S. W. Maloney. 2008. "Prediction of Environmental Impact of High-Energy Materials with Atomistic Computer Simulations." ADM002187. In *Proceedings of the 26th Army Science Conference*, Orlando, FL, 1–4 December 2008.
- Spear, R. J., C. N. Louey, and M. G. Wolfson. 1989. *A Preliminary Assessment of 3-Nitro-1,2,4-Triazol-5-One (NTO) as an Insensitive High Explosive*. MRL-TR-89-18. Maribyrnong, Australia: Defence Science and Technology Organisation, Materials Research Laboratory.
- Sunahara, G. I. 2009. *Ecotoxicology of Explosives*. Boca Raton, FL: CRC Press.
- Taylor S., J. H. Lever, J. Fadden, N. Perron, and B. Packer 2009. "Outdoor Weathering and Dissolution of TNT and Tritonal." *Chemosphere* 77:1338–1345.

- Taylor, S., J. H. Lever, M. E. Walsh, J. Fadden, N. Perron, S. Bigl, R. Spangord, M. Curnow, and B. Packer. 2010. *Dissolution Rate, Weathering Mechanics and Friability of TNT, Comp B, Tritonal, and Octol*. ERDC/CRREL TR-10-2. Hanover, NH: US Army Engineer Research and Development Center.
- Taylor, S., C. Richardson, J. H. Lever, J. S. Pitt, S. Bigl, N. Perron, and J. P. Bradley. 2011. "Dissolution of Nitroglycerin from Small Arms Propellants and Their Residues." *International Journal of Energetic Materials and Chemical Propulsion* 10:397–419.
- Taylor, S., K. Dontsova, S. Bigl, C. Richardson, J. Lever, J. Pitt, J. P. Bradley, M. Walsh, and J. Šimůnek. 2012. *Dissolution Rate of Propellant Energetics from Nitrocellulose Matrices*. ERDC/CRREL TR-12-9. Cold Regions Research and Engineering Laboratory, Hanover, NH.
- Taylor, S., D. B. Ringelberg, K. Dontsova, C. Daghljan, M. E. Walsh, and M. R. Walsh. 2013. "Insights into the Dissolution and the Three-Dimensional Structure of Insensitive Munitions Formulations." *Chemosphere* 93:1782–1788.
- Taylor, S., K. Dontsova, M. E. Walsh, M. R. Walsh. 2015a. "Outdoor Dissolution of Detonation Residues of Three Insensitive Munitions (IM) Formulations." *Chemosphere* 134:250–256.
- Taylor, S., E. Park, K. Bullion, and K. Dontsova. 2015b. "Dissolution of Three Insensitive Munitions Formulations." *Chemosphere* 119:342–348.
- US Climate Data. 2018. Climate Hanover – New Hampshire.
<http://www.usclimatedata.com/climate/hanover/new-hampshire/united-states/usnh0102>.
- U. S. Environmental Protection Agency. 1994. *Nitroaromatics and Nitramines by HPLC*. SW846 Method 8330. Washington, DC: Office of Solid Waste and Emergency Response.
- Walsh, M. R., M. E. Walsh, S. Taylor, C. A. Ramsey, D. B. Ringelberg, J. E. Zufelt, S. Thiboutot, G. Ampleman, and E. Diaz. 2013. "Characterization of PAX-21 Insensitive Munitions Detonation Residues." *Propellants, Energetics, Pyrotechnics* 38:399–409.
- Walsh, M. R., M. E. Walsh, C. A. Ramsey, S. Thiboutot, G. Ampleman, E. Diaz, and J. E. Zufelt. 2014. "Energetic Residues from the Detonation of IMX-104 Insensitive Munitions." *Propellants, Energetics, Pyrotechnics* 39:243–250.
- Walsh, M. R., M. E. Walsh, C. A. Ramsey, S. Thiboutot, G. Ampleman, and J. Dowden. 2015. *Energetic Residues from the Detonation of IMX101 and IMX-104 Munitions*. ERDC/CRREL TR-15-3. Hanover, NH: US Army Engineer Research and Development Center.
- Walton, M., and P. Workman. 1987. "Nitroimidazole Bioreductive Metabolism. Quantitation and Characterisation of Mouse Tissue Benzimidazole Nitroreductases In Vivo and In Vitro." *Biochemical Pharmacology* 36:887–896.
- Williams, R. T., W. E. Sisk, and A. R. MacGillivray. 1989. "Degradation of Nitroguanidine Wastewater Components in Soil." *Environmental Toxicology and Chemistry* 8:469–475.

- Vanderborght, J., M. Vanclooster, A. Timmerman, P. Seuntjens, D. Mallants, D. J. Kim, D. Jacques, L. Hubrechts, C. Gonzalez, J. Feyen, J. Diels, and J. Deckers. 2001. "Overview of Inert Tracer Experiments in Key Belgian Soil Types: Relation between Transport and Soil Morphological and Hydraulic Properties." *Water Resources Research* 37:2873–2888.
- Yaron, B., I. Dror, and B. Berkowitz. 2012. *Soil-Subsurface Change: Chemical Pollutant Impacts*. Heidelberg: Springer Berlin.
- Yoon, J. M., B. T. Oh, C. L. Just, and J. L. Schnoor. 2002. "Uptake and Leaching of Octahydro-1,3,5,7-Tetranitro-1,3,5,7-Tetrazocine by Hybrid Poplar Trees." *Environmental Science and Technology* 36:4649–4655.

Appendix A: Solubility of DNAN, NQ, and NTO as a Function of Temperature



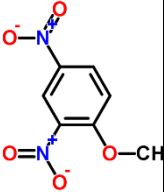
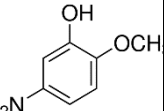
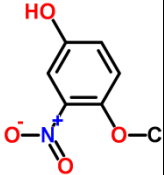
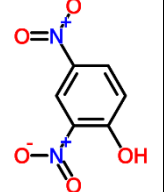
Appendix B: Studies Investigating the Transformation Products of DNAN


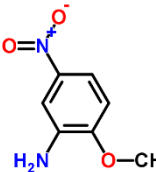
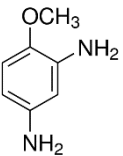
Compound [CAS] ^a	Matrix Containing DNAN	Reference
2-methoxy-5-nitrophenol [636-93-1]	Irradiated aqueous solutions; intermediate product with nitrate and nitrite as major products	Rao et al. 2013
	Molecular modeling of alkaline hydrolysis mechanism	Salter-Blanc et al. 2013
	Irradiation of aqueous solutions	Hawari et al. 2015
4-methoxy-3-nitrophenol [15174-02-4]	Molecular modeling of alkaline hydrolysis mechanism	Salter-Blanc et al. 2013
	Irradiation of aqueous solutions	Hawari et al. 2012
4-methoxy-3-nitroaniline [577-72-0]	Zero-valent iron treatment of PAX-21 wastewater; intermediate to formation of 2,4-diaminoanisole	Ahn et al. 2011
	<i>Rhizobium litchii</i> cultures	Schroer et al. 2015
	Suspensions of soils under aerobic and anaerobic conditions (iMENA, 4-methoxy-5-nitroaniline)	Olivares et al. 2016
2-methoxy-5-nitroaniline [99-59-2] (MENA)	Zero-valent iron treatment of PAX-21 wastewater; intermediate to formation of 2,4-diaminoanisole	Ahn et al. 2011
	Artificially contaminated soil microcosms (aerobic)	Perreault et al. 2012
	Sludge bioassays under aerobic, microaerophilic, and anaerobic conditions	Olivares et al. 2013
	Reduction with zero valent iron in lab solutions and bacteria in cell cultures	Hawari et al. 2015
	Earthworms and ryegrass shoots exposed to DNAN amended soil	Dodard et al. 2013
	<i>Rhizobium litchii</i> cultures	Schroer et al. 2015
	Suspensions of soils under aerobic and anaerobic conditions	Olivares et al. 2016
2,4-Dinitrophenol [51-28-5]	Irradiated aqueous solutions; minor (<3% of total nitrogen) product with nitrate and nitrite as major products	Rao et al. 2013
	Rhesus Macaques dosed with DNAN. Found in blood and urine; concentrations higher in blood due to presumed nitroreduction to amino-nitrophenols	Hoyt et al. 2013
	Aerobic cell cultures with bacteria isolated from Holston Army Ammunition Plant-activated sludge	Fida et al. 2014

Compound [CAS] ^a	Matrix Containing DNAN	Reference
	Enriched cell cultures (transient product)	Richard and Weidhaas 2014
	Irradiation (UV and sunlight) of aqueous DNAN solutions formed nitrocatechol (dihydroxy-nitrobenzene), an unstable product	Hawari et al. 2015
2,4- Dinitrophenolate [20350-26-9]	Molecular modeling of alkaline hydrolysis mechanism	Salter-Blanc et al. 2013
2,4-Diaminoanisole [615-05-4]	Anaerobic fluidized-bed reactor	Arnett et al. 2009
	Anaerobic fluidized-bed bioreactor	Platten et al. 2010
	Zero-valent iron treatment of PAX-21 wastewater	Ahn et al. 2011
	Sludge bioassays under aerobic, microaerophilic, and anaerobic conditions	Olivares et al. 2013
	Reduction with zero-valent iron in lab solutions and bacteria in cell cultures	Hawari et al. 2015
	Suspensions of soils under anaerobic conditions	Olivares et al. 2016
Azo Dimers from DAAN (2,4-Diaminoanisole)	Anaerobic fluidized-bed bioreactor	Platten et al. 2010
	Oxic (actively aerated) aqueous solutions of DAAN	Hawari et al. 2015
	Sludge bioassays under aerobic, microaerophilic, and anaerobic conditions	Olivares et al. 2013
	Suspensions of soils under aerobic and anaerobic conditions	Olivares et al. 2016
Nitrate/Nitrite	Irradiated aqueous solutions with nitrate and nitrite as major products	Rao et al. 2013
	Irradiation of aqueous solutions—For each mole of DNAN degraded, nitrate anion (0.7 mole), ammonium (1 mole), formaldehyde/formic acid (0.9 mole) was formed.	Hawari et al. 2015

^a Chemical Abstract Service

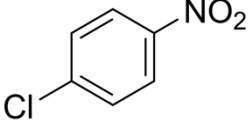
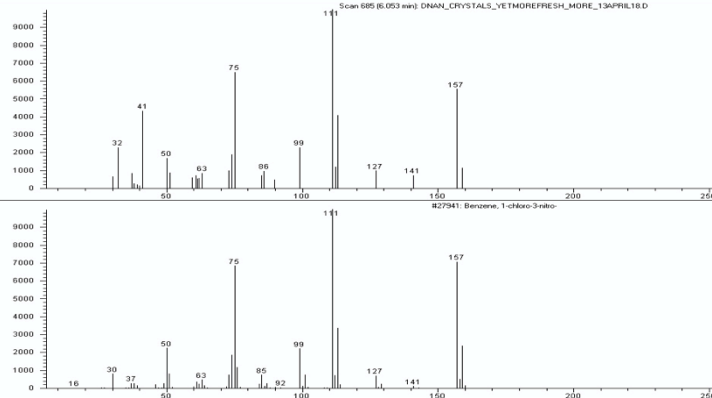
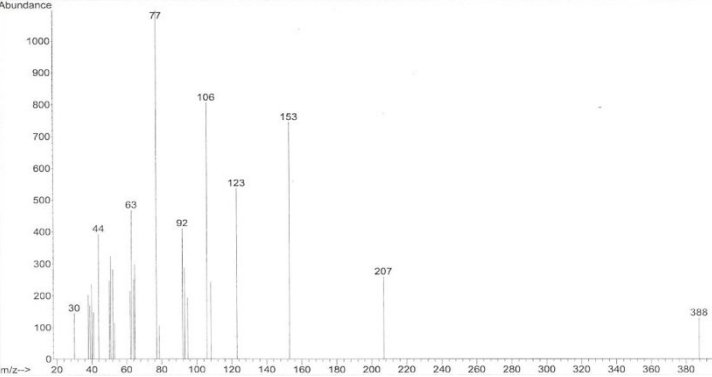
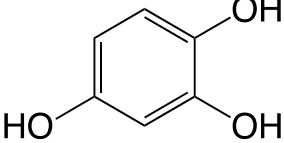
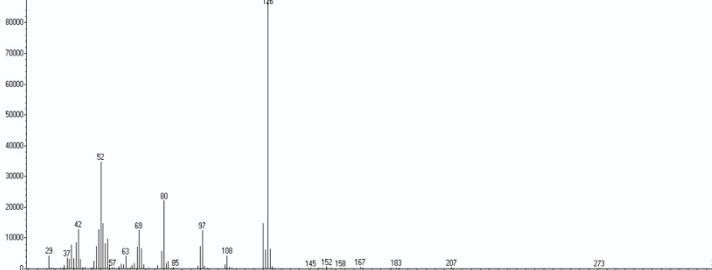
Appendix C: Properties of DNAN and Its Transformation Products

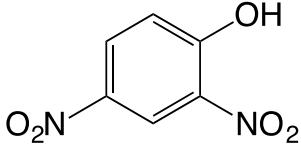
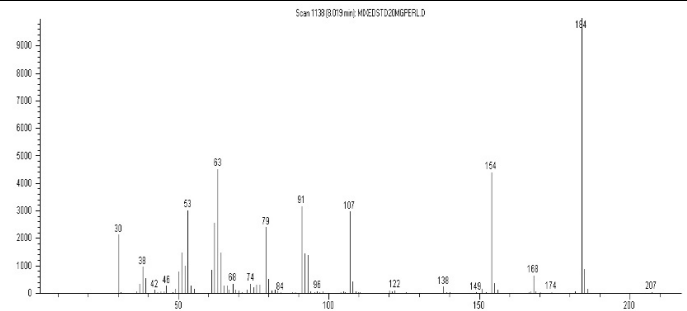
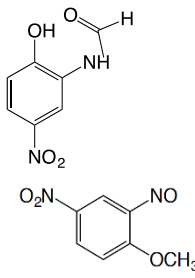
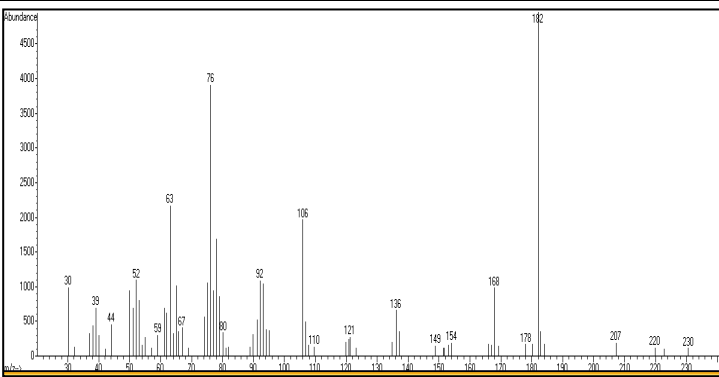
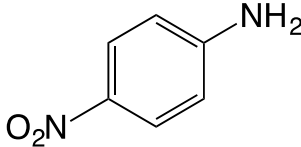
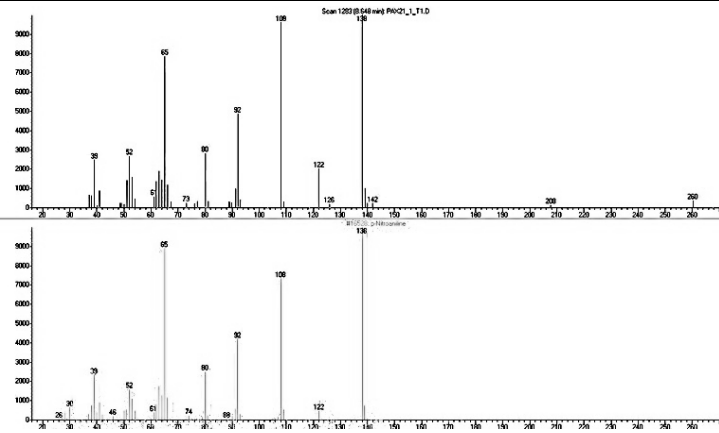
Name [CAS] Abbreviation [MW] [Formula]	Structure	Form	Melting Point	Boiling Point	Vapor Pressure (mm Hg, 25 °C)	Log K_{ow}	Hazard Classification from Safety Data Sheet	Other Properties
2,4-Dinitroanisole [119-27-7] DNAN [MW=198] [C ₇ H ₆ N ₂ O ₅]		Colorless to pale yellow crystals (AK Scientific Inc.)	88 °C –94 °C (Alfa Aesar)	207 °C (Alfa Aesar)	1.15 × 10 ⁻⁵ (Cuddy et al. 2014)	1.58 (Hawari et al. 2015)		S_w (25 °C) 0.213 g/L (Hawari et al. 2015) 0.276 g/L at 25 °C (Boddu et al. 2008)
2-methoxy-5-nitrophenol [636-93-1] 2-Me-5-NP [MW=169] [C ₇ H ₇ NO ₄]		Yellow-brown powder	104 °C–106 °C (Alfa Aesar) 96.5 °C (ChemSpider USEPA EPISuite)	294 °C (ChemSpider USEPA EPISuite)	1.9 × 10 ⁻⁴	1.73 (estimated) (ChemSpider USEPA EPISuite)	<ul style="list-style-type: none"> • Harmful if swallowed. • Skin and eye irritant • May cause respiratory irritation • Harmful to aquatic life with long-lasting effects 	
4-methoxy-3-nitrophenol [15174-02-4] 4-Me-3-NP [MW=169] [C ₇ H ₇ NO ₄]		Yellow powder (AK Scientific Inc.)	95 °C–103 °C (AK Scientific Inc.)	341 °C (ChemNet) 294 °C (ChemSpider USEPA EPISuite)	1.9 × 10 ⁻⁴	1.99 (estimated) (ChemSpider USEPA EPISuite)	<ul style="list-style-type: none"> • Skin and eye irritant • May cause respiratory irritation 	
2,4-Dinitrophenol [51-28-5] 2,4-DNP [184] [C ₆ H ₄ N ₂ O ₅]		Yellow crystals	106 °C–108 °C (Alfa Aesar)		3.9 × 10 ⁻⁴ mm Hg at 20 °C (Schwarzenbach et al. 1988; PubChem)	1.7 (PubChem)	<ul style="list-style-type: none"> • Toxic if inhaled or contacted by skin • Damage to organs through prolonged or repeated exposure • Very toxic to aquatic life 	2790 mg/L at 20 °C (Schwarzenbach et al. on PubChem) pK _a = 4.09

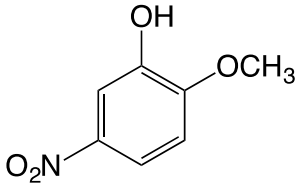
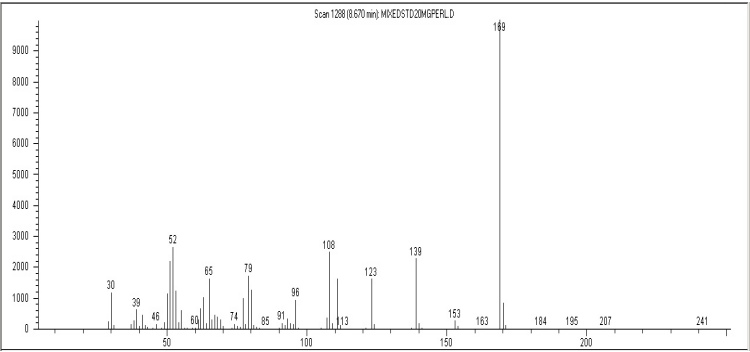
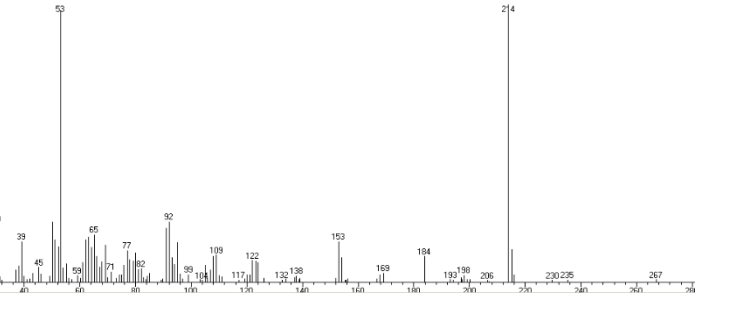
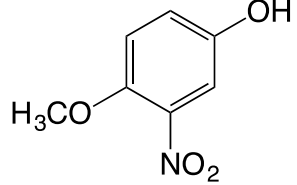
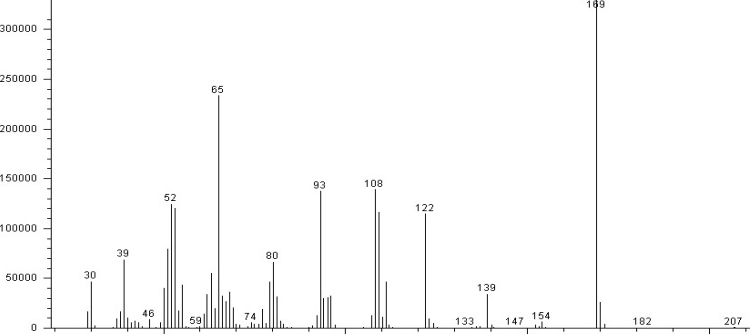
Name [CAS] Abbreviation [MW] [Formula]	Structure	Form	Melting Point	Boiling Point	Vapor Pressure (mm Hg, 25 °C)	Log K_{ow}	Hazard Classification from Safety Data Sheet	Other Properties
4-methoxy-3-nitroaniline [577-72-0] [MW=168] [C ₇ H ₈ N ₂ O ₃]		Red powder (ChemSpider NovoChem Ltd.)	97 °C (ChemSpider USEPA EPISuite)	304 °C (ChemSpider USEPA EPISuite)	3.2×10^{-4} (ChemSpider USEPA EPISuite)	0.92 (Enamine Safety Data Sheet) 0.80 (Hawari et al. 2015)	May cause an allergic skin reaction or breathing difficulties if inhaled	S_w (25 °C) 4.43 g/L (Hawari et al. 2015)
2-methoxy-5-nitroaniline [99-59-2] [MW=168] [C ₇ H ₈ N ₂ O ₃]		Orange-red needles or dull orange powder (MP Biomedicals Safety Data Sheet)	117 °C–119 °C (MP Biomedicals Safety Data Sheet)		1.3×10^{-4} (estimated) (MP Biomedicals Safety Data Sheet)	1.51 Enamine Safety Data Sheet 1.47 (Hawari et al. 2015)	<ul style="list-style-type: none"> Toxic if swallowed or in contact with skin Suspected of causing cancer 	Elutes on HPLC C18 before DNAN (Perreault et al. 2012) S_w (25 °C) 0.252 g/L (Hawari et al. 2015)
2,4-diaminoanisole [615-05-4] [138.17] [C ₇ H ₁₀ N ₂ O]		Dark brown crystals (Sigma- Aldrich SDS) Colorless solid (needles) (NIOSH through PubChem)	58 °C (Sigma-Aldrich SDS) 67 °C–68 °C (Merck)		0.047 mm Hg at 25 °C (PubChem)	0.5 (PubChem)	<ul style="list-style-type: none"> Harmful if swallowed Suspected of causing genetic defects May cause cancer Toxic to aquatic life with long-lasting effects 	S_w (25 °C) >40 g/L (Hawari et al. 2015) Miscible with water (PubChem)

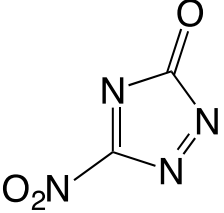
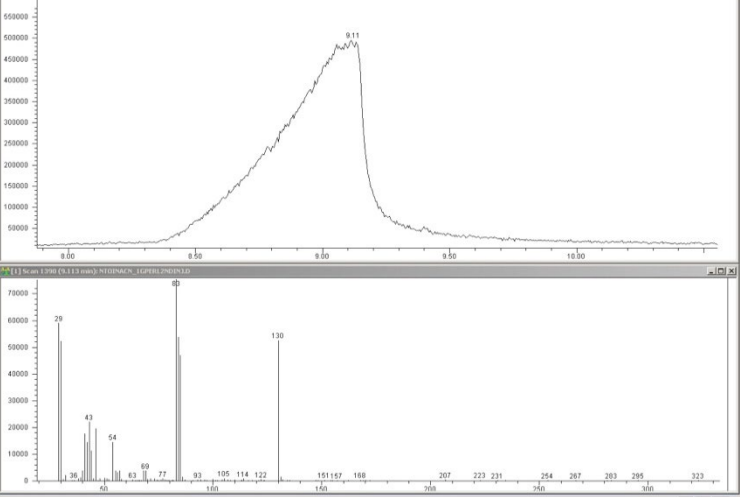
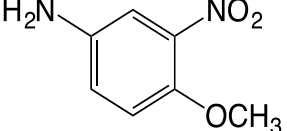
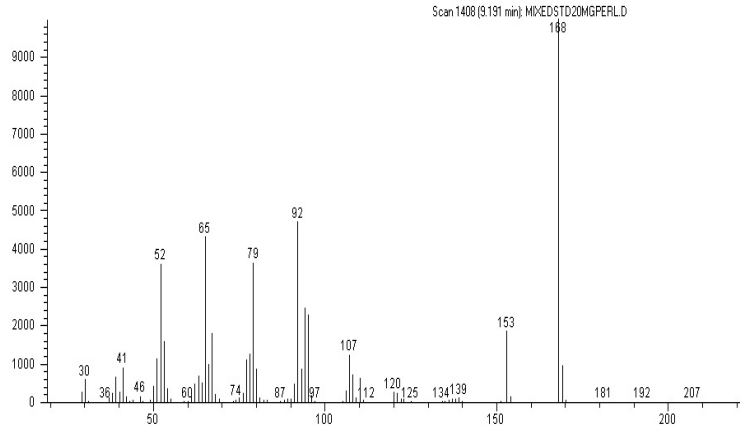
Appendix D: GC-MS Retention Times and Mass Spectra for Compounds Discussed in This Report

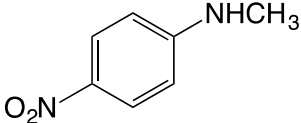
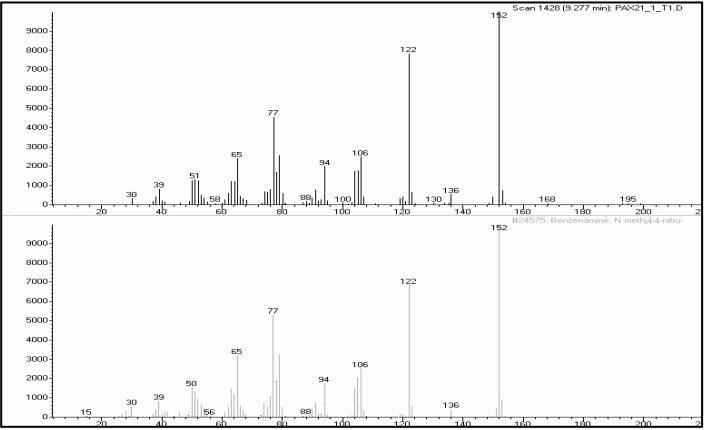
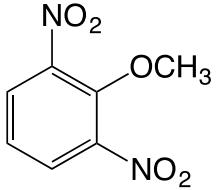
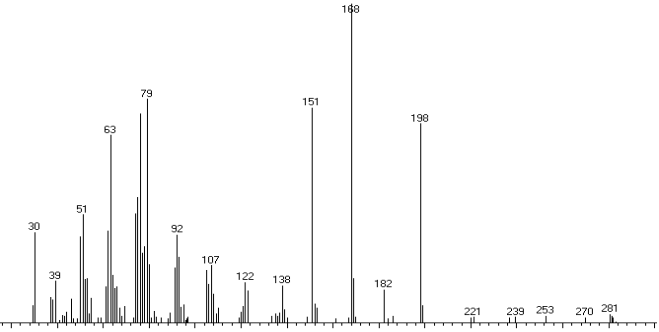
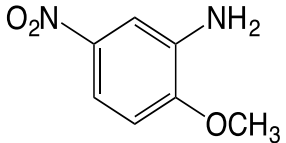
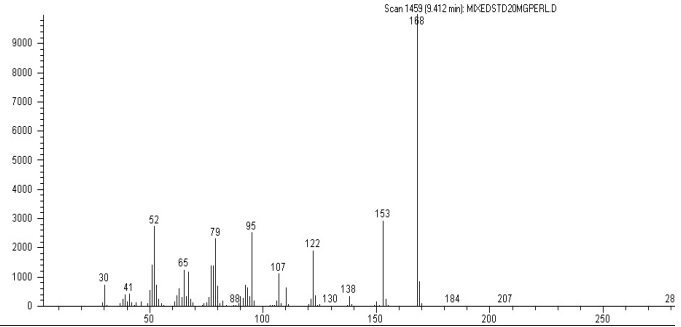
Note that NTO and NQ do not elute as sharp chromatographic peaks. Both compounds are thermally labile and degrade within the hot chromatography column.

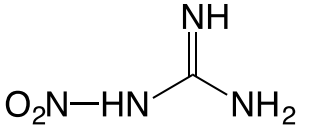
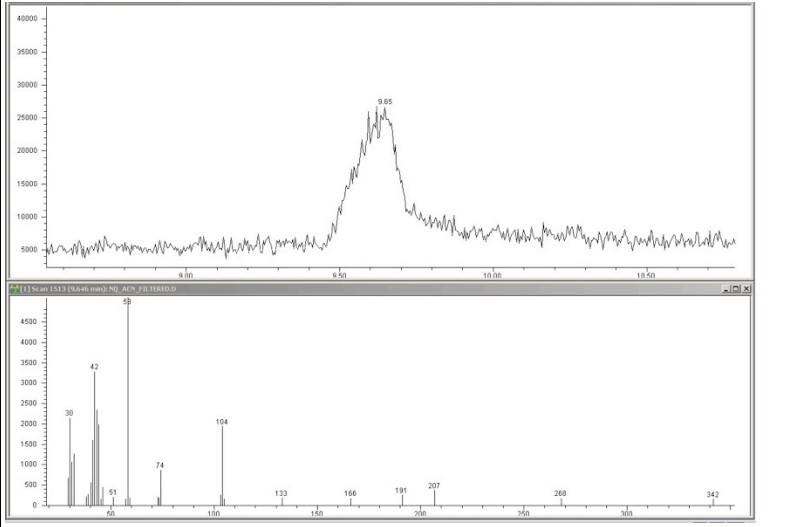
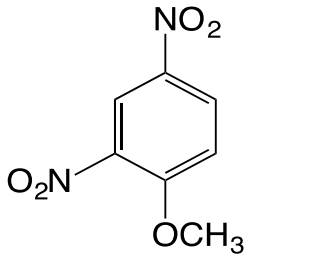
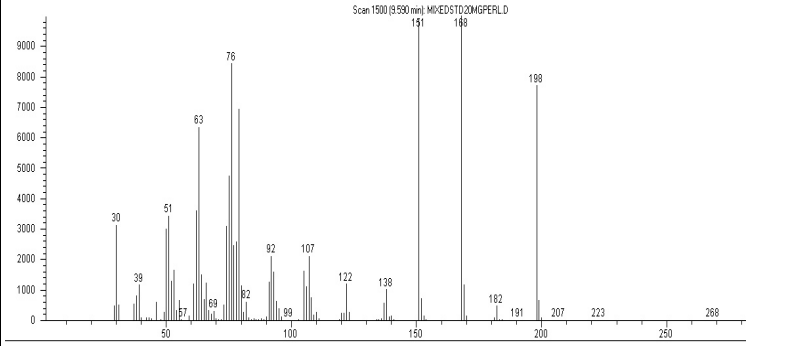
Retention Time (min)	Compound Molecular Weight, Formula	Mass of Fragments	GC Mass Spectra
6.1	1-Chloro-4-nitrobenzene MW = 157.5, C ₆ H ₄ ClNO ₂ 	Unknown	
6.95	Unknown	Unknown	
7.8	1,2,4-Benzenetriol MW = 126, C ₆ H ₆ O ₃ 	Unknown	

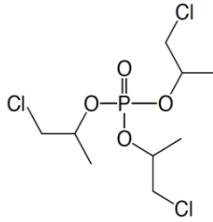
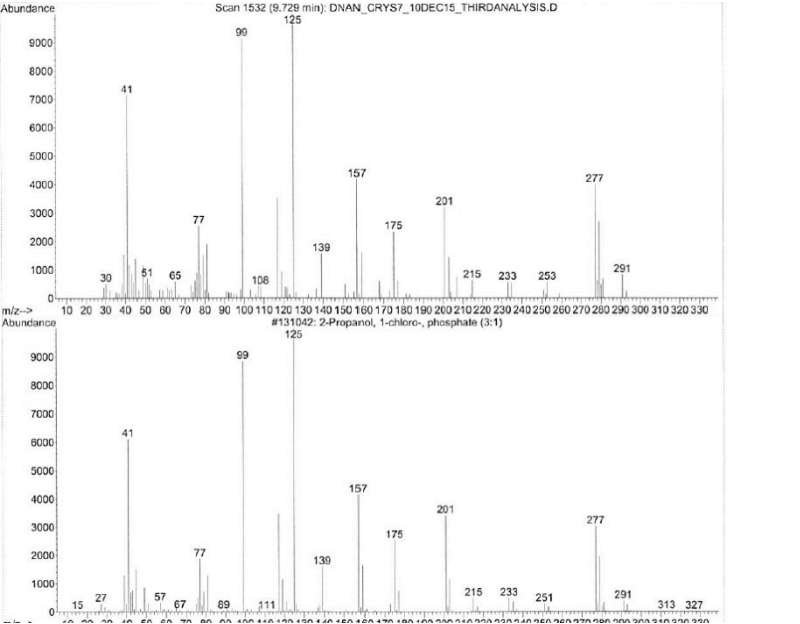
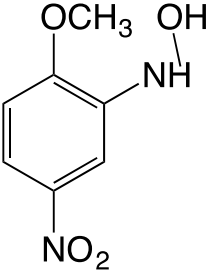
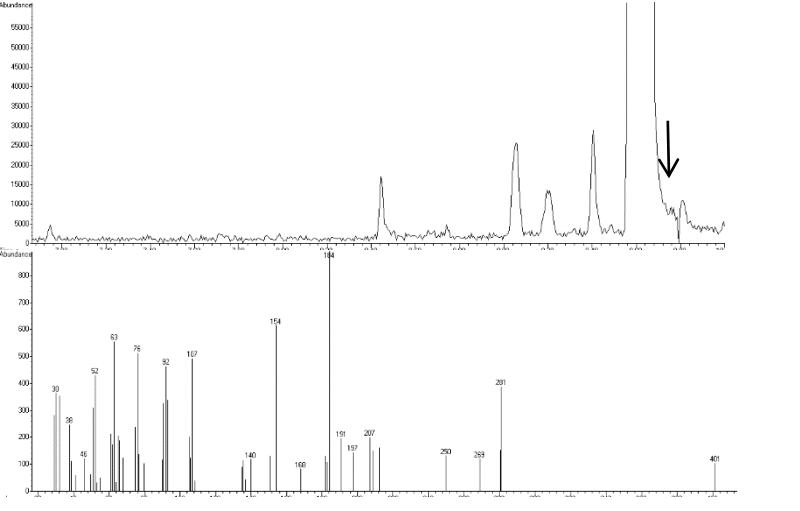
Retention Time (min)	Compound Molecular Weight, Formula	Mass of Fragments	GC Mass Spectra
8.02	2,4-Dinitrophenol MW = 184, C ₆ H ₄ N ₂ O ₅ 	184 (molecular ion) 154 (loss of NO (-30)) 91 79 63 53 30 (NO)	
8.45	Unknown A MW = 182, C ₇ H ₆ N ₂ O ₄ 	182 (Consistent with C ₇ H ₆ N ₂ O ₄) 136 (Loss of NO ₂ (-46)) 106 (Loss of CH ₂ ONO ₂ (-76)) 76 63 51 39 30 (NO)	
8.65	4-Nitroaniline MW = 138, C ₆ H ₆ N ₂ O ₂ 	138 (molecular ion) 108 (Loss of NO (-30)) 92 80 65 39 30	

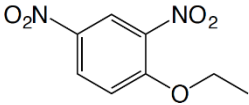
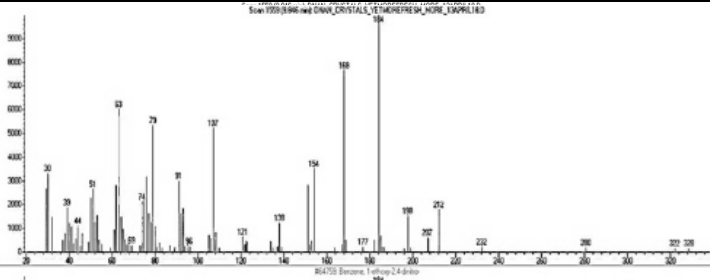
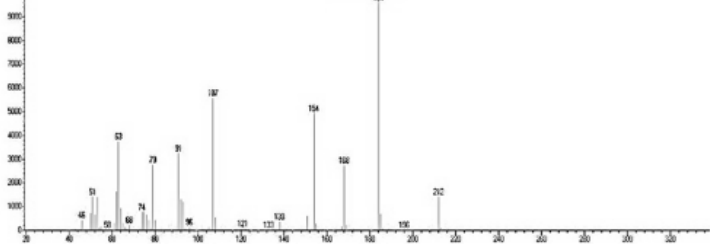
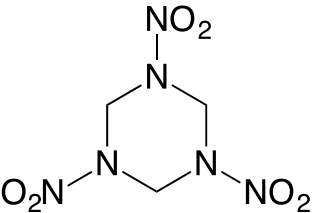
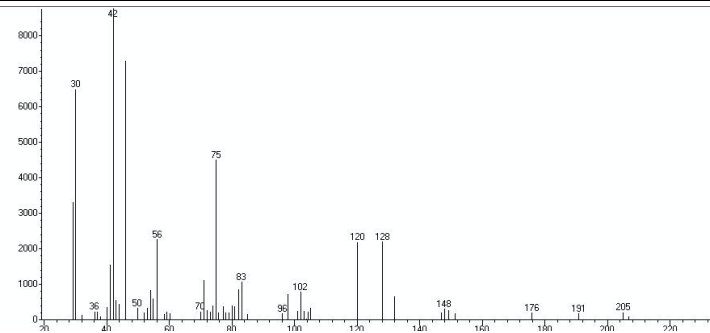
Retention Time (min)	Compound Molecular Weight, Formula	Mass of Fragments	GC Mass Spectra
8.67	2-methoxy-5-nitrophenol MW = 169, C ₇ H ₇ NO ₄ 	169 (molecular ion) 139 (Loss of NO (-30)) 123 (Loss of NO ₂ (-46)) 108 (Loss of CH ₃ NO ₂ (-61)) 79 65 52 30 (NO)	
9.03	Unknown C MW = 214, C ₇ H ₆ N ₂ O ₆	Unknown	
9.06	4-methoxy-3-nitrophenol MW = 169, C ₇ H ₇ NO ₄ 	169 (molecular ion) 153 (Loss of O ₂ =16) 122 (Loss of NO+OH=47) 108 (Loss of CH ₃ NO ₂ =61) 65 53 39 30 (NO)	

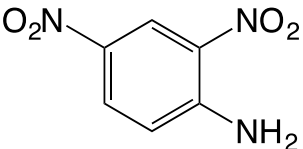
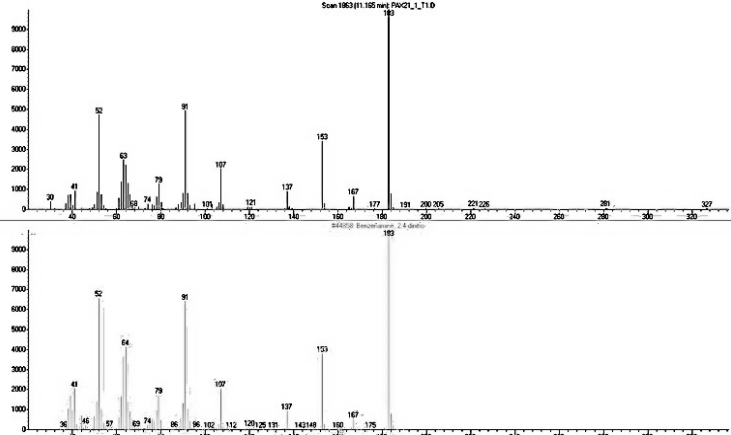
Retention Time (min)	Compound Molecular Weight, Formula	Mass of Fragments	GC Mass Spectra
9.1	NTO MW = 128, C ₂ N ₄ O ₃ 	130 83	
9.20	4-methoxy-3-nitroaniline MW = 168, C ₇ H ₈ N ₂ O ₃ 	168 (molecular ion) 153 (Loss of CH ₃ (-15)) 123 107 (Loss of CH ₃ NO ₂ (-61)) 92 (Loss of CH ₂ ONO ₂ (-76)) 79 65 52 30 (NO)	

Retention Time (min)	Compound Molecular Weight, Formula	Mass of Fragments	GC Mass Spectra
9.28	MNA (n-methyl-p-nitroaniline) MW = 152, C ₇ H ₈ N ₂ O ₂ 	152 (molecular ion) 122 (Loss of NO (-30)) 77 65 50 39 30	
Unknown	B-DNAN isomer, MW 198, (2,6-DNAN?) 	198 (molecular ion) 168 (Loss of NO (-30)) 151 76 63 30	
9.41	2-methoxy-5-nitroaniline MW = 168, C ₇ H ₈ N ₂ O ₃ 	168 (molecular ion) 153 (Loss of CH ₃ (-15)) 122 107 (Loss of CH ₃ NO ₂ (-61)) 95 (Loss of NO ₂ and HCN (-73)) 79 65 52 30 (NO)	

Retention Time (min)	Compound Molecular Weight, Formula	Mass of Fragments	GC Mass Spectra
9.6	NQ MW = 104, CH ₄ N ₄ O ₂ 	Unknown	
9.67	2,4-Dinitroanisole (DNAN) MW = 198, C ₇ H ₆ N ₂ O ₅ 	198 (molecular ion) 168 (Loss of NO (-30)) 151 (Loss of HNO ₂) 76 (Benzene ring with 4 H) 63 (CH ₃ + NO ₂ + H ₂) 30 (NO)	

Retention Time (min)	Compound Molecular Weight, Formula	Mass of Fragments	GC Mass Spectra
9.73	2-proponol, 1-chloro-phosphate (3:1) MW = 328, C ₉ H ₁₈ Cl ₃ O ₄ 	Unknown	
9.81	2-hydroxyl amino-4-nitroanisole MW = 184, C ₇ H ₈ N ₂ O ₄  Structure from Hawari et al. (2011)	184 63 30	

Retention Time (min)	Compound Molecular Weight, Formula	Mass of Fragments	GC Mass Spectra
9.85	1-ethoxy-2,4-dinitrobenzene MW = 212, C ₈ H ₈ N ₂ O ₅ 	Unknown	 
10.3	RDX MW = 222, C ₃ H ₆ N ₆ O ₆ 	Unknown	

Retention Time (min)	Compound Molecular Weight, Formula	Mass of Fragments	GC Mass Spectra
11.2	2,4-Dinitrobenzamine MW = 183, C ₆ H ₅ N ₃ O ₄ 	183 153 107 91 52 30	

Appendix E: Additional Figures for Dissolution and Transport of Insensitive Munitions Formulations IMX-101 and IMX-104 in Saturated Soil Columns

This appendix includes the results of additional analysis conducted to investigate the dissolution and transport of insensitive munitions formulations IMX-101 and IMX-104 in saturated soil columns.

Figure E-1. Breakthrough curves for individual explosives for detonated IMX-101 in Camp Guernsey soil: NTO, 3-nitro-1,2,4-triazol-5-one; NQ, nitroguanidine; DNAN, 2,4-dinitroanisole; 2-ANAN, 2-amino-4-nitroanisole; and 4-ANAN, 4-amino-2-nitroanisole. The *vertical solid line* indicates a switch to saturating solution.

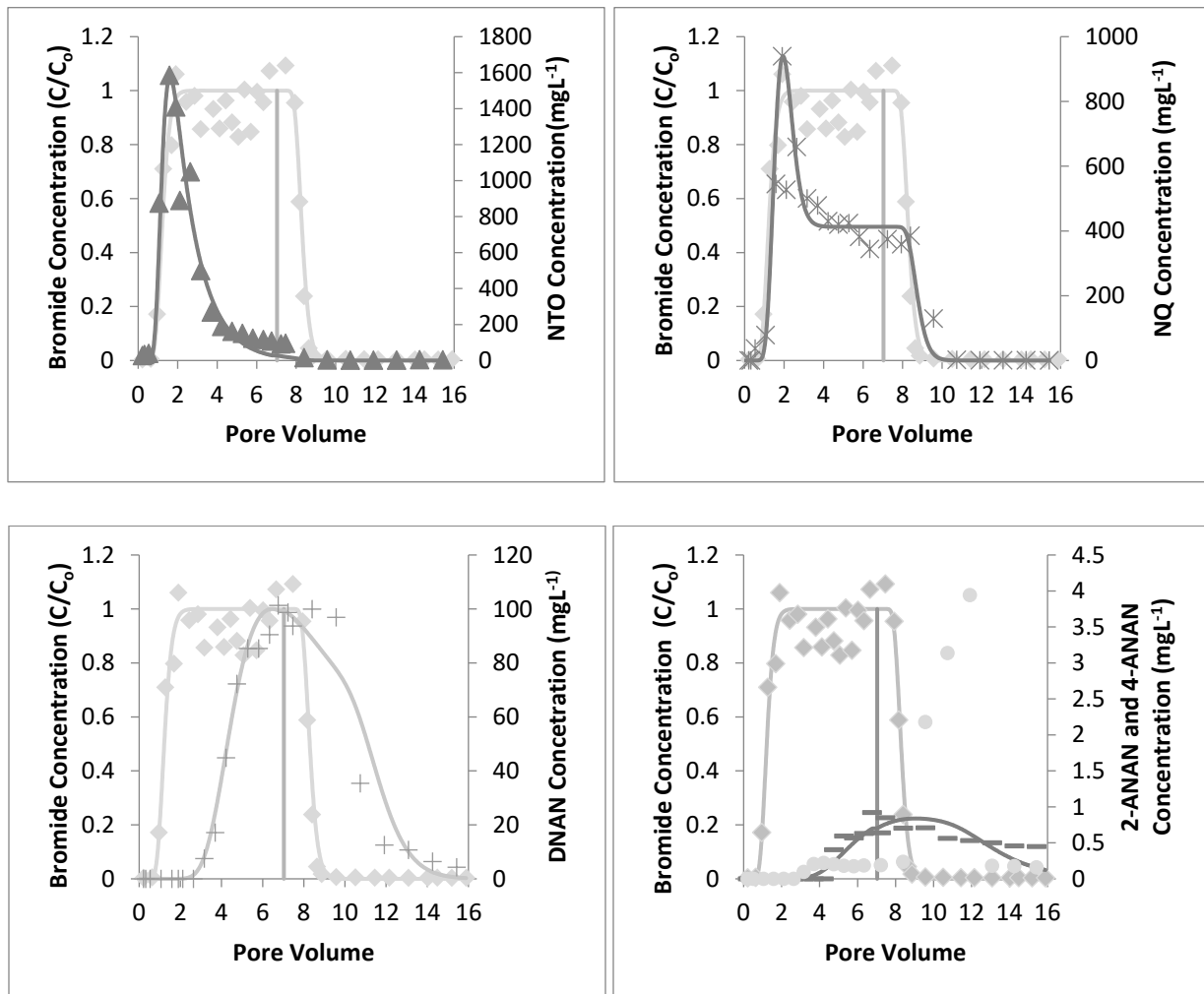


Figure E-2. Breakthrough curves for individual explosives for nondetonated IMX-101 in Camp Guernsey soil: NTO, 3-nitro-1, 2, 4-triazol-5-one; NQ, nitroguanidine; DNAN, 2,4-dinitroanisole; 2-ANAN, 2-amino-4-nitroanisole; and 4-ANAN, 4-amaino-2- nitroanisole. The *vertical solid line* indicates a switch to saturating solution.

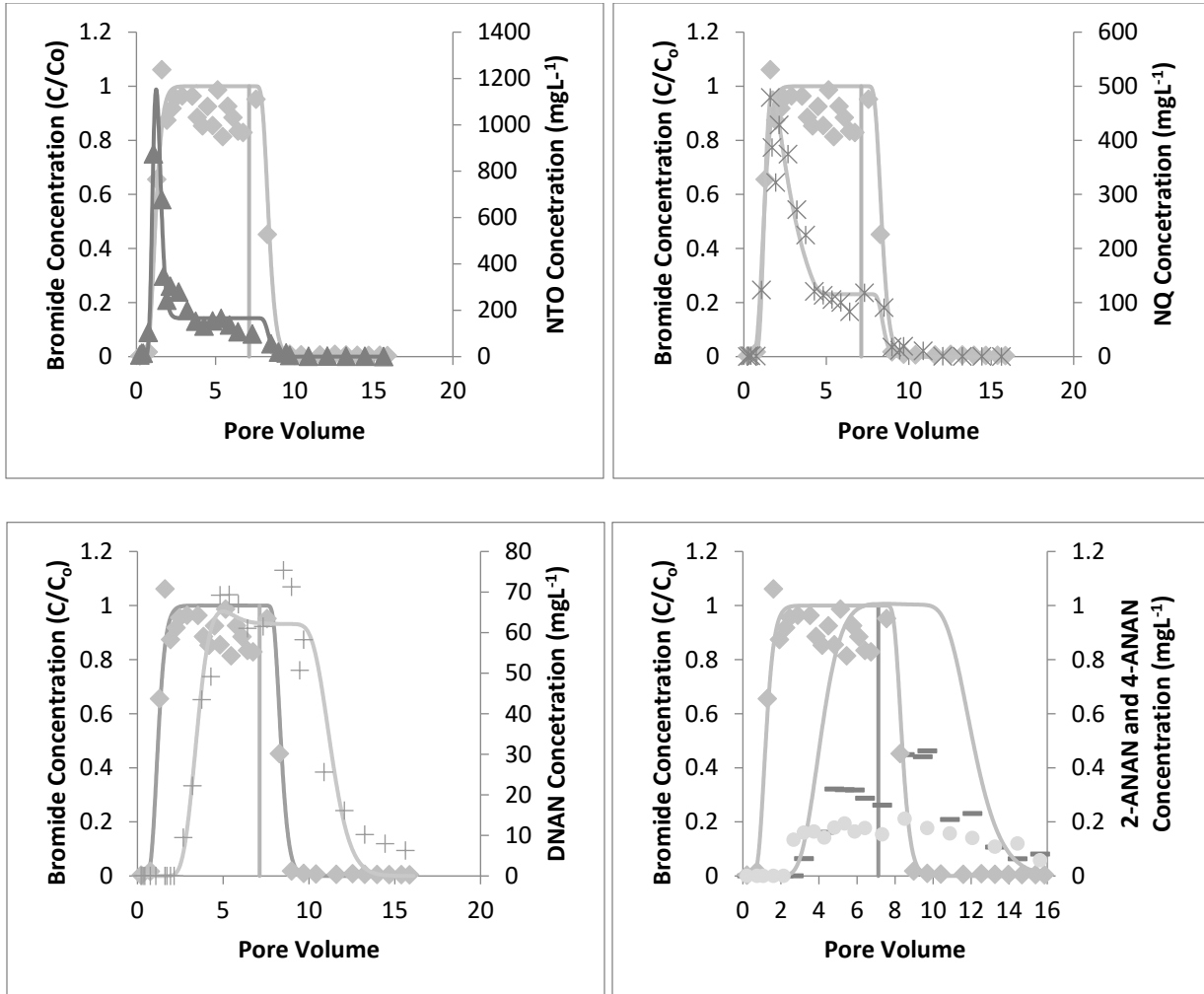


Figure E-3. Breakthrough curves for individual explosives for nondetonated IMX-101 in Camp Swift soil: NTO, 3-nitro-1,2,4-triazol-5-one; NQ, nitroguanidine; DNAN, 2, 4-dinitroanisole; 2-ANAN, 2-amino-4-nitroanisole; and 4-ANAN, 4-amino-2-nitroanisole. The *vertical solid line* indicates a switch to saturating solution.

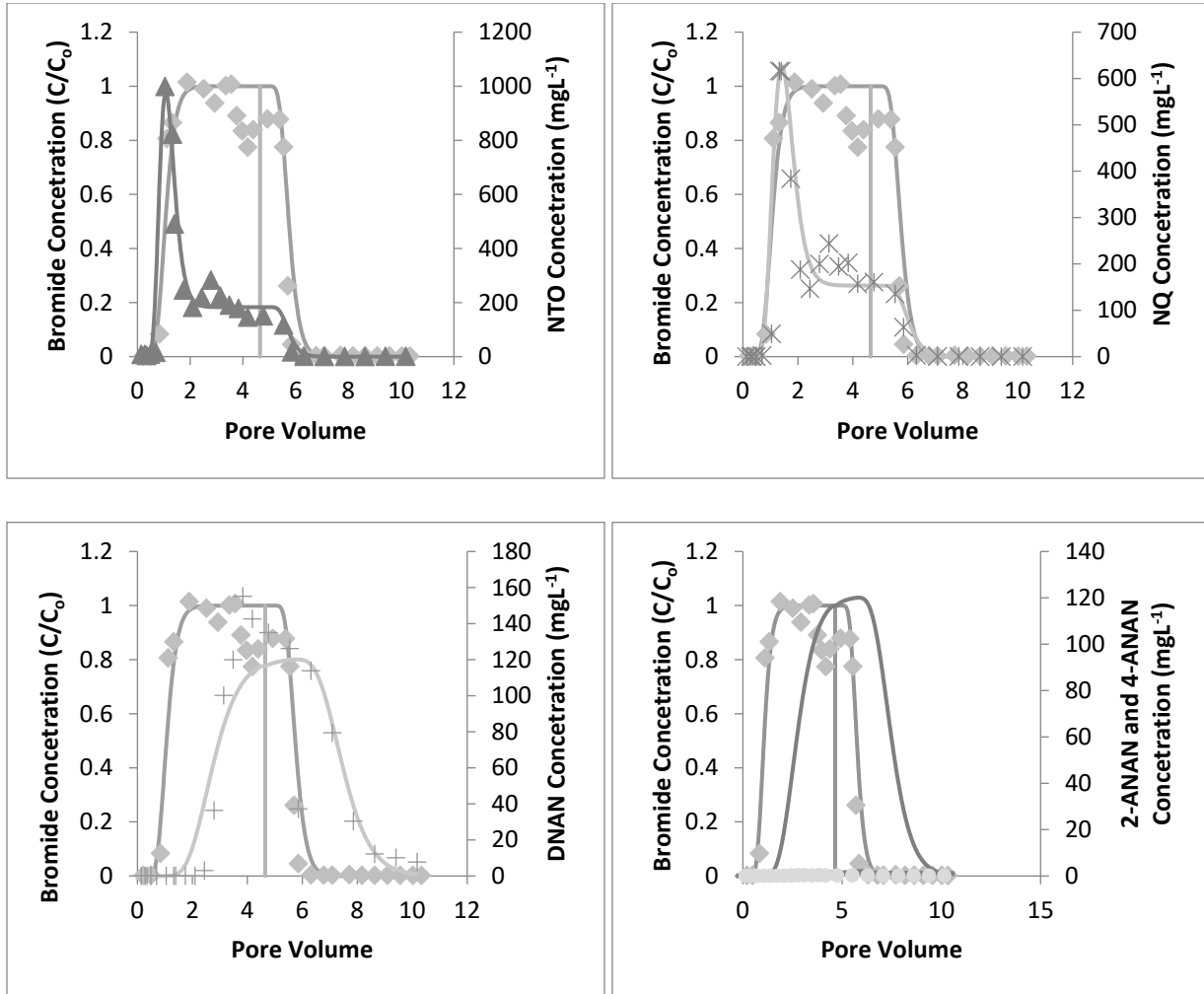


Figure E-4. Breakthrough curves for individual explosives for detonated IMX-101 flow interruption in Camp Guernsey soil: NTO, 3-nitro-1,2,4-triazol-5-one; NQ, nitroguanidine; DNAN, 2,4-dinitroanisole; 2-ANAN, 2-amino-4-nitroanisole; and 4-ANAN, 4-amino-2-nitroanisole. The *vertical dashed line* indicates the start of 24 hr flow interruption. The *vertical solid line* indicates a switch to saturating solution.

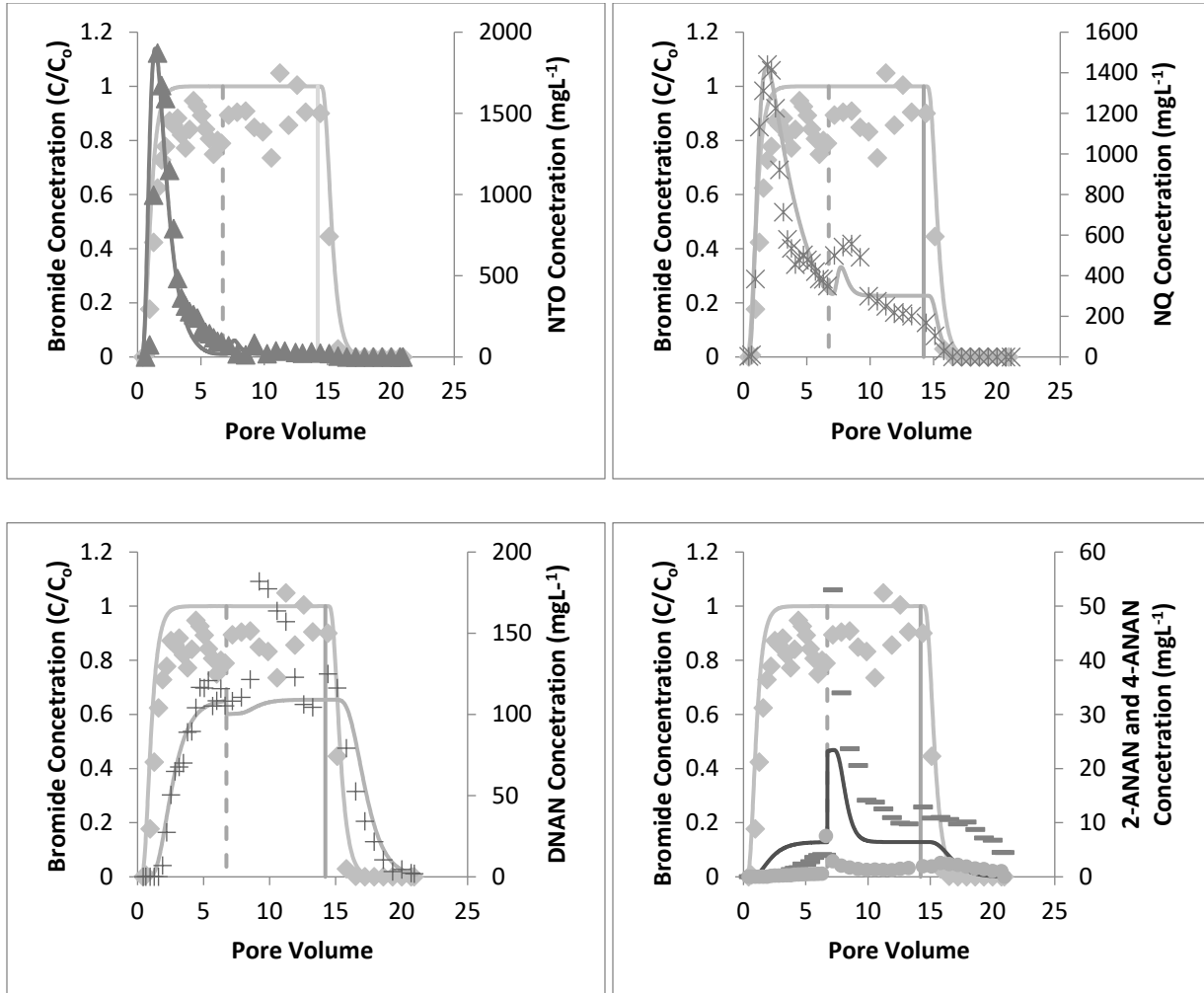


Figure E-5. Breakthrough curves for individual explosives for nondetonated IMX-104 particle in Camp Guernsey soil: NTO, 3-nitro-1,2,4-triazol-5-one; RDX, hexahydro-1,3,5-trinitro-1,3,5-triazine; HMX, octahydro-1,3,5,7-tetranitro-1,3,5,7-tetrazocine; DNAN, 2, 4- dinitroanisole; 2-ANAN, 2-amino-4-nitroanisole; and 4-ANAN, 4-amino-2-nitroanisole. The *vertical solid line* indicates a switch to saturating solution.

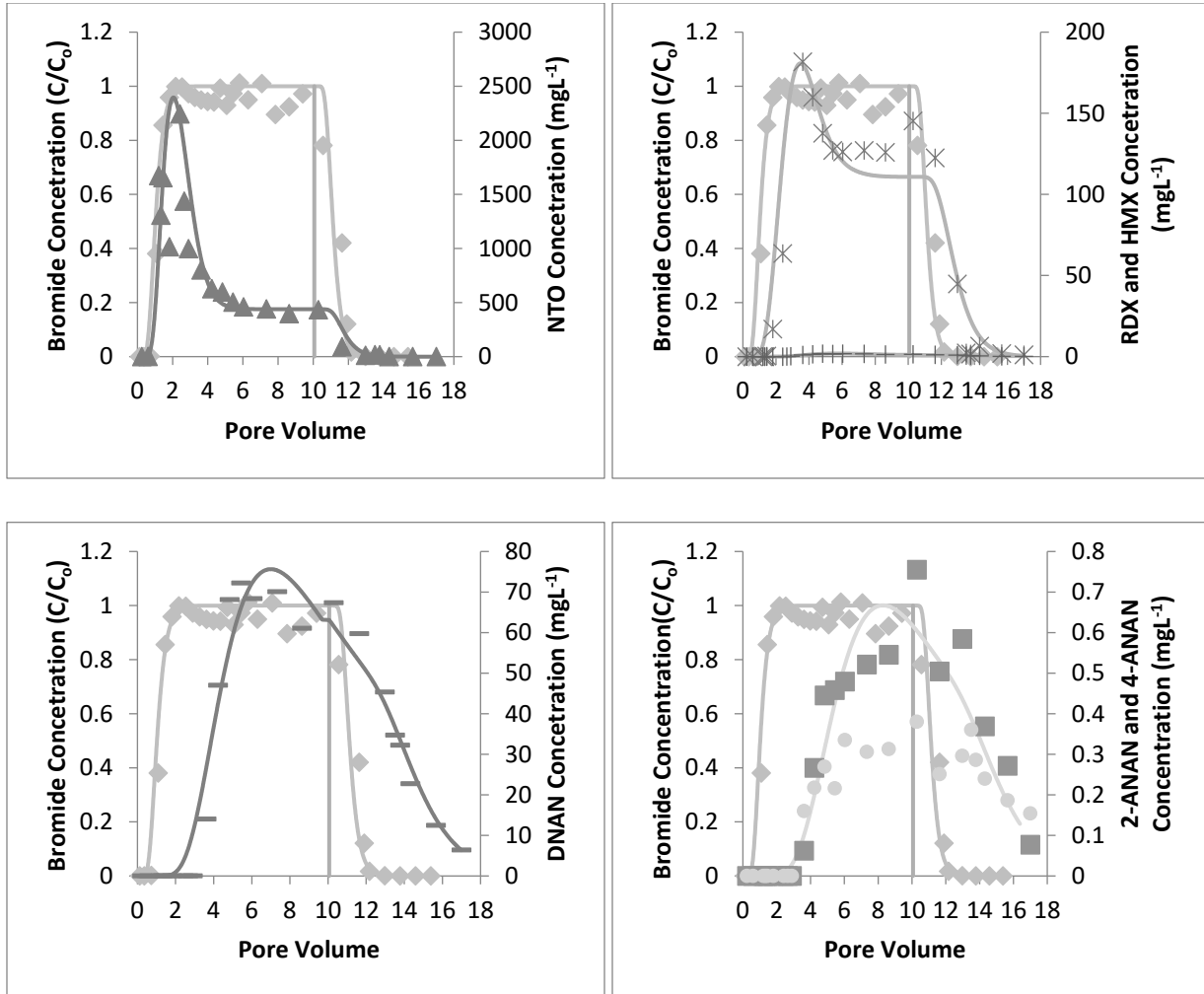


Figure E-6. Breakthrough curves for individual explosives for nondetonated IMX-104 particle in Camp Swift soil: NTO, 3-nitro-1,2,4-triazol-5-one; RDX, hexahydro-1,3,5-trinitro-1,3,5-triazine; HMX, octahydro-1,3,5,7-tetranitro-1,3,5,7-tetrazocine; DNAN, 2, 4- dinitroanisole; 2-ANAN, 2-amino-4-nitroanisole; and 4-ANAN, 4-amino-2-nitroanisole. The *vertical solid line* indicates a switch to saturating solution.

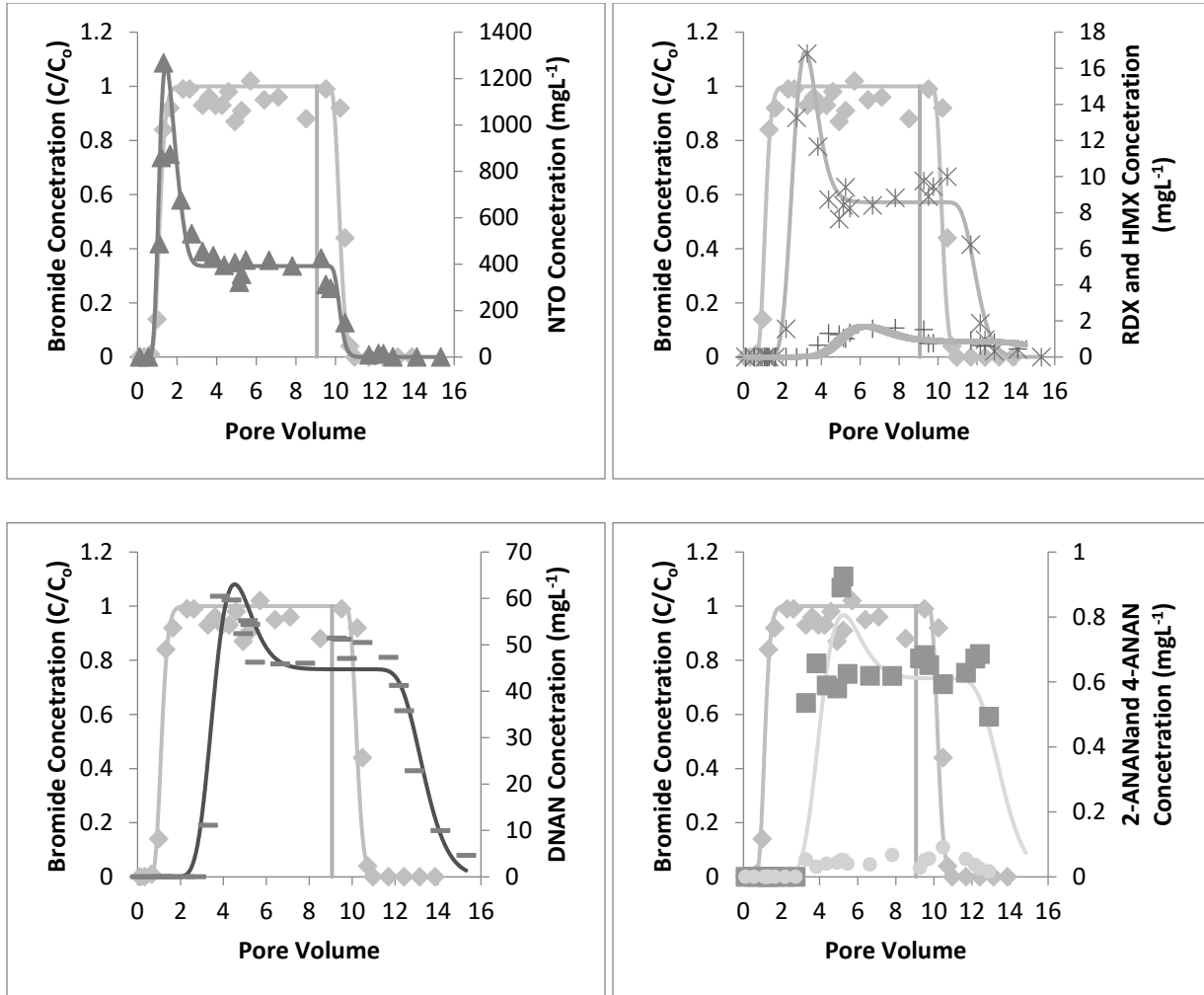


Figure E-7. Breakthrough curves for individual explosives for detonated IMX-104 flow interruption in Camp Guernsey soil: NTO, 3-nitro-1,2,4-triazol-5-one; RDX, hexahydro-1,3,5-trinitro-1,3,5-triazine; HMX, octahydro-1,3,5,7-tetranitro-1,3,5,7-tetrazocine; DNAN, 2,4- dinitroanisole; 2-ANAN, 2-amino-4-nitroanisole; and 4-ANAN, 4-amino-2-nitroanisole. The *vertical dashed line* indicates the start of 24 hr flow interruption. The *vertical solid line* indicates a switch to saturating solution.

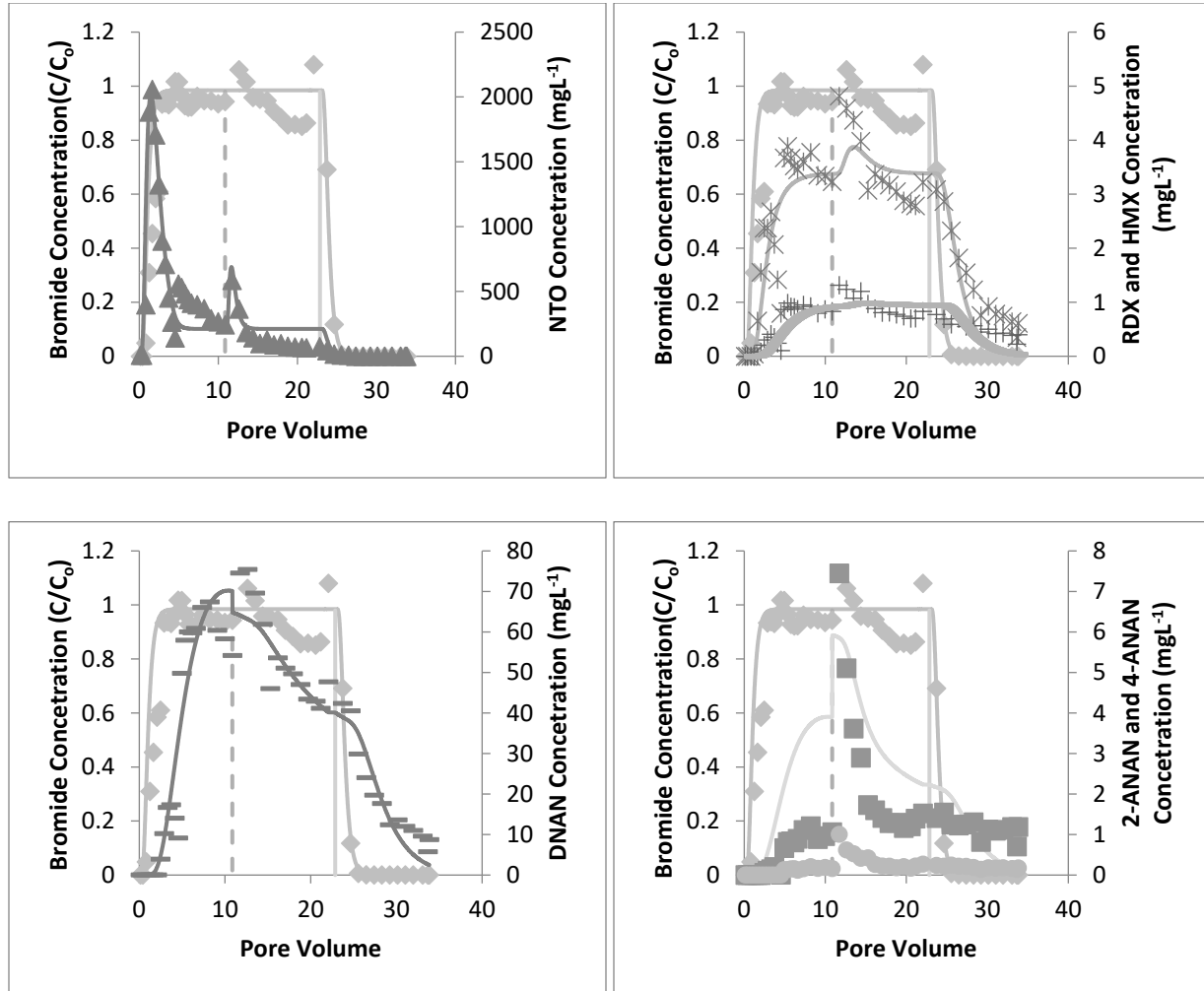
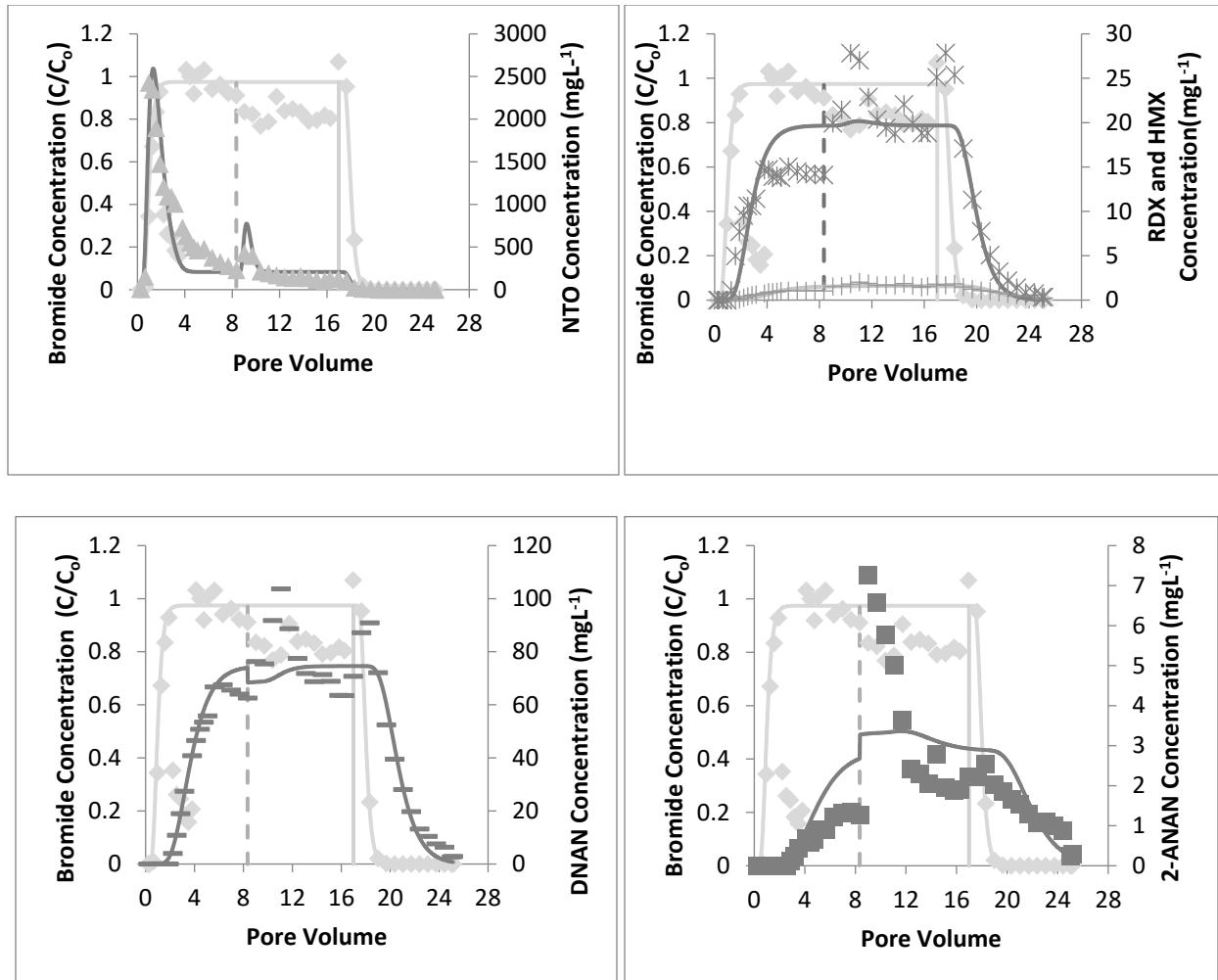


Figure E-8. Flow interruption breakthrough curves for individual explosives for detonated IMX-104 particle in Camp Guernsey soil: NTO, 3-nitro-1, 2, 4-triazol-5-one; RDX, hexahydro-1,3,5-trinitro-1,3,5-triazine; HMX, octahydro-1,3,5,7-tetranitro-1,3,5,7-tetrazocine; DNAN, 2, 4- dinitroanisole; and 2-ANAN, 2-amino-4-nitroanisole. The *vertical dashed gray line* indicates the start of 24 hr flow interruption. The *vertical solid gray line* indicates a switch to saturating solution.



Abbreviations

2-ANAN	2-amino-4-nitroanisole (same as MENA or 2-MeO-5-NA)
4-ANAN	4-amino-2-nitroanisole (same as 4-MeO-3-NA)
AP	Ammonium perchlorate
ARDEC	US Army Armament Research, Development, and Engineering Center
ATO	5-amino-1,2,4-triazol-3-one
BTC	Breakthrough curve
C4	Composition 4, a common plastic explosive
CAS	Chemical Abstract Service
CEC	Cation exchange capacity
CI	Confidence interval
ClO ₄ ⁻	Perchlorate ion
Comp B	Composition B, a 60-40 RXD-TNT mix
CRREL	Cold Regions Research and Engineering Laboratory
D	Detonated
DAAN	2,4-diaminoanisole
D2/WI	Deuterium/tungsten lamp designations
DNAN	2,4-dinitroanisole
DNP	Dinitrophenol
DNT	2,4- or 2,6-dinitrotoluene
EC	Electrical conductivity
ERDC	US Army Engineer Research and Development Center
FI	Flow interruption

FTIR	Fourier transfer infrared
GC-MS	Gas chromatography–mass spectrometry
HMX	High explosive 1,3,5,7,-octahydro-1,3,5,7-tetranitrotetrazocine
HPLC	High-precision liquid chromatography
IC	Ion chromatography
IM	Insensitive munitions
IMX	Insensitive munitions explosive
k	Mass-loss rate coefficient (first-order transformation rate constant)
K_d	Soil adsorption coefficient
K_{oc}	Soil organic carbon adsorption coefficient
KOH	Potassium hydroxide
K_{ow}	Octanol-water partition coefficient
LD ₅₀	Lethal dose (LD ₅₀) is the amount of an ingested substance that kills 50 percent of a test sample.
m/z	Mass / atomic number
MENA	2-methoxy-5-nitroaniline (same as 2-ANAN or 2-MeO-5-NA)
2-MeO-5-NA	2-methoxy-5-nitroaniline (same as MENA and 2-ANAN)
4-MeO-3-NA	4-methoxy-3-nitroaniline (same as 4-ANAN)
2-MeO-5-NP	2-methoxy-5-nitrophenol
4-MeO-3-NP	4-methoxy-3-nitrophenol
μCT	Micro-computed tomography
M_{diss}	Mass dissolved
M_f	Final mass
M_i	Initial mass

M_{miss}	Mass missing= $M_i - (M_f + M_{diss})$
MNA	<i>N</i> -methyl- <i>p</i> -nitroaniline
MW	Molecular weight
n	Porosity
na	Not available
NA	Not applicable
NH_4^+	Ammonium
NIST	National Institute of Standards and Technology
NO_3^-	Nitrate
NP	NovaPak C8
NQ	Nitroguanidine
NTO	3-nitro-1,2,4-triazol-5-one
OC	Organic carbon
PAX	Picatinny Arsenal Explosive
ρ_b	Bulk density
pK_a	Acid dissociation constant
PTFE	Polytetrafluoroethylene
R^2	Coefficient of determination
RDX	1,3,5-hexahydro-1,3,5-trinitro-1,3,5-triazine
SERDP	Strategic Environmental Research and Development Program
SIM	Selective ion monitoring
SSA	Specific surface area
TFA	Trifluoroacetic acid
TNT	2,4,6-trinitrotoluene

UD	Undetonated
UK	Unknown
USEPA	United States Environmental Protection Agency
UV	Ultraviolet
UV-vis	Ultraviolet to visible
v/v	Volume/volume
λ	Longitudinal dispersivity
Y_{max}	Initial (Maximum) dissolution rate
Y_{min}	Minimum or steady-state dissolution rate
χ	Decay Constant for Dissolution Rate

REPORT DOCUMENTATION PAGE

Form Approved
OMB No. 0704-0188

Public reporting burden for this collection of information is estimated to average 1 hour per response, including the time for reviewing instructions, searching existing data sources, gathering and maintaining the data needed, and completing and reviewing this collection of information. Send comments regarding this burden estimate or any other aspect of this collection of information, including suggestions for reducing this burden to Department of Defense, Washington Headquarters Services, Directorate for Information Operations and Reports (0704-0188), 1215 Jefferson Davis Highway, Suite 1204, Arlington, VA 22202-4302. Respondents should be aware that notwithstanding any other provision of law, no person shall be subject to any penalty for failing to comply with a collection of information if it does not display a currently valid OMB control number. PLEASE DO NOT RETURN YOUR FORM TO THE ABOVE ADDRESS.

1. REPORT DATE (DD-MM-YYYY) November 2022			2. REPORT TYPE Technical Report / Final		3. DATES COVERED (From - To) FY12-FY17	
4. TITLE AND SUBTITLE Dissolution of NTO, DNAN, and Insensitive Munitions Formulations and Their Fates in Soils: SERDP ER-2220					5a. CONTRACT NUMBER	
					5b. GRANT NUMBER	
					5c. PROGRAM ELEMENT	
6. AUTHOR(S) Katerina M. Dontsova, Susan Taylor, Jennifer D. Arthur, Julie B. Becher, Mark L. Brusseau, Edward Hunt, Noah W. Mark, Dave B. Ringelberg, Jiří Šimůnek, and Marianne E. Walsh					5d. PROJECT NUMBER	
					5e. TASK NUMBER	
					5f. WORK UNIT NUMBER	
7. PERFORMING ORGANIZATION NAME(S) AND ADDRESS(ES) US Army Engineer Research and Development Center (ERDC) Cold Regions Research and Engineering Laboratory (CRREL) 72 Lyme Road Hanover, NH 03755-1290					8. PERFORMING ORGANIZATION REPORT NUMBER ERDC/CRREL TR-22-22	
9. SPONSORING / MONITORING AGENCY NAME(S) AND ADDRESS(ES) Strategic Environmental Research and Development Program Environmental Restoration Program Area 4800 Mark Center Drive, Suite 16F16 Alexandria, VA 22350-3605					10. SPONSOR/MONITOR'S ACRONYM(S) SERDP	
					11. SPONSOR/MONITOR'S REPORT NUMBER(S)	
12. DISTRIBUTION / AVAILABILITY STATEMENT Approved for public release; distribution is unlimited.						
13. SUPPLEMENTARY NOTES Funding provided by the Strategic Environmental Research and Development Program (SERDP) under ER-2220, "Dissolution of NTO, DNAN, and Insensitive Munitions Formulations and Their Fates in Soils."						
14. ABSTRACT The US military is interested in replacing TNT (2,4,6-trinitrotoluene) and RDX (1,3,5-hexahydro-1,3,5-trinitro-1,3,5-triazine) with DNAN (2,4-dinitroanisole) and NTO (3-nitro-1,2,4-triazol-5-one), which have similar explosive characteristics but are less likely to detonate unintentionally. Although these replacements are good explosives, basic information about their fate and transport was needed to evaluate their environmental impact and life-cycle management. This project measured their dissolution, photodegradation, and how aqueous solutions interact with soils, data critical to determining exposure potential and, consequently, risk.						
15. SUBJECT TERMS Explosives, Military--Environmental aspects, Explosives, Military--Residues, Explosives, Military--Dissolution (Chemistry), Soil absorption and adsorption, Soil pollution						
16. SECURITY CLASSIFICATION OF:			17. LIMITATION OF ABSTRACT SAR	18. NUMBER OF PAGES 150	19a. NAME OF RESPONSIBLE PERSON	
a. REPORT Unclassified	b. ABSTRACT Unclassified	c. THIS PAGE Unclassified			19b. TELEPHONE NUMBER (include area code)	

7. PERFORMING ORGANIZATION NAME(S) AND ADDRESS(ES) (CONT.)

University of Arizona
Biosphere 2 and Soil, Water, and Environmental Science Department
845 N. Park Avenue
Tucson, AZ 85721-0158

Dartmouth College
Hanover, NH 03755

University of California, Riverside
Department of Environmental Sciences
2258 Geology Building
Riverside, CA 92521-0424